Using ensemble simulations for robust process analyses and statistical evaluations of very extreme daily precipitation events

Dissertation

Submitted in Partial Fulfillment of the
Requirements for the Degree of Doctor rerum naturalium (Dr. rer. nat.)

to the Department of Earth Sciences
of Freie Universität Berlin

by

Florian Ruff

Berlin, September 2023

1st reviewer: Prof. Dr. Stephan Pfahl
2nd reviewer: Prof. Dr. Erich Fischer

Day of disputation: 23rd January 2024

Abstract

Flooding events are one of the most dangerous hazards for society. Central Europe was regularly affected by high-impact river floods within the last few decades, causing high socioeconomic losses. In order to improve flood protection, a detailed understanding of the underlying processes and precise return value estimates of the associated extreme precipitation is from importance, especially when these characteristics change in a warmer climate. For process analysis, past studies have either analysed individual events or systematically studied events with smaller return periods on the order of one year, due to the limited length of observational time series. The main objective of this thesis is, hence, to perform such a systematic analysis of 100-year precipitation events.

In order to improve the understanding of atmospheric processes during extreme precipitation, robust process analyses are performed in this thesis. For this, ensemble simulations are used to generate a large set of daily precipitation events. With this approach, time series can be obtained that are considerably longer than observational time series, resulting in a more systematic assessment of processes (beyond individual events) and in reduced uncertainties of return value estimates. Firstly, ensemble weather prediction (EPS) data from the ECMWF are used to investigate atmospheric processes of realistic 100-year events over central European river catchments and their differences to less extreme events. 100-year events are generally associated with an upper-level cut-off low over central Europe in combination with a surface cyclone southeast of the specific catchment. Differences to less extreme events vary between the catchments, indicating that either dynamic processes (intensified upper-level cut-off low and surface cyclone) or thermodynamic mechanisms (higher lower-tropospheric moisture content) are more relevant. Secondly, 100-year return values of daily precipitation are estimated on a global scale from the EPS data, substantially reducing the uncertainty compared to observational estimates. Despite a general agreement of spatial patterns, the model-generated data set leads to systematically and significantly higher return values in several regions (e.g. the Amazon, western Africa, the Arabian Peninsula). This may point to an underestimation of very extreme precipitation events in observations. Finally, changes of daily 10-year precipitation events (due to the too small sample size for a robust analysis of 100-year events) over central European river catchments are analysed from ensemble climate simulations between the historical and a projected warmer climate. Precipitation extremes are projected to intensify and occur more frequently in spring and autumn. Dynamical changes of these events are often associated with a slight westward shift of the upper-level cut-off low, an intensified ridge over eastern Europe and less pronounced changes near the surface. Thermodynamic changes such as an increased horizontal temperature gradient and higher lower-tropospheric moisture content play an important role as well.

Zusammenfassung

Hochwasserereignisse sind sehr gefährlich für die Gesellschaft. Mitteleuropa wurde in den letzten Jahrzehnten regelmäßig von schweren Überschwemmungen heimgesucht, die hohe sozioökonomische Verluste verursachten. Um den Hochwasserschutz zu verbessern, ist ein detailliertes Verständnis der zugrundeliegenden Prozesse und eine genaue Abschätzung der Wiederkehrwerte der damit verbundenen Extremniederschläge von großer Bedeutung, insbesondere wenn sich diese Charakteristika in einem wärmeren Klima ändern. Für Prozessanalysen wurden in früheren Studien, aufgrund der begrenzten Länge der Beobachtungszeitreihen, entweder einzelne Ereignisse analysiert oder Ereignisse mit geringeren Wiederkehrperioden in der Größenordnung von einem Jahr systematisch untersucht. Das Hauptziel dieser Studie ist daher, eine solche systematische Analyse von 100-jährigen Niederschlagsereignissen durchzuführen.

Um das Verständnis atmosphärischer Prozesse dieser Extrema zu verbessern, werden in dieser Arbeit robuste Prozessanalysen durchgeführt. Dazu werden Ensemblesimulationen verwendet, um einen großen Datensatz täglicher Niederschlagsereignisse zu erzeugen. Mit diesem Ansatz können Zeitreihen erzeugt werden, die deutlich länger sind als Beobachtungen, was zu einer systematischeren Bewertung von Prozessen (über Einzelereignisse hinaus) und zu geringeren Unsicherheiten von Wiederkehrwerten führt. Im ersten Teil werden Ensemble-Wettervorhersagedaten (EPS) des ECMWF verwendet, um atmosphärische Prozesse realistischer 100-jähriger Ereignisse über Mitteleuropa und deren Unterschiede zu schwächeren Extrema zu untersuchen. 100-jährige Ereignisse sind oft mit einem abgegrenzten Höhentief über Mitteleuropa und einer Bodenzyklone südöstlich der Einzugsgebiete verbunden. Die Unterschiede zu schwächeren Extrema variieren zwischen den Einzugsgebieten, in denen entweder dynamische Prozesse (verstärktes Höhentief und Bodenzyklone) oder thermodynamische Mechanismen (höherer Feuchtegehalt) von größerer Bedeutung sind. Im zweiten Teil werden 100-jährige Wiederkehrwerte des täglichen Niederschlags auf globaler Ebene aus den EPS-Daten geschätzt. Die Unsicherheit wird dadurch im Vergleich zu den Beobachtungsschätzungen erheblich verringert. Trotz einer allgemeinen Übereinstimmung der räumlichen Muster werden mit den EPS-Daten in mehreren Regionen (z. B. Amazonas, Westafrika, Arabische Halbinsel) systematisch höhere Wiederkehrwerte geschätzt. Dies könnte darauf hindeuten, dass Extremniederschläge in Beobachtungen unterschätzt werden. Im dritten Teil werden Veränderungen der täglichen 10-jährigen Niederschlagsereignisse (aufgrund zu geringer Stichprobengröße 100-jähriger Ereignisse für eine robuste Analyse) über Mitteleuropa anhand von Ensemble-Klimasimulationen zwischen dem historischen und einem wärmeren Klima analysiert. Die Simulationen zeigen, dass sich Extremniederschläge verstärken und im Frühling und Herbst häufiger auftreten. Dynamische Veränderungen dieser Ereignisse sind oft mit einer leichten westlichen Verschiebung des Tiefs in 500 hPa, einem verstärkten Hochdruckrücken über Osteuropa und weniger ausgeprägten Veränderungen in Bodennähe verbunden. Thermodynamische Veränderungen wie ein verstärkter horizontaler Temperaturgradient und ein höherer atmosphärischer Feuchtegehalt in der unteren Troposphäre spielen ebenfalls eine wichtige Rolle.

Table of Contents

Chapter 1

Introduction to research questions

Within the last few decades, central Europe has regularly been affected by severe flooding events, which resulted in devastating socioeconomic losses. Especially in highly populated areas, flooding events are one of the main natural hazard for society (Hammond et al., 2015; Kreibich et al., 2014; Barredo, 2007). Several hundreds of people lost their life and thousands got injured, regional infrastructure, buildings and properties got destroyed or remained unusable for weeks, while economic losses of several million to billion euros have been accumulated (Korswagen et al., 2022; Munich Re, 2022; Schüttrumpf et al., 2022; Engel, 2004). Some outstanding historical events, just within the current century, are the Rhine flood in June 2021, the inundation over the Berlin metropolitan area in June 2017, the central European flood in June 2013 (see Fig. 1.1a), the Oder flood in May 2010 and the central European flood in August 2002 (see Fig. 1.1b), during which several river catchments (mainly Elbe and Danube) were affected. According to Statista (2022), the Rhine flood in 2021 was worldwide the second most expensive natural hazard in 2021. In Altenahr, which was mainly affected by the flood, peak discharges of up to 1300 m^3/s were measured (Lehmkuhl et al., 2022). The flooding event around Berlin in 2017 was the costliest natural hazard in the Berlin metropolitan area between 2002 and 2017 with accumulated losses of around EUR 60 million, which resulted from extreme precipitation with return periods above 100 years (Caldas-Alvarez et al., 2022) leading to flooded basements and disrupted infrastructure. During the central European flood in 2013, several rain gauges measured record-breaking water levels of about 12.75 m in the German city Passau, bordering the Danube (Merz et al., 2014). Also several other German cities were inundated, such as Deggendorf as shown in Fig. 1.1a. The central European flood in 2002 was even the most expensive natural hazard in central Europe as several billion of euros were accumulated due to damages to public and private properties (Mueller, 2003). This was caused by large inundations of several cities, such as Dresden as shown in Fig. 1.1b, due to extreme precipitation that was expected to occur less than once in a hundred years (Kundzewicz et al., 2005). The historical events have shown that a detailed understanding

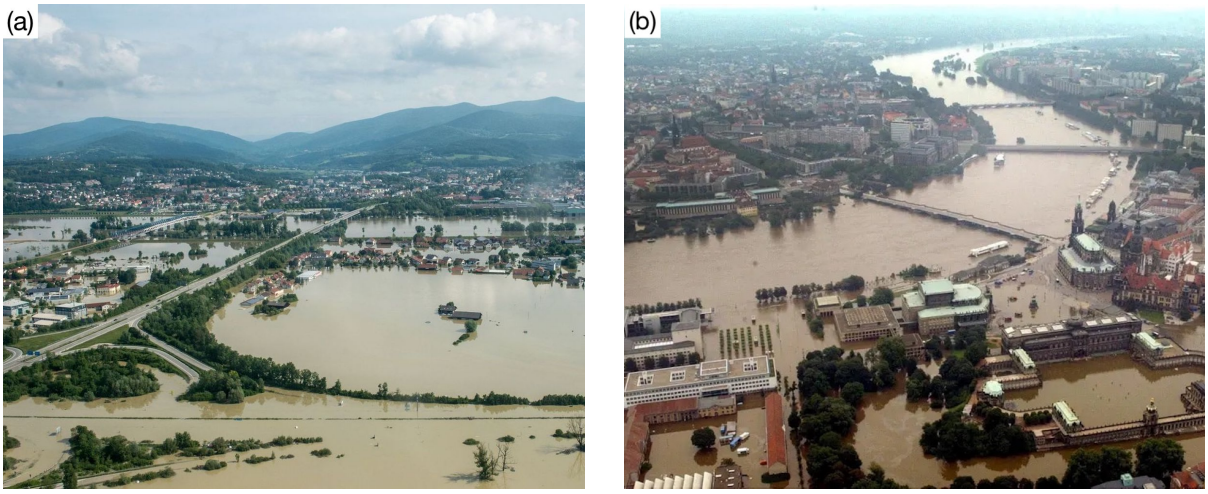

Figure 1.1: Aerial view on the cities **(a)** Deggendorf (Bavaria, Germany) during the central European flood in June 2013 (Weigel, 2017) and **(b)** Dresden (Saxony, Germany) during the central European flood in August 2002 (Kappeler, 2017).

of the underlying processes, that lead to such severe flooding events, are necessary in order to provide precise forecasts and early warnings for the society.

These river floods in central Europe can typically be classified into two types. On the one hand, a flooding event can emerge relatively fast in form of a flash flood. They often occur in smaller rivers and are associated with a very high precipitation intensity, typically caused by heavy convection (thunderstorms) over a spatially limited domain. Relatively quickly, a peak discharge of the specific river is reached (Sene, 2016), which puts the society along the river at risk, even several kilometers away from the extreme precipitation. On the other hand, a flooding event can emerge over several hours and affect the socioeconomic system on a larger scale, often occurring in larger rivers. This thesis focuses on such large-scale flooding events, as they are often associated with a higher risk to society than flash floods. Large-scale flooding events emerge from a slow increase of the river's runoff and water levels and are typically associated with extreme large-scale precipitation over a wider area, which last particularly long with a duration of around one day. In some cases, the extreme precipitation can even impact surrounding river catchments as well. Although the location and intensity of extreme precipitation are not the only factors that influence the occurrence of a flooding event, they are one of the main drivers. Other important factors that affect the severeness of flooding events are hydrological preconditions such as a (almost) saturated soil and a high river runoff prior to the extreme precipitation event (Grams et al., 2014; Bissolli et al., 2011; Engel, 1997). Still, the precise prediction of upcoming extreme precipitation events has the largest impact on preventing socioeconomic losses of the society. Additionally, an accurate representation of statistical features such as return values of extreme precipitation events with certain return periods can also help to improve flood protection systems as estimated precipitation intensities are known in advance.

Several previous studies have investigated extreme precipitation events over central Europe, which are typically associated with a mid-latitude surface cyclone that remains quasi-stationary over central or eastern Europe for one to a few days (Mohr et al., 2023; Caldas-Alvarez et al., 2022; Pfahl, 2014; Blöschl et al., 2013; Bissolli et al., 2011; Ulbrich et al., 2003). An example of such a surface cyclone is presented in Fig. 1.2 (left panel), showing the atmospheric configuration during the extreme precipitation event over the Berlin metropolitan area in June 2017. The origin of the surface cyclone is linked to upper-level Rossby wave breaking and the development of an upper-level trough or cut-off low over western or central Europe, shown in case studies from Caldas-Alvarez et al. (2022), Lehmkuhl et al. (2022), Grams et al. (2011), and Ulbrich et al. (2003). Blöschl et al. (2013) have additionally shown that the stationarity of the upper-level cut-off low can be increased by anticyclones over the North Atlantic and western Russia, which block the low from a fast propagation. With such an upper-level configuration, surface cyclones often move from western Europe around the southern flank of the Alps, or cyclogenesis occurs over the Ligurian Sea, followed by a northeastward movement of the cyclone to central or eastern Europe (Bissolli et al., 2011; Mudelsee et al., 2004; Ulbrich et al., 2003), which is widely known as a "Vb" cyclone track as introduced by van Bebber (1891). However, Grams et al. (2014) showed that the surface cyclone can also originate from eastern Europe as it was the case for the central European flood in 2013. Additionally, the surface cyclone is not necessarily associated with extremely low pressure (Grams et al., 2014; Pfahl, 2014), so that other processes are important as well. All previously mentioned historical extreme events occurred in the summer season, which facilitated the evaporation of moisture into the troposphere prior to the extreme precipitation. Moisture typically evaporates from water sources such as the North Atlantic and Mediterranean Sea (Blöschl et al., 2013; Sodemann et al., 2009; Ulbrich et al., 2003) and from continental regions such as central and eastern Europe (Caldas-Alvarez et al., 2022; Grams et al., 2014; Winschall et al., 2014). Continental areas may also seem to be slightly more relevant for evaporating moisture during the summer season, as more moisture evaporated from eastern Europe than from all water sources before precipitated during the Berlin event in 2017 (see Fig. 1.2, right panel). The surface cyclone facilitates the transport of moisture towards the river catchment, over which air masses regionally ascend shortly before and during the extreme event. Orographic effects of the Alps and other mountainous regions increase the ascent even more (Grams et al., 2014; Szalińska et al., 2014; Ulbrich et al., 2003). These previous studies have mainly focused on single historical events with various return periods. Other studies analysed statistical features of precipitation events with return periods of up to just a few years as in Donat et al. (2013), Sillmann et al. (2013), and Kenyon and Hegerl (2010). However, return periods of extreme precipitation events, possibly triggering a severe flooding event, can range from 10 to even 100 years. Additionally, dynamical drivers may be different between extreme precipitation events of such diverging return periods. A robust analysis of dynamical mechanisms of several 100-year precipitation events over central European river catchments in combination with an analysis of differences to less extreme events has not been performed so far and is investigated

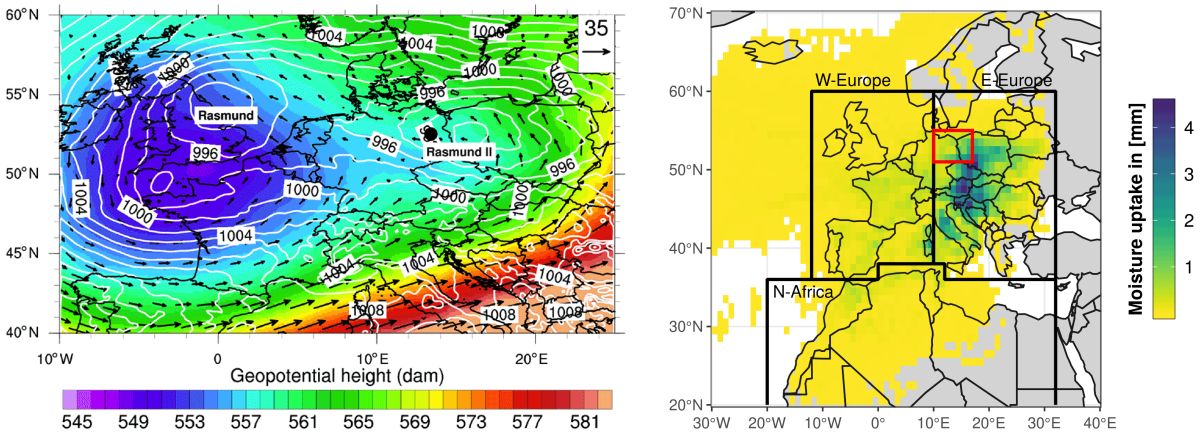

Figure 1.2: Figures 3 (adjusted) and 9 of Caldas-Alvarez et al. (2022), showing the **(left)** geopotential height (colour shading) and wind speed (arrows) at 500 hPa in combination with sea level pressure (contours) and the **(right)** moisture uptake within the planetary boundary layer from Lagrangian backward trajectories, both for the extreme precipitation event over the Berlin metropolitan area in June 2017.

in this thesis as the first research task.

Besides a detailed understanding of the atmospheric processes associated with 100-year precipitation events, long-term prevention of socioeconomic losses from flooding events can be achieved by establishing flood protection systems at vulnerable locations. These systems are usually build to prevent the neighboring areas from high water levels that are associated with precipitation intensities from events of a certain return period. Merz et al. (2014) and Bissolli et al. (2011) already showed that the flood risk management has been improved in the beginning of the 21st century, which helped to prevent large socioeconomic losses for certain areas. Still, there is potential to reduce flood losses in the future (Jongman et al., 2015). Thus, a precise representation of the resulting return values, also called "probable maximum precipitation" in practical water management (World Meteorological Organization, 2009), is needed for appropriate constructions of flood protection systems. Previous studies have evaluated probable maximum precipitation for extreme events with return periods below 100 year and/or just for specific regions or nations (Rodrigues et al., 2020; Donat et al., 2013; Maraun et al., 2011), using extreme value statistics for observational time series. According to Rajulapati et al. (2020), such estimates from observations are affected by certain limitations such as possible spatial inhomogeneities from a combination of rain gauge data (for global coverage) or trends due to, e.g., anthropogenic climate change over the last decades. Alternatively, model simulations from seasonal forecasts or climate models provide long time series, allowing robust estimates of return values of even 100 years (Kelder et al., 2020; Mizuta & Endo, 2020). Still, a robust analysis of return values of daily precipitation with return periods of 100 years on a global scale has not been performed so far and is investigated in this thesis as the second research task.

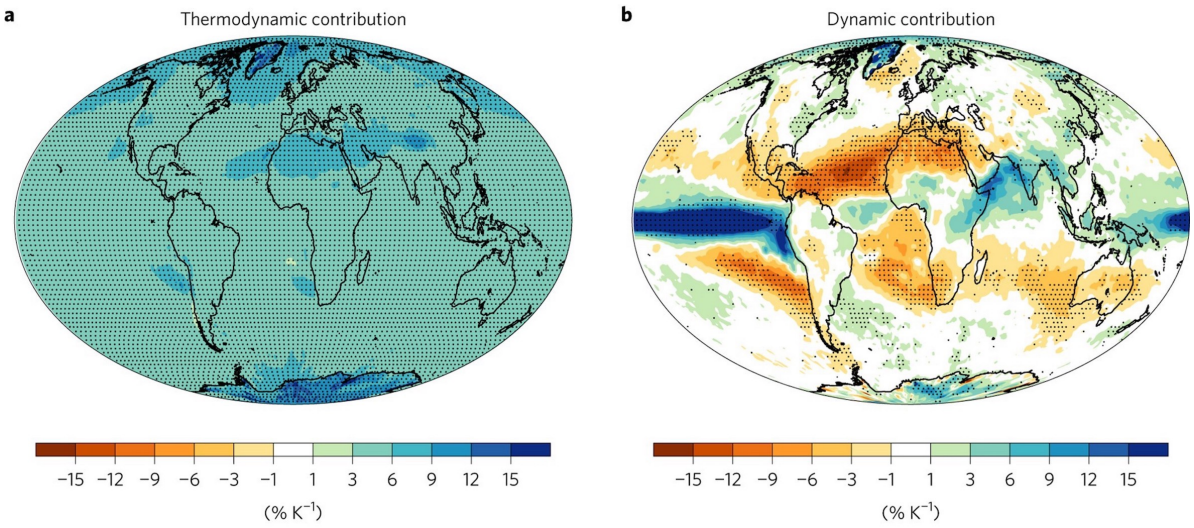

Figure 1.3: Figure 3 (adjusted) of Pfahl et al. (2017), evaluating multi-model mean fractional changes of **(left)** thermodynamic scaling (thermodynamic contribution) and **(right)** the effects of changes in vertical wind (dynamic contribution) to projected future changes in annual maximum daily precipitation.

Within the last several decades, the influence of a changing climate on extreme weather events has increased. Observational data show that the intensity and frequency of extreme precipitation events increased in the last decades (Myhre et al., 2019; Fischer & Knutti, 2014; Madsen et al., 2014). Besides this, the global population increases as well, especially in vulnerable areas, possibly enhancing the risk of flood disasters, even on a global scale (Tellman et al., 2021; Alfieri et al., 2017; Kron, 2015). As the global CO_2 emissions are not supposed to largely decrease within the next few years, the effects of climate change on extreme weather events, especially extreme precipitation, will enhance in the future. Several previous studies have focused on the projected future changes of extreme precipitation until 2100 with the help of climate simulations. They show that the frequency and intensity of extreme precipitation in the mid-latitudes is projected to increase in a warmer climate (Gründemann et al., 2022; Myhre et al., 2019; Ban et al., 2015; Pendergrass & Hartmann, 2014; Fischer et al., 2013; O'Gorman & Schneider, 2009). Such increases are also projected for central Europe (Nissen & Ulbrich, 2017; Madsen et al., 2014; Collins et al., 2013), possibly resulting in an intensity increase of 10-15% for 5-day annual maximum precipitation and 2.5-5.0%/K for 20-year return values (Collins et al., 2013). However, there are rather weak changes in the seasonal mean precipitation over central Europe. According to Tabari (2020) and Alfieri et al. (2015), the frequency of flooding events will, thus, possibly increase as well. In order to analyse the underlying mechanisms, some studies decomposed precipitation changes in a warmer climate into dynamic (atmospheric motion) and thermodynamic (atmospheric moisture content) contributions (Pfahl et al., 2017; Emori & Brown, 2005). On the one hand, thermodynamic contributions would globally lead to a homogeneous increase of the precipitation intensity of about 3-9%/K, as Pfahl et al. (2017) showed from global climate

simulations, which can also be seen in Fig. 1.3 (left panel). At least for the extratropics, this is overall in line with the expected precipitation increase from the Clausius-Clapeyron equation of about 6-7% (Ban et al., 2015; O'Gorman, 2015; Emori & Brown, 2005), as warmer air masses can contain more water vapour that can additionally precipitate. On the other hand, dynamic contributions modify the extreme precipitation on a regional scale (see also Fig. 1.3, right panel) by amplifying or weakening the precipitation increases from the thermodynamic contribution (Tandon et al., 2018; Emori & Brown, 2005). On a regional scale, precipitation changes depend on both dynamic and thermodynamic contributions. The thermodynamic contribution is rather well understood, so that uncertainties in precipitation changes primarily emerge from the dynamic contribution. However, these previous studies mainly focused on events with return periods on the order of one year. A robust analysis of the underlying changes in the atmospheric circulation for high-impact events with multi-annual return periods has not been performed so far, which is investigated in this thesis as the third research task.

Given all the previously mentioned research task, the aim of this thesis is to answer the following questions, which can help to understand the atmospheric mechanisms associated with extreme daily precipitation events in more detail:

1. **What distinguishes 100-year daily precipitation extremes over central European river catchments from more moderate extreme events?**
2. **How reliable are global estimates of 100-year return values of daily precipitation from ensemble weather prediction data in comparison to observational data sets?**
3. **How do very extreme daily precipitation events over central European river catchments change in a warmer climate?**

In order to properly investigate these three research topics on very extreme daily precipitation events, time series of meteorological parameters are needed for the identification and analysis of such extreme events. Observational time series of meteorological parameters typically do not range back longer than the 19th century. However, measurements were taken in different temporal intervals and were available just at specific locations and primarily near the surface. In the 20th century, the development of numerical weather prediction (NWP) models started. Besides typical weather forecasts for a few days in advance, the NWP models also enable realistic representations of historical weather situations by initialising the models with historical measurements of meteorological parameters and by assimilating these measurements on a regular basis. The resulting product is called reanalysis and, thus, provides information for several meteorological parameters at various altitudes with a high spatial and temporal resolution, compared to observational records. Given that, time series with a length of several decades up to about 100

years can be obtained. Although such time series would be long enough for a robust analysis of extreme events with return periods on the order of 10 years, more intense, e.g. 100-year, events can not be robustly analysed. Additionally, data before the 1950s are less reliable as just a few surface observations were typically assimilated. The time series obtained from reanalysis data are, thus, still too short.

Reanalysis data typically just represent one realistic state of the atmosphere. However, neither observational records nor NWP models can perfectly represent the reality. Slightly changed observational data can result in totally different atmospheric situations, simulated by the models. Alternative atmospheric conditions, that potentially could have occurred with a similar probability, are not provided by reanalysis data. Weather forecasts from NWP, however, partly rely on ensemble predictions in order to evaluate uncertainties of the weather forecasts. Ensemble predictions produce individually developed atmospheric situations for typically the next several days. This is performed by initialising the NWP model with (slightly changed) observational data and by randomly perturbing some uncertain processes during the model runs (stochastic physics). The larger the number of ensemble members, the more atmospheric situations can be simulated. One of the most commonly used systems is the ensemble prediction system (EPS) from the European Centre for Medium-Range Weather Forecasts (ECMWF), at which ensemble predictions are performed with their operational weather prediction model. The EPS has been applied in several previous studies. E.g., Osinski et al. (2016) tracked European wind storms and identified storm characteristics such as severity, size and duration, Magnusson et al. (2014) evaluated the EPS forecasts on the basis of Hurricane Sandy over the U.S. East Coast in October 2012, while Breivik et al. (2013) estimated return values of significant wave height over the northeast Atlantic, the Norwegian Sea and the North Sea.

Typically, the differences between the individual realisations of the ensemble prediction increase with longer forecast times. The forecast skill of the NWP of the ECMWF has been steadily improved over the last years due to improvements in the forecast models, in the data assimilation and due to a larger amount of observations (Magnusson & Källén, 2013). However, the forecast times has been extended as well so that ensemble predictions at the highest lead times still simulate a large variety of realistic weather situations with only minor predictability left from the initial conditions. Such realisations of weather situations can be evaluated as a large climatological data set, which was already performed by Magnusson et al. (2014) and Breivik et al. (2013). The advantage of using the EPS data as a climatological data set in particular is the large reduction of uncertainties of either the identified storm characteristics in Osinski et al. (2016) or the estimated 100-year return values of significant wave height in Breivik et al. (2013). As this thesis tries to better understand the atmospheric drivers of very extreme precipitation events in a robust way by answering the three research questions mentioned above, the approach of Breivik et al. (2013) on identifying extreme events from a large climatological data set, based on ensemble prediction data at high lead times from the ECMWF, is applied.

Using the EPS data as a large climatological data set is based on a few assumptions. Firstly, the daily precipitation fields must not significantly correlate with the initial conditions, especially the extreme precipitation events. For daily precipitation at high lead times of e.g. 10 days, this criteria is met as precipitation is highly variable in space and time. Secondly, the precipitation fields between the individual ensemble members have to be considered as independent and identically distributed. Thirdly, the precipitation intensity distributions between the EPS data and observational data sets have to be as similar as possible. And finally, no significant trend in the occurrence of extreme precipitation events must be found. All these assumptions are statistically evaluated before the analyses and for each chapter, adapted to the respective data set. Such an approach can, in a similar way, also be applied to ensemble simulations from a global climate model, which is presented in Ch. 4 for the investigation of the third research question.

In Ch. 2, the first research question is discussed by investigating the atmospheric drivers of 100-year precipitation events over central European river catchments and their differences to more moderate extreme precipitation events, using EPS data from the ECMWF as a large climatological data base. The second research question is examined in Ch. 3 by evaluating global estimates of 100-year return values of daily precipitation and their uncertainties on the estimates from the EPS data with three quasi-global observational data sets. This is followed by Ch. 4, in which atmospheric characteristics of 10-year daily precipitation events over central European river catchments between the historical and a warmer climate from ensemble simulations of a global climate model are analysed. For this research task, the return period of extreme precipitation events is reduced from 100 to 10 years as the climatological data base from ensemble climate simulations is not large enough in order to robustly analyse climatological changes of 100-year precipitation events. Finally, an overarching conclusion and discussion about the most important findings and limitations of this thesis, including a short outlook for future studies, is presented in Ch. 5.

The presented work in Ch. 2 is published as a research article (highlight paper) in the peer-review journal *Weather and Climate Dynamics*, while the presented work in Ch. 3 is submitted in the peer-review journal *Natural Hazards and Earth System Sciences*. The work in Ch. 2 and Ch. 3 are both distributed under the terms of the Creative Commons Attribution 4.0 License. In both papers, I designed the study, performed the analysis, produced the figures as well as drafted and edited the manuscript. The references are as follows.

Ruff, F. and Pfahl, S.: What distinguishes 100-year precipitation extremes over central European river catchments from more moderate extreme events?, Weather Clim. Dynam., 4, 427–447, `https://doi.org/10.5194/wcd-4-427-2023`**, 2023.**

Ruff, F. and Pfahl, S.: Global estimates of 100-year return values of daily precipitation from ensemble weather prediction data, EGUsphere [preprint], `https://doi.org/10.5194/egusphere-2023-2057`**, 2023.**

Some additional work is done, which is not discussed in this thesis. There, I performed a moisture uptake analysis over Europe within the planetary boundary layer from Lagrangian backward trajectories for the extreme precipitation event over the Berlin metropolitan area in June 2017, produced the associated figure (see right panel of Fig. 1.2) and drafted and edited the corresponding manuscript section. This additional work is part of the following research article, which is published in the peer-review journal *Natural Hazards and Earth System Sciences*.

Caldas-Alvarez, A., Augenstein, M., Ayzel, G., Barfus, K., Cherian, R., Dillenardt, L., Fauer, F., Feldmann, H., Heistermann, M., Karwat, A., Kaspar, F., Kreibich, H., Lucio-Eceiza, E. E., Meredith, E. P., Mohr, S., Niermann, D., Pfahl, S., Ruff, F., Rust, H. W., Schoppa, L., Schwitalla, T., Steidl, S., Thieken, A. H., Tradowsky, J. S., Wulfmeyer, V., and Quaas, J.: Meteorological, impact and climate perspectives of the 29 June 2017 heavy precipitation event in the Berlin metropolitan area, Nat. Hazards Earth Syst. Sci., 22, 3701–3724, `https://doi.org/10.5194/nhess-22-3701-2022`**, 2022.**

Chapter 2

What distinguishes 100-year precipitation extremes over central European river catchments from more moderate extreme events?

2.1 Introduction

Flooding events in highly populated areas are one of the main natural hazards for modern society (Hammond et al., 2015; Kreibich et al., 2014; Barredo, 2007). Central Europe has regularly been affected by substantial flooding events in the last few decades in several river catchments due to extreme precipitation events. Remarkable flooding events were the Rhine floods in June 2021 and in December 1993, the Oder floods in May 2010 and in July and August 1997, and the flooding events in central Europe in June 2013 and in August 2002. During the two latter events, several catchments, but mainly the Danube and Elbe, were affected. Such an impact on several river catchments often occurs with spatially very extended extreme precipitation events. Many of the flood events had devastating impacts such as several to hundreds of human life losses, thousands of evacuations and economic losses of several million to billion euros (Munich Re, 2022; Engel, 2004; Munich Re, 1999). The central European flood in August 2002 was the most expensive natural hazard for central Europe, caused accumulated costs of about EUR 15 billion for both public and private properties and even impacted business interruptions after the event (Mueller, 2003), while the Rhine flood in June 2021 was globally the second most expensive natural hazard in 2021 (Statista, 2022). These damages were associated with high water levels, partly even the highest water levels on record. For instance, during the central European flood in June 2013,

several gauges measured record water levels including in the German city Passau (at the Danube) where the highest water levels of about 12.75 m were recorded since 1501 (Merz et al., 2014). However, several improvements in flood risk management implemented in the beginning of the 21st century following the floods at the end of the 20th century prevented some areas from socioeconomic losses to a large extent (Merz et al., 2014; Bissolli et al., 2011). Nevertheless, as losses can never be totally eliminated, it is important to gain more knowledge about the atmospheric triggering mechanisms that induce such extreme floods to improve forecasts of these events and warn the public at an early stage. Additionally, flooding events can become even more relevant in the future as climate simulations show a higher frequency of extreme precipitation events in the mid-latitudes in a warmer climate (Pendergrass & Hartmann, 2014; Fischer et al., 2013; O'Gorman & Schneider, 2009).

Central European flooding is typically associated with large-scale extreme precipitation events over a river catchment, which are linked to mid-latitude cyclones that become quasi-stationary over central or eastern Europe for a few days as described in Grams et al. (2014), Pfahl (2014), Blöschl et al. (2013), Bissolli et al. (2011), and Ulbrich et al. (2003). In case studies, Grams et al. (2014) and Ulbrich et al. (2003) found that the origin of such a circulation anomaly was linked to upper-level Rossby wave breaking and the formation of an upper-level cut-off low over western Europe. The stationarity of such a cut-off low can be facilitated by a blocking anticyclone over the North Atlantic, sometimes in combination with a blocking over western Russia as shown by Blöschl et al. (2013). Such an upper-tropospheric configuration is often associated with either a surface cyclone moving from western Europe southeastwards around the southern flanks of the Alps or with cyclogenesis over the Ligurian Sea, followed by a northeastward track of the surface cyclone towards central or eastern Europe (Bissolli et al., 2011; Mudelsee et al., 2004; Ulbrich et al., 2003). Such cyclone tracks are typically known as a "Vb" weather type (van Bebber, 1891). However, the central European flood in June 2013 was triggered by surface cyclones that formed over eastern Europe but moved towards central Europe as well (Grams et al., 2014). Although a surface cyclone is often of high relevance for producing extreme precipitation, it is not necessary that this cyclone is associated with extremely low pressure (Pfahl & Wernli, 2012). This was also shown by Grams et al. (2014), as the surface cyclones during the central European flood in June 2013 were rather shallow with minimum pressure between 995 hPa and 1000 hPa. Hence, other important processes such as the transport of atmospheric moisture and the quasi-stationarity of the weather pattern have to be taken into account.

Surface cyclones can facilitate the transport of atmospheric moisture in the lower troposphere towards a certain area. For extreme flooding events, typically several moisture sources are important. On the one hand, moisture can evaporate into the atmosphere from the North Atlantic as well as from the Mediterranean (Blöschl et al., 2013; Sodemann et al., 2009; Ulbrich et al., 2003). On the other hand, a high amount of moisture evaporates over continental areas such as central and eastern Europe along the tracks of cyclones (Grams et al., 2014; Winschall

et al., 2014). Especially during the northward movement of Vb cyclones towards central or central eastern Europe, continental moisture sources become more dominant (Winschall et al., 2014; James et al., 2004). Regional ascent of these moist air masses occurs shortly before and during the extreme precipitation events over the specific river catchment. The orographic effects of the Alps and other mountainous areas additionally play an important role in the location of the extreme precipitation as was the case in several of the extreme flooding events (Grams et al., 2014; Szalińska et al., 2014; Blöschl et al., 2013; Ulbrich et al., 2003).

However, just the occurrence of an extreme precipitation event does not necessarily trigger a major flood event. Besides the precipitation intensity, the time period over which precipitation accumulates is an important factor. While short-term extreme precipitation often triggers flash floods, precipitation accumulated over at least several hours up to a few days is more likely to cause large flooding events. As the case studies cited above show, hydrological preconditions such as (almost) saturated soil and a high river runoff already prior to the event are also important prerequisites for the development of a flooding. Such conditions are often the result of the accumulation of precipitation during the days or weeks before the extreme flooding (Grams et al., 2014; Merz et al., 2014; Bissolli et al., 2011; Engel, 1997).

In most previous studies, detailed analyses of the atmospheric dynamics of historical extreme precipitation events associated with central European flooding have been done in case studies. Some of these studies have compared their results with a few other floods in the same river catchment. However, due to the shortage of the observational record it is difficult to determine the return value of the most severe historical floods, and there are too few events to systematically investigate the generic atmospheric processes leading to such events. Today's knowledge about the mechanisms of such extreme events is, therefore, based on analyses of single events as well as on statistical investigations of more moderate precipitation events with return periods on the order of one up to a few years (Donat et al., 2013; Sillmann et al., 2013; Pfahl & Wernli, 2012; Kenyon & Hegerl, 2010). Higher return values are typically estimated based on extreme value theory such as in Maraun et al. (2011). Still, the length of observational time series plays an important role in the precision of such statistical estimates as well. Additionally, a detailed analysis of the underlying meteorological processes is complicated, as the extreme events are usually not explicitly identified in such statistical assessments. Kelder et al. (2020) recently showed that a large ensemble simulation approach can yield novel insights into more extreme events and their changes during the last few decades. They investigated 3-day precipitation extremes with return periods of up to 100 years in Norway and showed that a 100-year precipitation event in 1981 is equivalent to a 40-year event in 2015. Nevertheless, there is still a systematic lack of knowledge on the mechanisms leading to very extreme precipitation events with return periods on the order of 100 years. It is also unclear how these mechanisms of 100-year events distinguish from more moderate extreme precipitation events. These knowledge gaps are addressed in the present study.

This study focuses on the dynamical mechanisms behind very extreme large-scale precipitation events with a return period of 100 years in five major central European river catchments, which have the potential to cause devastating flooding events. In order to robustly analyse these mechanisms, data from operational ensemble weather prediction simulations are used to generate a large set of multiple realisations of possible weather situations for a quasi-stationary climate following Breivik et al. (2013). This set of multiple possible realisations has an equivalent length of 1200 years and, hence, is several times longer than conventional observational time series. Several extreme precipitation events with return periods of at least 100 years are identified in this data set with the help of extreme value theory. Estimates of such extreme return values from observational time series are compared with the ensemble prediction data to evaluate the realistic representation of extreme precipitation magnitudes. The atmospheric processes associated with the 100-year events are then systematically analysed. In a second step, the results are compared to the conditions during more moderate extreme precipitation events.

Section 2.2 describes the ensemble prediction data set that is used for the identification and meteorological analysis of 100-year precipitation events. In addition, three observational data sets are introduced that are used for verification. All methodological aspects regarding the processing of ensemble data and further statistical methods are explained in Sect. 2.3. In Sect. 2.4, both the atmospheric processes associated with 100-year events and the differences to less extreme precipitation events as well as an analysis of tracks, frequencies and intensities of objectively identified surface cyclones during the extreme events are presented. Finally, conclusions and a discussion of the most important findings are provided in Sect. 2.5.

2.2 Data

For this study, a large data set of daily precipitation events is constructed from operational ensemble weather prediction data. Additional observational data are used to evaluate this model-based data set. All these data sets are described in the following.

2.2.1 Ensemble prediction data

The archive of the operational weather prediction model of the Integrated Forecasting System (IFS), provided by the European Centre for Medium-Range Weather Forecasts (ECMWF), is used to get a large set of simulated but realistic daily weather and precipitation events from their ensemble prediction system (EPS). The workflow of the EPS is described in more detail in Molteni et al. (1996). The IFS is a comprehensive earth system model, combining the atmospheric model of ECMWF with community models for other components of the earth system and a data assimilation system (ECMWF, 2023e). It is used for all forecasting activities of ECMWF.

The full documentation of the model and the assimilation system can be found in ECMWF (2023c). Using an operational weather model ensemble instead of a single climate model initial-condition large ensemble (SMILE) has the advantage that the data are available with a higher spatial resolution and that the weather model is very well calibrated due to extensive comparison with observations on a daily basis, even though surface precipitation observations are not assimilated. On the contrary, the weather prediction ensemble may suffer from temporal inhomogeneities and interdependence between ensemble members, which is not the case for SMILEs. Although SMILEs can be used in a similar manner to obtain large sample sizes, the approach of using weather prediction ensemble data for extreme event analyses is still studied little. The interdependence between ensemble members is investigated in Sect. 2.3.2, while temporal inhomogeneities as well as additional limitations of the approach are discussed in more detail in Sect. 2.5.

Every day, ensemble simulations are started with lead times of at least 10 days and 51 ensemble members. One member represents the control run with no perturbed initial conditions, while the other 50 members represent perturbed runs with slightly changed initial conditions between each ensemble member and additional stochastic perturbations introduced during the model integration. Since 25th of March 2003, these ensemble simulations have been operated two times a day, starting at 00:00 and 12:00 UTC. The combination of 51 ensemble members and two daily initialisations results in 102 simulations per real day. The basis for this study is daily precipitation sums from these forecasts computed by adding up the large-scale and convective precipitation over 24 hour time periods contiguously.

Instead of the daily precipitation sums for all 10 days of each simulation, just the 10th day of each simulation (accumulated precipitation between forecast hour 216 and forecast hour 240, resulting in a 24-hour time period each) is used in this study, following Breivik et al. (2013). They used a large data set from ensemble simulations to estimate return values of wave heights over the oceans. To this end, Breivik et al. (2013) assumed that the weather conditions, and especially the wave heights, of the 10th day of each simulation are independent between the different ensemble members due to the advanced lead time. During the first days, the simulations of the different members are correlated due to a strong dependency on the initial conditions, but this correlation weakens when the forecasts advance in time. Breivik et al. (2013) also performed several statistical evaluations to demonstrate this independence on the 10th forecast day and to evaluate the statistics of the simulated wave heights in comparison to observations. Also for the daily precipitation events investigated in this study, due to the high spatial and temporal variability of precipitation, it is assumed that the weather conditions of each 10th simulation day do not strongly correlate with the initial conditions of the simulations and the daily precipitation events can thus be regarded as independent realisations. Following Breivik et al. (2013), this assumption is evaluated statistically as described in Sect. 2.3.2.

There were several IFS model updates between the years 2003 and 2019 that may influence the modelled precipitation amounts as well as the forecast skill at advanced lead times and, thus, the results of the analyses of this study. A collection of all changes (from Cycle 25r1, implemented before 1st January 2003, to Cycle 46r1, last implemented cycle before 31th December 2019) can be found in ECMWF (2023d), while the full documentation (incl. data assimilation, dynamical processes and parameterisation) of all the individual IFS model cycles is provided in ECMWF (2023c). Typically, several small changes/improvements were implemented in each new model cycle, and precipitation forecasts were slightly improved over several years, but no notable large improvement can be identified for a specific model cycle. Noteworthy updates have been a new formulation of the humidity analysis (Cycle 26r1), a new moist boundary layer scheme (Cycle 29r1), improved precipitation forecasts over Europe due to several technical changes such as bias corrections and assimilation improvements (Cycle 32r3), changes in the cloud scheme (Cycle 41r1), and improvements in near-coastal precipitation forecasts due to changes in cloud physics (Cycle 45r1) as well as several changes in the data assimilation and other technical improvements. In order to evaluate the effect of these updates on the data set, the temporal distribution of extreme precipitation events, including possible trends, over the years is studied in Sect. 2.3.3.

The first tests showed that very high percentiles (99th, 99.9th and 99.99th), which represent the most extreme precipitation events of this daily data set, are systematically higher for the first years of the ensemble prediction data (see Supplementary Fig. A.1 for the Danube catchment). Since 2008, the data have shown a more consistent amplitude of these different percentiles, comparable to the observational data sets (not shown). Hence, to exclude any possible inconsistencies due to the temporal inhomogeneity of the data, just the ensemble prediction data from 1st of January 2008 until 31th December 2019 are used in the following. No trend can be detected in the percentiles shown in Supplementary Fig. A.1 during this restricted period according to the Mann-Kendall test (95% confidence level), except for the 99.9th percentile in the Weser and Ems and Elbe catchments. The combination of 102 different simulated precipitation events per real day and 12 years of simulations from the archive of the EPS leads to an overall data set of 1224 years of simulated but realistic daily precipitation events. The data cover the entire globe and are available on a regular lat–long grid, whose resolution changes over time due to updates of the model system. Since these precipitation data are further used to compute daily precipitation sums for large central European river catchments (see Sect. 2.3), they are first interpolated on a relatively coarse grid of 1°x 1°.

To study the atmospheric conditions during and before the most extreme daily precipitation events, several additional meteorological parameters are extracted from simulations that included an extreme precipitation event (as defined below) and used for composite and single-event analyses during and up to 4 d ahead of the events. All parameters are available every 6 h from forecast hour 120 (4 d before the event occurred) until forecast hour 240 (the end of the event) on a regular lat–long grid with a spatial resolution of 0.1°x 0.1°. These data cover a large European

region, ranging from 25° to 75°N and from 30°W to 45°E.

2.2.2 Observational data sets

Three observational precipitation data sets (Rainfall Estimates on a Gridded Network (REGEN); Hydrometeorologische Rasterdaten (HYRAS); and ENSEMBLES daily gridded observational data set for precipitation, temperature and sea level pressure in Europe (E-OBS)) are used to evaluate the precipitation climatologies obtained from the ensemble simulations. These data sets are all based on station observations and mainly differ in their spatial resolution, region of coverage and method used for the interpolation of available station data to a regular spatial grid.

REGEN data

The REGEN data set (Contractor et al., 2020a) is an observational precipitation data set covering global land areas. It is based on the spatial interpolation of in situ surface precipitation measurements from several large observational archives, such as the Global Historical Climatology Network daily, hosted by the National Oceanic and Atmospheric Administration, and the Global Precipitation Climatology Centre, hosted by Deutscher Wetterdienst (DWD). All observed precipitation time series are quality-controlled before interpolation. The station density differs strongly between specific regions and continents. Africa and central Asia have a low density of stations, while many parts of North America, Australia and especially Europe have a high density. Besides daily precipitation sums, this data set provides parameters like the standard deviation of these precipitation sums as well as the number of rain gauges within each grid box. For this study, just the daily precipitation sums of Version 1-2019 based on around 135.000 stations are used for further investigations. These data are available on a regular lat–long grid for all global land areas with a spatial resolution of 1°x 1° from 1st of January 1950 until 31th of December 2016.

HYRAS data

The HYRAS data set represents a climatology of daily precipitation sums for Germany and river catchments of major rivers in neighbouring countries, provided by the DWD. This data set is based on thousands of in situ observations. The number of stations increases over time, and the station density differs between countries and is much higher in Germany and the Netherlands compared to parts of e.g. Poland and France. All these observational station data were quality-controlled by the DWD and were interpolated to a Lambert conformal conic projection by using the REGNIE (Regionalisierte Niederschläge) method, which is described in more detail in Rauthe et al. (2013a). Here, these data are interpolated again on a regular lat–long grid with a spatial resolution of 0.05°x 0.05°. They are available from 1st of January 1951 until 31th December

2015 and cover an area of Germany and adjacent river catchments ranging from about 45.10° to 55.65°N and 1.85° to 20.80°E.

E-OBS data

The E-OBS data set is an ongoing observational data set for European land areas, provided by the European Climate Assessment & Dataset (ECAD) initiative. This data set combines observational data from a large set of stations across several countries, provided by National Meteorological Services, in an ensemble approach with 100 ensemble members for several meteorological parameters such as temperature and precipitation, as described in Cornes et al. (2018a). The observational data are quality-controlled, both by each national meteorological service and by the ECAD itself. As for the other data sets, the temporal and especially the spatial availability of station data differs, especially across national borders, with higher densities in central and northern Europe. Through the ensemble simulations, the uncertainties of the interpolation of the data to a regular grid are reduced. For this study, just the daily precipitation sums are used. Based on E-OBS version 21.0e, these precipitation data are available on a regular lat–long grid with a spatial resolution of 0.1°x 0.1° from 1st of January 1950 until 31th of December 2019 and cover a large European region, ranging from 25.0° to 71.5°N and 25.0°W to 45.5°E.

2.3 Methodology

In this section, the methodology to identify and analyse extreme precipitation events in ensemble prediction data is described, starting with the catchment definitions of the selected rivers, followed by the statistical evaluation of the suitability of the ensemble data. Afterwards, the determination of the extreme events is introduced as well as the composite analysis and cyclone identification and tracking method that are used for characterising the underlying atmospheric processes.

For simplicity, all figures and analyses in Sect. 2.3.2 are only shown for the Danube catchment as representative of all catchments. In the case that results for other catchments differ substantially from those of the Danube catchment, this is mentioned in the text.

2.3.1 River catchments

Five major central European river catchments are considered in this study. Four river catchments represent the rivers Rhine, Elbe, Oder and the upper (most western) part of the Danube, while the fifth catchment covers the region of the two rivers Weser and Ems in northern Germany, here denoted as Weser/Ems. As explained in Sect. 2.1, flooding events in the past have shown that

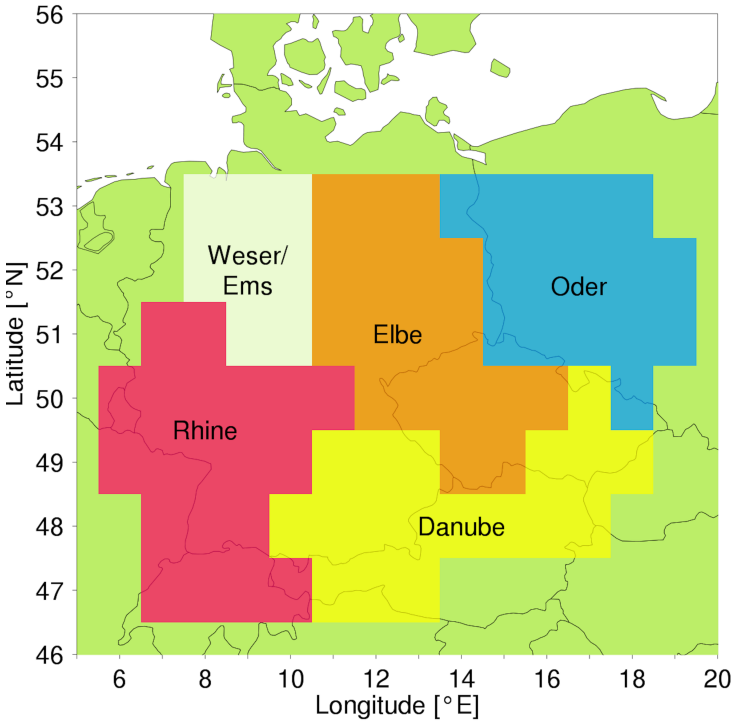

Figure 2.1: River catchments of the rivers Rhine; Elbe; Oder; Danube; and the combination of the rivers Weser and Ems, denoted Weser/Ems, based on a 1°x 1° lat–long grid over central Europe.

all these regions are affected by risks of flooding and associated socioeconomic impacts during extreme precipitation events.

The spatial coverage of these selected river catchments as adopted in this study is shown in Fig. 2.1. The spatial resolution of 1°x 1° is due to the resolution of the daily precipitation data of the ensemble prediction data (see Sect. 2.2.1). Each grid point has been allocated to one of the five river catchments based on a river basin map by the Waterways and Shipping Administration of Germany (Wasserstraßen- und Schifffahrtsverwaltung des Bundes, 2022). Due to the relatively coarse resolution, this does not exactly reproduce the river catchments but still provides a clear separation of the larger-scale precipitation patterns potentially associated with flooding in the different catchments.

Precipitation time series for each river catchment are constructed by averaging the time series from the associated 1°x 1° grid boxes, both from the ensemble predictions and observational data sets. Only for the comparison with HYRAS data is the methodology slightly adapted because HYRAS does not cover the entire catchments shown in Fig. 2.1. Therefore, only 1°x 1° boxes with a HYRAS data coverage of at least 90% are considered for the comparison of simulated precipitation with the HYRAS observations.

2.3.2 Statistical evaluation of the ensemble prediction data

In order to evaluate the suitability of the precipitation data set obtained from the ensemble weather prediction database for the analysis of extreme precipitation events, several statistical properties of the data are considered following Breivik et al. (2013). The following statistical evaluations cover the independence of events between ensemble members, as well as within a specific member, and a comparison of the statistical distributions of daily precipitation between the members, as well as with observational data. For these analyses, the 10th day (last 24 hours) of each ensemble forecast is taken into account, independent of the initialisation time. For each 24-hour period, the precipitation is spatially averaged over all grid points within the respective catchment to produce daily time series for each catchment and ensemble member. Figure 2.2 shows the results of the statistical evaluation exemplarily for the Danube catchment.

A basic assumption in the application of the ensemble prediction data set as a climatological data basis for the following analysis is that the precipitation accumulated over the 10th forecast day is independent between the ensemble members. To statistically evaluate this independence, Fig. 2.2a shows the statistical distribution of Spearman correlation coefficients between all possible combinations of ensemble members (5151 in total), in which low (high) correlations show a higher (lower) independence between ensemble members. The correlations are computed between time series as mentioned in the previous paragraph. The left boxplot represents the correlations between the entire daily time series of two ensemble members with a total length of 12 years. These correlation coefficients vary between 0.12 to 0.32, with a mean correlation of about 0.19. All correlations are statistically significant, which is also due to the long time series. Physically such relative small correlations between the precipitation time series may arise from low-frequency (longer than 10 days) variability in the climate system, which affects all ensemble members from the same initialisation date in a similar manner. However, in order to estimate 100-year return values and identify 100-year precipitation events, in this study not the entire time series but only the annual maxima of daily precipitation is used (block maximum approach, see Sect. 2.3.3). Therefore, the right boxplot in Fig. 2.2a indicates the distribution of correlation coefficients between such annual maximum values (12 values for each ensemble member). Most of the correlation coefficients are around 0 (mean correlation of 0.04), but there is a huge spread between -0.90 and +0.85. In order to estimate the statistical significance in such a situation of multiple correlation coefficients, the false discovery rate (FDR) test of Benjamini and Hochberg (1995) is applied, as described in Ventura et al. (2004), to the entire sample of p values associated with the individual correlation coefficients from the various combinations of ensemble members. According to this FDR test, only 1 out of the 5151 correlation coefficients for the Danube catchment can be considered significant, and this number of significant correlations varies between zero and two for the other catchments. These very low numbers of significant correlation coefficients, together with the relatively small correlations of the entire time series, justify the assumption of independence, in particular when considering extreme (such as annual

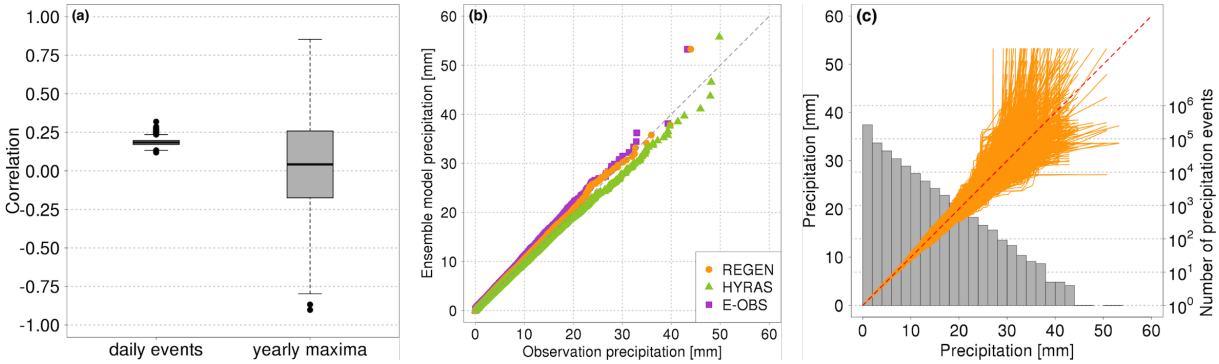

Figure 2.2: Statistical evaluation of daily precipitation data obtained from ensemble weather predictions for the Danube catchment. **(a)** Distribution of Spearman correlation coefficients between (left) daily precipitation time series and (right) annual maximum daily precipitation values for every combination of ensemble members (5151 in total). The box is bordered by the 25th and 75th percentile, while the whiskers extend to the most outer point, which is not more than 1.5 times the interquartile range from the box. **(b)** Quantile–quantile plot of daily precipitation from the ensemble weather prediction data (vertical axis) and three observational data sets (REGEN, HYRAS and E-OBS; horizontal axis). Differences in simulated precipitation for HYRAS observations are due to the reduced area with HYRAS coverage (only grid points with at least 90% HYRAS coverage are taken into account). **(c)** Quantile–quantile plot of daily precipitation from every ensemble member combination (5151 in total). Grey bars indicate the intensity distribution from the entire ensemble prediction data set.

maximum) daily precipitation events.

A second important criterion for the applicability of the ensemble weather prediction data to analyse extreme precipitation events is a realistic representation of observed precipitation statistics. This is evaluated by comparing quantiles from the statistical distributions of daily precipitation between the ensemble data (taking all members together) and three observational data sets (REGEN, HYRAS and E-OBS) in quantile-quantile plots (Q–Q plots), as shown in Fig. 2.2b. A perfect match of the distributions would be indicated by quantiles falling on the diagonal. This is the case for precipitation intensities below about 20 mm, which occur most frequently (see Fig. 2.2c). In this range, the distributions of daily precipitation from the ensemble data and the three observational data sets are thus almost equal. For higher intensities, there are some differences between the quantiles, with the ensemble data overestimating the higher quantiles compared to E-OBS data but underestimating them in comparison to HYRAS. The deviations from the diagonal are mostly smaller in other catchment areas (see Supplementary Fig. A.2), which may be related to the relatively complex topography of the Danube catchments and the limited spatial resolution of both model and observational data. All together, this analysis shows that the ensemble weather prediction data set represents the statistical distribution of daily precipitation reasonably well and lies within the observational uncertainties (differences between the observational data sets) even for high quantiles corresponding to extreme precipitation events.

Finally, the statistical distributions of daily precipitation are also compared between the individual ensemble members. Figure 2.2c shows the Q–Q plots for every possible combination of ensemble members (5151 in total), each one as an orange line. The grey bars show the precipitation distribution of all daily events from all ensemble members. All Q–Q plots show nearly identical distributions for all members and low precipitation intensities (20 mm and lower). For higher precipitation intensities, the Q–Q plots start to diverge. Such a divergence is expected since the time series are 12 years long and a daily precipitation event of 30 mm roughly corresponds to a 10-year event. Random fluctuations in the occurrence of such rare events can thus lead to large differences in the higher quantiles between the members.

In conclusion, the analyses in this section have shown that the ECMWF ensemble prediction system produces realistic statistical distributions of daily precipitation in the selected catchments (see Fig. 2.2b) throughout each ensemble member (see Fig. 2.2c) and that extreme precipitation events obtained from the ensemble prediction data set can be considered statistically independent, as the correlations between precipitation time series from different ensemble members are small, and (almost) no significant correlations are obtained between extreme precipitation events in different members (see Fig. 2.2a). The data set is thus considered to be suitable for a systematic analysis of very extreme, 100-year precipitation events.

2.3.3 Determination of extreme precipitation events

Building on the statistical evaluation presented in Sect. 2.3.2, the daily precipitation data from all ensemble members are now pooled together. To determine return values corresponding to 100-year (and also 20- and 50-year) return periods and select the corresponding precipitation events, the block maximum approach from extreme value statistics is applied (see Coles et al., 2001). A yearly period is selected to determine block maxima, resulting in 1224 block maxima in total. Such a yearly block size is large enough to fulfil the Fisher-Tippett theorem, such that a generalised extreme value distribution (GEV) can be fitted to the block maxima by the maximum likelihood approach. Three parameters, the location (μ), scale (σ) and shape (ξ), are estimated to obtain the best fit of the extreme value distribution, as can be seen in Supplementary Fig. A.3 for the Danube catchment. From these three parameters, the return value v can be computed by the following equation:

$$\begin{aligned} v &= \mu + \sigma \cdot \frac{(x^{\xi} - 1)}{\xi} \\ x &= \frac{-1}{log(1 - \frac{1}{p})} \end{aligned} \tag{2.1}$$

where a specific return period in years is denoted by p following Stephenson (2002). Confidence

Catchments	Return values (mm)	Confidence intervals (mm)	
Rhine	34.49	33.28	35.84
Weser/Ems	42.56	39.80	45.32
Elbe	36.62	34.78	38.75
Oder	38.58	36.87	40.50
Danube	40.21	38.65	41.92

Table 2.1: Return values and confidence intervals for 100-year daily precipitation events in different river catchments, obtained from the procedure in Sect. 2.3.3.

intervals of the return value are obtained from bootstrap resampling (see Coles et al., 2001). A new set of block maxima is drawn with replacement from the original set, and the return value is again obtained from a GEV fit and Eq. (2.1). This procedure is repeated 1000 times, leading to 1000 different return values from which the 0.025 and 0.975 quantiles are used as confidence intervals.

Table 2.1 shows the 100-year return values and confidence intervals estimated for the different catchments following this procedure. For the explicit analysis of 100-year events, all daily precipitation events in a specific river catchment with a precipitation amount above the 100-year return value are selected. This results in 13 events for the Danube catchment (Rhine: 13, Weser/Ems: 10, Elbe: 11, Oder: 13). For comparison, more moderate extreme precipitation events that fall in between the 20-year and 50-year return value are chosen (Danube: 41 events, Rhine: 42, Weser/Ems: 29, Elbe: 38, Oder: 36). For simplicity, the 100-year precipitation events are abbreviated as MEPEs (most extreme precipitation events) and the more moderate, 20- to 50-year events as LEPEs (less extreme precipitation events) in the following.

The reasoning behind using LEPEs with return periods between 20 and 50 years for comparison is that it would be of interest to compare MEPEs to a clearly distinct distribution of less extreme events. Of course, there are also events with return periods between 50 and 100 years, that is, in between the two groups. Nevertheless, since MEPEs and LEPEs generally occur in similar synoptic-scale environments, as discussed in detail in Sect. 2.4, it is not expected that such intermediate events behave entirely different.

To further demonstrate the temporal homogeneity of this set of extreme events, their temporal distribution over the period 2008-2019 is investigated, which is shown in Supplementary Fig. A.4. First, no significant trend (according to the Mann-Kendall test, 95% confidence level) exists in the number of MEPEs and LEPEs per year over the 12 years (taking data from all catchments together to obtain a sufficient sample size). Based on the Kolmogorov–Smirnov test, again with a 95% confidence level, the temporal distribution of both MEPEs and LEPEs (again for all catchments together) over the 12 years cannot be distinguished from a Poisson distribution, which is the case for independent events with a constant mean rate. Finally, in the individual

catchments the occurrences of the MEPEs and LEPEs per year almost all lie within the expected 95% confidence interval from a Poisson distribution with a constant mean rate (for MEPEs there is only one outlier in the Rhine catchment and for LEPEs two outliers in the Weser/Ems and Rhine catchments, which is both below 2% given the total numbers of 60 MEPEs and 186 LEPEs). In summary, all these tests are consistent with the hypothesis that the extreme events are distributed randomly over the entire period.

2.3.4 Composite analysis

To analyse the generic meteorological conditions associated with extreme precipitation events, composites are constructed by averaging an atmospheric field from a specific lead time over all events from a given catchment and intensity (100-year or moderate, 20- to 50-year events). Such a composite analysis emphasises the structures that are common to all or most of the events. In addition, all 100-year events have been examined individually, and specifically noticeable anomalies are mentioned in the text. By averaging fields from a fixed lead time, the composites are representative of a specific time step relative to the occurrence of the daily extreme event, but not of a specific time of the day, as the forecasts have been initialised at both 00:00 and 12:00 UTC. Composites of meteorological parameters with a strong diurnal cycle thus have to be interpreted with care. Differences between composite patterns are tested for statistical significance at each grid point using Student's t test on a significance level of 0.05 (see Coles et al., 2001).

2.3.5 Cyclone identification and tracking

As precipitation extremes in Europe are known to be linked to the occurrence of mid-latitude cyclones on the synoptic scale (Pfahl, 2014), the composite analysis is complemented by an automated cyclone identification and tracking method following Wernli and Schwierz (2006) in a slightly updated version as documented in Sprenger et al. (2017). Cyclones are identified and tracked based on 6-hourly sea-level-pressure (SLP) fields from the ECMWF ensemble forecasts. Cyclone centres are determined as local minima of the SLP, and subsequent cyclone centres are connected to form a cyclone track if they occur within a search area determined by the previous cyclone track. This cyclone tracking algorithm has been included in several recent inter-comparison studies (e.g. Flaounas et al., 2023; Neu et al., 2013). It has also been widely used to study the relationship between cyclones and extreme precipitation (e.g. Pfahl, 2014; Pfahl & Wernli, 2012).

Here, this algorithm is used to find the surface cyclone that is associated with a specific extreme precipitation event. For each event, all cyclone tracks are considered possible candidates that exist at least up to 6 h after the beginning of the 24-hour event. The closest cyclone located in a

specific area around the river catchment during that time step (Danube: 40°–50°N & 10°–25°E; Rhine: 42°–52°N & 5°–20°E; Weser/Ems: 45°–55°N & 5°–20°E; Elbe: 45°–55°N & 10°–25°E; Oder: 45°–55°N & 15°–30°E) is then associated with the event. These areas are mainly located southeast of the river catchments, where the composite analysis indicates an SLP minimum (see below). There are a few cases when no cyclone is located in the predefined area, when the SLP field is rather flat and does not possess a well-defined minimum. These cases are excluded from the analysis of cyclone tracks. Additionally, the cyclone tracks associated with the extreme events do not have the same length, such that the number of considered cyclones differs between lead times.

2.4 Results

In the first part of this section, the temporal and spatial distributions of 100-year and more moderate extreme events are shown (Sect. 2.4.1). Afterwards, the main results of this study are presented, covering the atmospheric conditions associated with 100-year events and their differences to more moderate events (Sect. 2.4.2). The results of the cyclone identification and tracking approach are then shown for both types of events in Sect. 2.4.3. Several figures and analyses are only shown for the Danube catchment, but results for other catchments are also discussed, in particular if they are substantially different.

2.4.1 Spatial and temporal distribution

Precipitation events with 100-year return periods

In this section, 100-year events are characterised in terms of their spatial precipitation patterns and time of occurrence. The MEPEs are typically associated with high precipitation amounts over the entire river catchment. In most catchments, the composite precipitation patterns have a maximum near the centre and a relatively flat decrease in the average daily precipitation towards the boundaries, except for the Danube (see Fig. 2.3a) and partly the Rhine catchment. There, the highest precipitation rates are found along the northern flank of the Alps, indicating the importance of orographic precipitation enhancement in these two catchments. The mean composite precipitation amounts (spatially averaged over the catchment) are the largest for the Weser/Ems and Danube catchments with 52.6 mm and 44.1 mm, respectively, followed by the Oder (42.1 mm), Elbe (40.9 mm) and Rhine (37.6 mm) catchments. The high values in the Weser/Ems region are associated with the relatively small catchment size. Higher values, of course, occur at single grid points. For the maximum grid-point values, the ranking changes as follows: Elbe (77.7 mm), Danube (74.3 mm), Rhine (68.1 mm), Weser/Ems (63.8 mm) and Oder (62.7 mm).

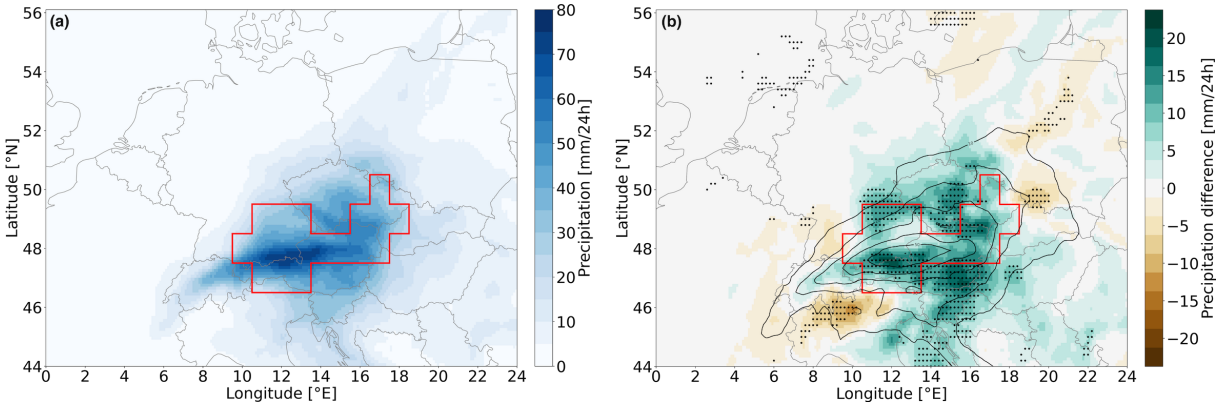

Figure 2.3: **(a)** Composite of the accumulated daily precipitation amount during all MEPEs. **(b)** Composite difference between the accumulated precipitation amount of MEPEs and LEPEs. Results are shown for events over the Danube catchment, which is indicated by the red line. In **(b)**, positive (negative) values represent higher (lower) precipitation amounts during MEPEs, significant differences are marked by a black dot and the LEPE composite is shown as black contours (contour interval of 10 mm).

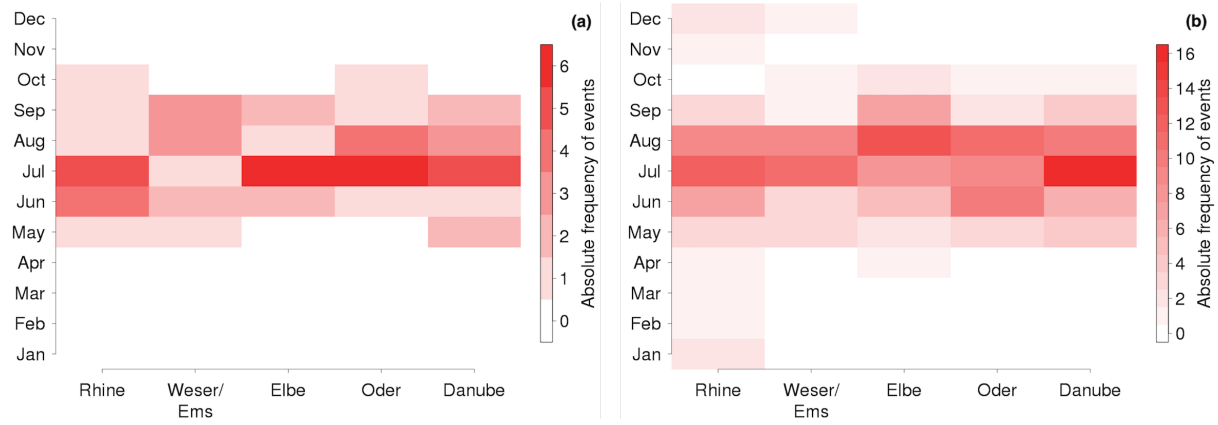

Figure 2.4: Monthly distribution of **(a)** MEPEs and **(b)** LEPEs for all five river catchments.

Interesting aspects of 100-year precipitation events are their time of occurrence during the year and their temporal variability during the day of the event. The monthly frequencies of MEPEs for all river catchments are presented in Fig. 2.4a, which clearly shows that such events occur most frequently during the extended summer months June–September. While the frequency over e.g. the Oder catchment is relatively high in July and August, the events over the Weser/Ems catchment are rather evenly distributed over the warmer months. A few events, for instance over the Rhine catchment, also occur in May or October, which is, however, rather rare.

To quantify the temporal variability of precipitation during the day of the MEPEs, the 6-hourly precipitation values of each event are ranked by their intensity, starting with the highest intensities, as shown in Supplementary Fig. A.5 for the Danube catchment. Large differences between the red boxes would indicate that the daily MEPEs are mainly caused by very intense 6-hourly

precipitation periods, whereas relatively equal distributions would indicate that the MEPEs are due to persistent precipitation during the entire day. For the Danube catchment, there is no clear indication that just one of these types dominates. There is some sub-daily variability during the MEPEs, with the 6-hourly precipitation during the most intense period being about 75% higher than in the weakest period. Similar sub-daily distributions are found for the Rhine and Oder catchments. Just the Weser/Ems and Elbe events show a tendency towards larger differences, that is MEPEs being more influenced by intense 6-hourly precipitation.

Differences to 20-50-year precipitation events

By construction, the accumulated daily precipitation amounts for LEPEs are significantly smaller than for MEPEs, as shown in Fig. 2.3b for the Danube catchment. Over the entire catchment, the MEPE composite indicates higher precipitation amounts, and most of these differences are statistically significant. The LEPE composite, which is displayed as black contours, shows a similar spatial pattern as the MEPE composite with high precipitation amounts within the catchment and a maximum over the northern part of the Alps. However, MEPEs are also associated with significantly higher precipitation rates over southeast Germany and the Czech Republic as well as around the eastern parts of the Alps. In some regions in the western Alps and eastern Europe, significantly more precipitation occurs during LEPEs. Also in the other river catchments, the spatial patterns of the LEPE composites are similar to the corresponding MEPE composite (see Supplementary Fig. A.6, mind the different colour scale).

A comparison of the temporal occurrence and sub-daily variability of LEPEs illustrates a lot of similarities to the 100-year events. The monthly frequencies of LEPEs (Fig. 2.4b) indicate a similar seasonality as for MEPEs. LEPEs occur most frequently during the extended summer as well, mainly from May to October with a maximum frequency during June, July and August in all river catchments. Hence, although the seasonality of LEPEs is less well defined, there is no shift in the maximum frequency towards other months compared to MEPEs. However, especially over the Rhine catchment, a few events also occur during the other seasons. This low frequency of winter events is interesting given the fact that historical extreme floods in the Rhine catchment occurred primarily in the winter season. Monthly distributions of even weaker extreme precipitation events in the Rhine catchment, with return values of about 1-10 years, show rather equally distributed frequencies with slightly more events in the winter season (see Supplementary Fig. A.7 where HYRAS observations are used due to their high spatial resolution). The seasonal distribution of events in the Rhine catchment might thus shift from winter to summer with increasing event intensity.

Also the sub-daily variability of precipitation during LEPEs is similar to MEPEs (see again Supplementary Fig. A.5). The precipitation differences between MEPEs and LEPEs are similar in all 6-hourly sub-periods, indicating that the differences between the events cannot be explained

by differences in either peak intensity or persistence alone. The same is true for the other river catchments; only the tendency towards larger differences between 6-hourly intensities during MEPEs observed for the Weser/Ems and Elbe catchments is less pronounced for LEPEs.

2.4.2 Atmospheric conditions associated with extreme events

Precipitation events with 100-year return periods

In order to characterise the atmospheric conditions associated with 100-year precipitation events, composites of various fields 12 hours after the start of daily MEPEs over the Danube catchments are shown in Fig. 2.5. The temporal evolution of the geopotential height composites prior to the events is shown in Fig. 2.6. The geopotential height composite at 500 hPa (Fig. 2.5a) indicates a negative anomaly over central Europe with its centre southeast of the Danube catchment and the Alps, which has the form of an upper-level cut-off low. Similar cut-off low anomalies are found for the other river catchments, with the low-pressure centre typically located slightly east of the respective catchment (see Supplementary Fig. A.8). The additional southward shift to the southern side of the Alps observed for the Danube catchment thus is slightly exceptional. In addition, positive geopotential height anomalies are located over the North Atlantic and over eastern Europe (see again Fig. 2.5a). The presence of such ridges may lead to a quasi-stationary situation in which the cut-off low is prevented from moving farther east. In the sea-level-pressure composite for the Danube catchment (contours in Fig. 2.5a), an extended area of relatively low pressure covers large parts of central and eastern Europe, with the low-pressure centre being located close to and slightly east of the centre of the upper-level cut-off low, which is a configuration conductive to baroclinic cyclone growth. An area of high pressure is found over the North Atlantic, underneath the 500 hPa ridge.

The upper-level cut-off low is also visible as a positive potential vorticity (PV) anomaly on the 320 K isentrope (Fig. 2.5b). The centre of the PV cut-off is shifted slightly southeastward compared to the centre of the geopotential height anomaly at 500 hPa. Such stratospheric PV cut-offs or streamers are created by upper-level Rossby wave breaking (Grams et al., 2011) and have been shown to be often associated with extreme precipitation events in Europe (Martius et al., 2008). Also for the present case of MEPEs in the Danube catchment, the composite temporal evolution of the geopotential height field at 500 hPa (Fig. 2.6) indicates that the cut-off low develops from a trough located over northwestern Europe 24 hours before the event (Fig. 2.6a). Subsequently, Rossby wave breaking is likely associated with the separation of the negative geopotential height anomaly from the main northern region of low geopotential height (high PV) and its southeastward displacement and slowdown south of the Danube catchment (Fig. 2.6b–d). The formation of the cut-off is associated with an intensification of the upstream and downstream ridges as well as surface cyclogenesis (see also Sect. 2.4.3). MEPEs in the other

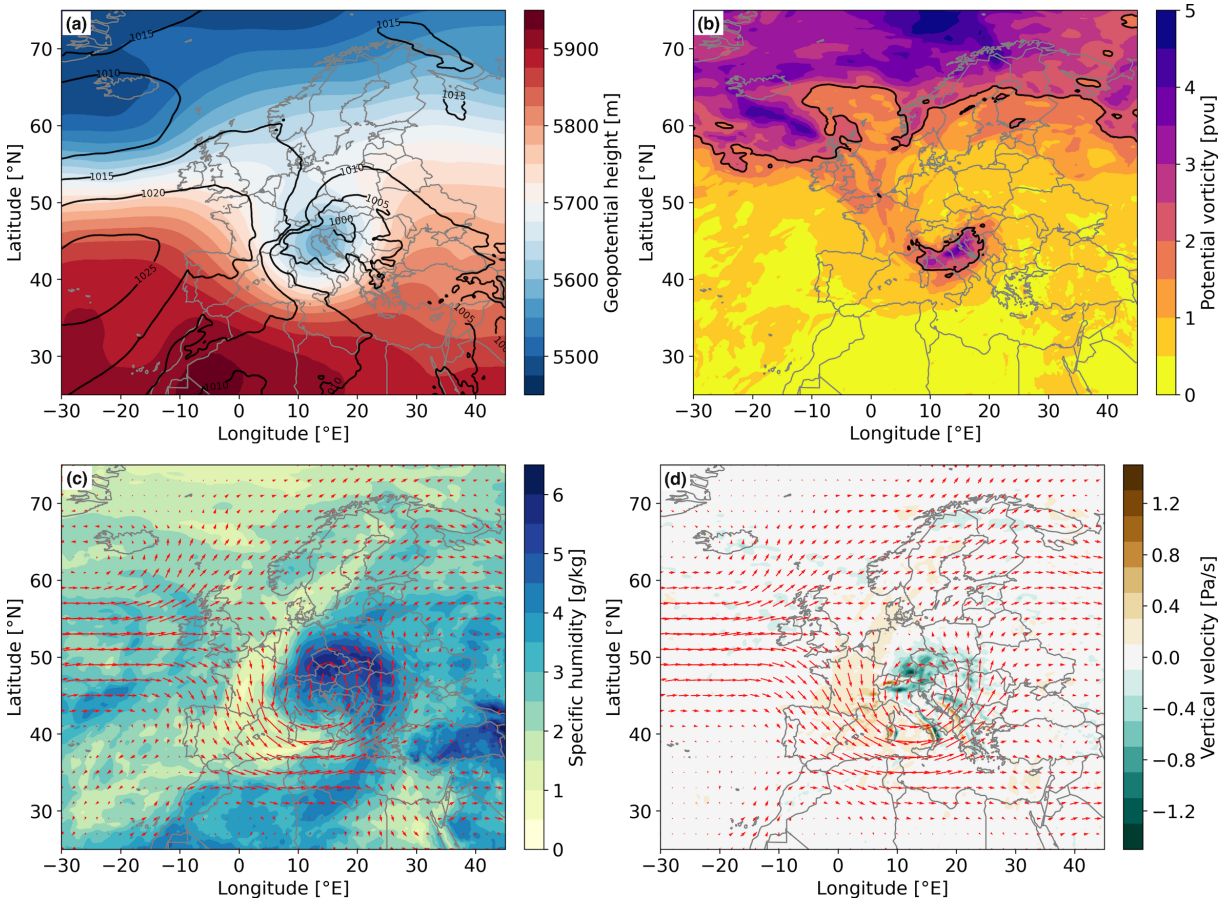

Figure 2.5: Composite of atmospheric conditions 12 hours after the start of daily MEPEs in the Danube catchment of **(a)** geopotential height at 500 hPa (colour shading) and sea-level pressure (contours); **(b)** potential vorticity at 320 K, with the 2 pvu contour indicated in black; **(c)** specific humidity (colour shading) and horizontal wind (red arrows) at 700 hPa; and **(d)** vertical velocity (colour shading) and horizontal wind (red arrows) at 500 hPa.

catchments follow a similar development, with the composite trajectory of the upper-level cut-off low and the location of surface cyclogenesis slightly displaced towards the respective catchment region (not shown).

The configuration of low pressure over central Europe and high pressure over the North Atlantic and eastern Europe is associated with northwesterly winds over western Europe, westerly winds over the Mediterranean, and southerly winds over eastern Europe in the lower and middle troposphere (see Fig. 2.5c,d). Such a horizontal wind field facilitates the advection of moist air masses over the eastern Mediterranean and eastern Europe towards central Europe (Fig. 2.5c). In addition to the Mediterranean, continental evapotranspiration can act as an important (and often main) moisture source in such situations, as shown in previous case studies (Grams et al., 2014; Winschall et al., 2014; Sodemann et al., 2009; James et al., 2004). The moist air is transported towards the Danube catchment with northeasterly winds, where strong ascent (Fig. 2.5d) leads

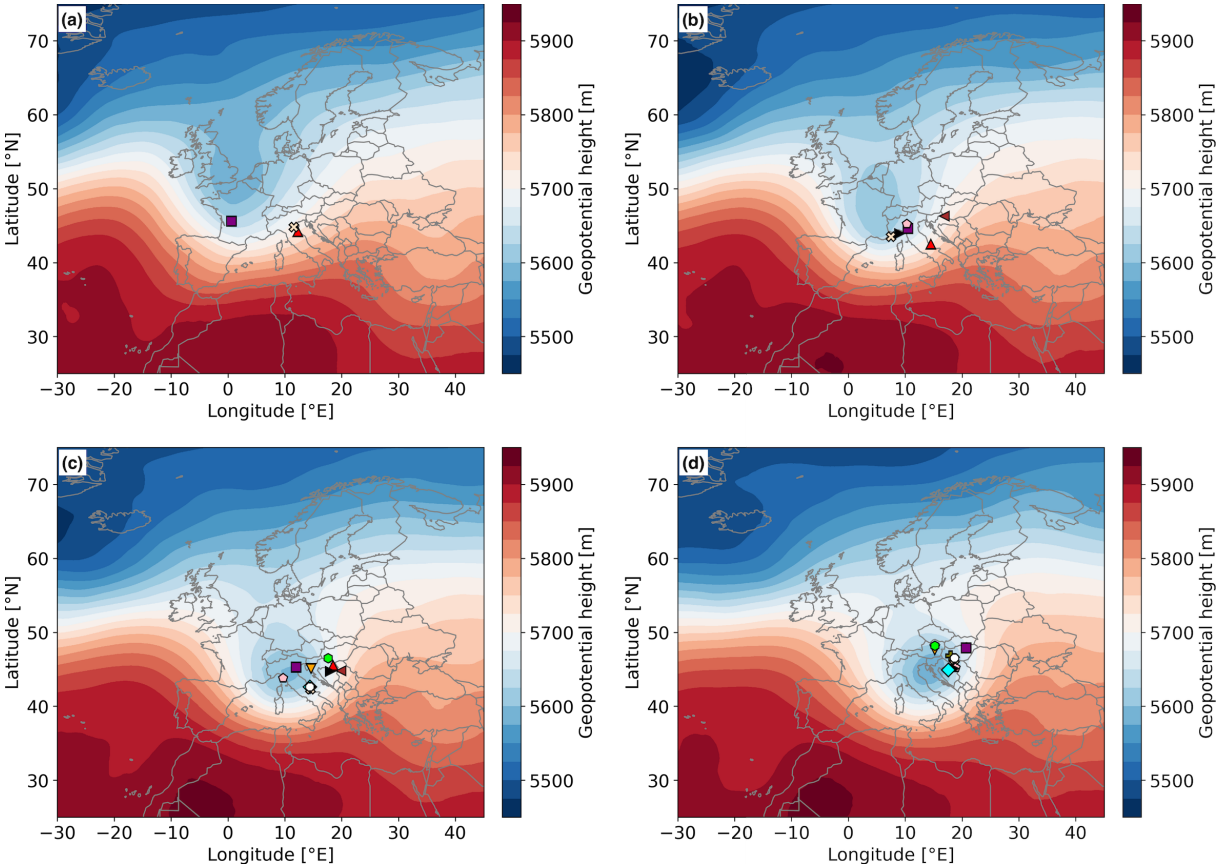

Figure 2.6: Composites of the geopotential height at 500 hPa for all MEPEs over the Danube catchment **(a)** 24 h before the event, **(b)** 12 h before the event, **(c)** at the beginning of the event and **(d)** 12 h after the beginning of the event. The surface cyclone centres (sea-level-pressure minima) from the cyclone identification and tracking approach are shown as coloured symbols. Since not every cyclone was identified for all time steps, later images show higher numbers of identified cyclone centres.

to rainout. Dynamical forcing, evident from positive vorticity advection, plays a role in this lifting in all catchments but is the weakest for the Danube (not shown). In addition, orographic effects can intensify the ascent, in particular in the case of the Danube (and also the Rhine) catchment, when the air masses are transported towards the Alpine ridge from the north. The slow displacement of the cut-off low can lead to continual ascent in the same catchment region and high accumulation of precipitation during the day of the MEPEs.

These composites show the average conditions during all 100-year precipitation events over a river catchment. Although most of the individual events develop in a similar way as shown in these composites, based on a visual analysis of the individual events, there are a few exceptions with a different progression. Two events over the Danube catchment are characterised by an upper-level low that moves north of the Alps but a surface cyclone also developing east of the catchment (see Supplementary Fig. A.9a for one case, 12 hours before the event). One event over

the Weser/Ems catchment results from a rather weak, northward-moving surface cyclone over Germany, east of a large upper-level trough over the British Isles and the North Atlantic (see Supplementary Fig. A.9b). Although the cyclone does not strongly intensify, it facilitates the transport of warm and moist air masses from the south towards the river catchment. During two events over the Elbe catchment, a large upper-level cut-off low over southeastern Europe moves northward to Poland in combination with the intensification of a surface cyclone to the north and moisture transport also from the Black Sea region. Two other events are characterised by an Omega blocking centred over Scandinavia and a large ridge over central/eastern Europe in between two lows over the eastern North Atlantic and eastern Europe but no clear surface cyclone (see Supplementary Fig. A.9c for one case). Moist air masses are transported from southern to central Europe ahead of the western low-pressure system, and lifting over the catchment is associated with a near-surface convergence zone. Additionally, an event over the Oder catchment is linked to a "high over low" blocking system over the British Isles and a convergence zone over the catchment (see Supplementary Fig. A.9d). Three events over the Rhine catchment are characterised by a positive upper-level geopotential height anomaly over eastern Europe with an upper-level trough that slowly moves from the British Isles towards the catchment while surface cyclones develop north of the Alps.

In addition to the primarily synoptic-scale environment and processes investigated in the composites of Fig. 2.5, convective processes may also influence the intensity of MEPEs. To quantify such a potential influence, composites of the convective available potential energy (CAPE) on the day of the events and the previous day are analysed (see Supplementary Fig. A.10a for a CAPE composite at the day of the Danube events). The composites show very low CAPE over central Europe and just weak-to-medium CAPE over eastern Europe on both days (similar to all other catchments). For single events, there are some areas with weak CAPE in most of the cases, but only one to three events per catchment are associated with medium-to-high CAPE values over or nearby the specific catchment. This indicates that convective processes, here measured in terms of CAPE, appear to play a minor role in very extreme, 100-year precipitation events in the large river catchments investigated in this study. Note, however, that this conclusion may be sensitive to the underlying data set, since the simulations applied here do not explicitly resolve moist convection.

Differences to 20-50-year precipitation events

The previous section has shown that the atmospheric conditions during 100-year precipitation events are often similar between the different river catchments. In this section, differences between 100-year and more moderate, 20- to 50-year precipitation events are identified through differences between the MEPE and LEPE composites. Figures 2.7 and 2.8 show such composite differences for the Danube and Elbe catchments, respectively, as different mechanisms distinguish

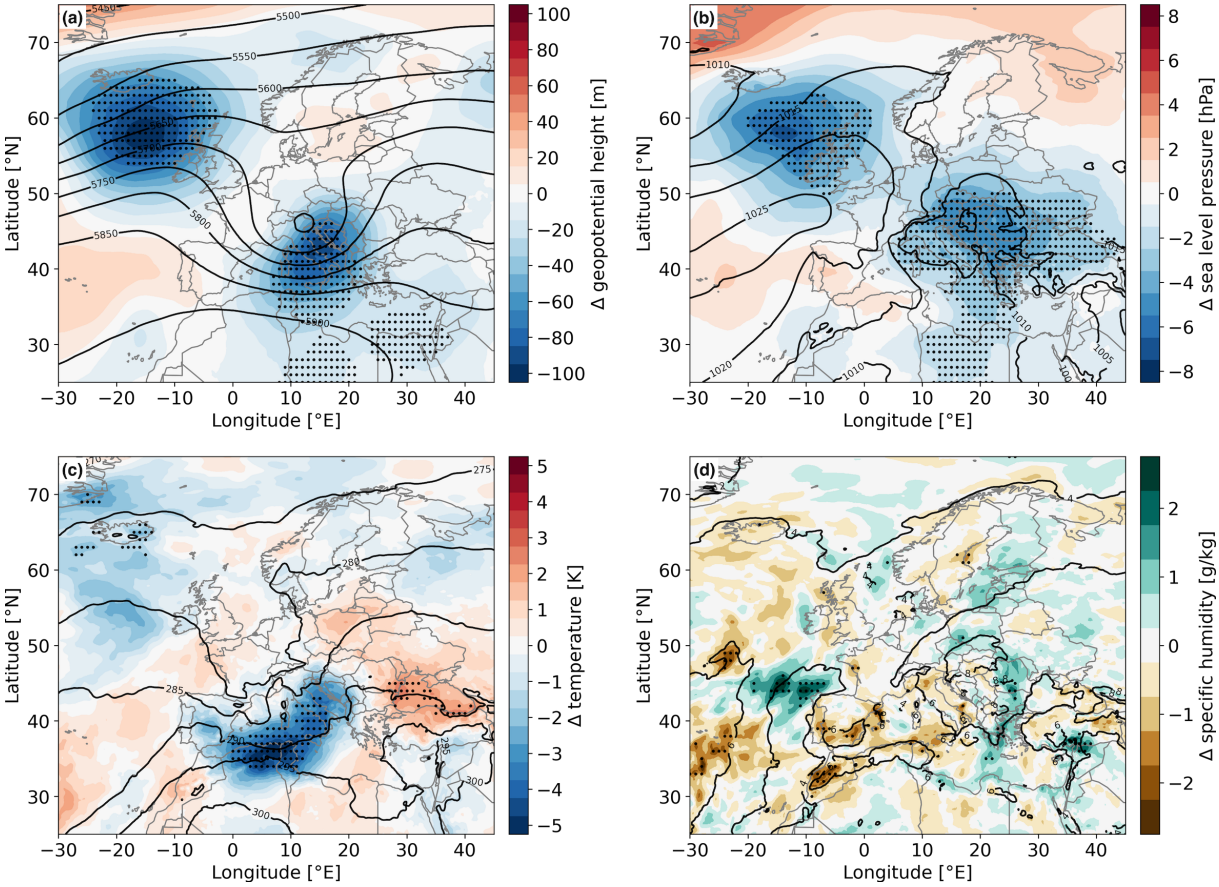

Figure 2.7: Differences between the composites of MEPEs and LEPEs 12 hours after the start of daily MEPEs in the Danube catchment, showing **(a)** geopotential height at 500 hPa, **(b)** sea-level pressure, **(c)** temperature at 850 hPa and **(d)** specific humidity at 850 hPa. Positive (negative) values indicate higher (lower) values in the MEPE composite. Significant differences are marked by black dots. The LEPE composites are shown as black contours.

MEPEs from LEPEs over these catchments.

LEPEs over the Danube catchment are associated with a similar upper-level pattern as MEPEs, with an upper-level cut-off low located over central Europe centred slightly south of the river catchment in combination with ridges over the North Atlantic and eastern Europe (Fig. 2.7a). Also the surface pressure configuration is similar with a large area of low pressure over eastern Europe and high pressure over the North Atlantic (Fig. 2.7b). However, MEPEs are characterised by a significantly intensified low-pressure anomaly at 500 hPa that also extends further south compared to LEPEs. In addition, the surface pressure is significantly lower over large parts of central and eastern Europe. Pressure is also lower around Iceland both at the surface and in the middle troposphere. The intensified cut-off low and associated cyclonic circulation during MEPEs are associated with intensified cold air advection, bringing colder air masses over the Mediterranean Sea along the southern flank of the cut-off low (Fig. 2.7c). Over the Danube

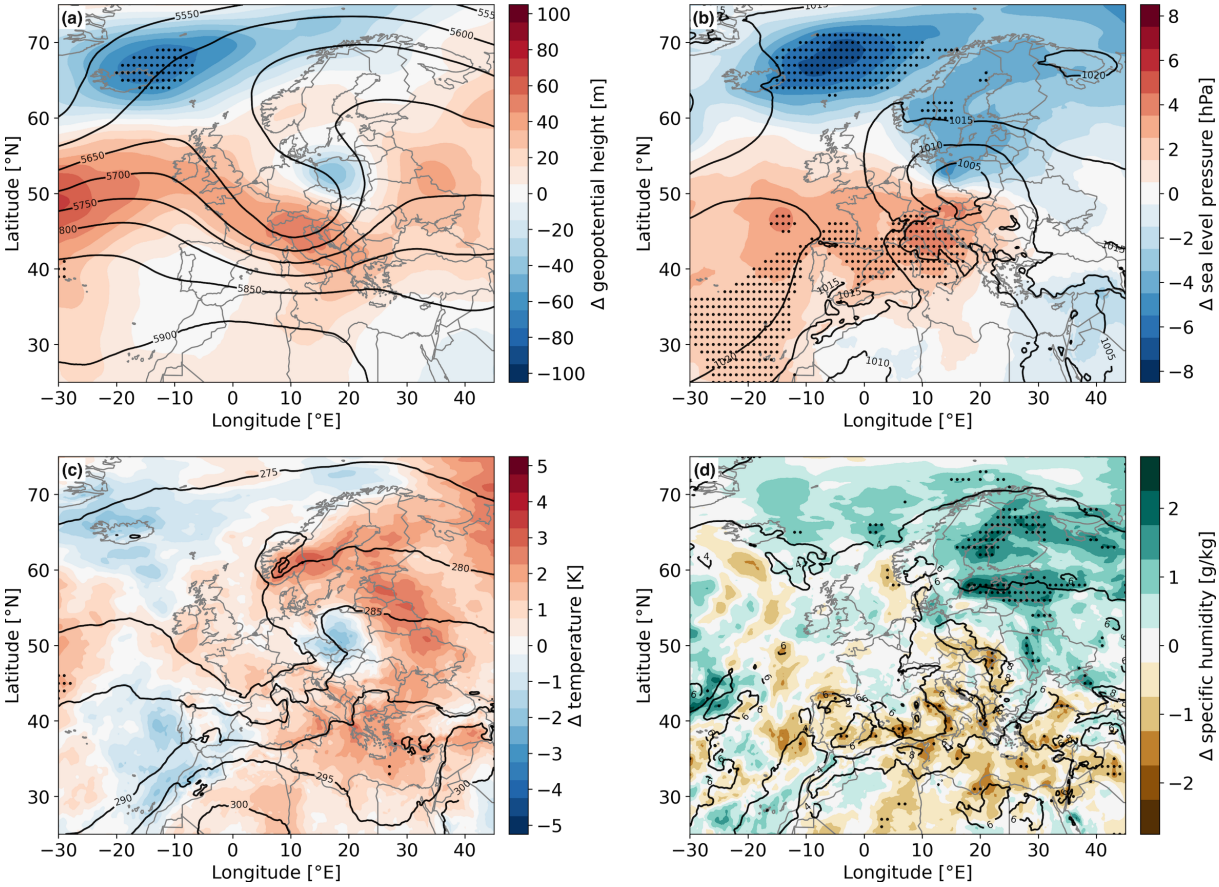

Figure 2.8: The same as in Fig. 2.7 but for events over the Elbe catchment.

catchment itself, no significant temperature difference occurs, but still the temperature is slightly higher during MEPEs northeast of the catchment. There is also no particular increase of the moisture content in the lower troposphere over most parts of central and eastern Europe, although some areas are characterised by minor increases during MEPEs (Fig. 2.7d). Figures 2.7a and b thus clearly show that dynamical mechanisms such as an intensified cut-off low at 500 hPa and intensified low-pressure systems at the surface play a more important role than thermodynamic mechanisms (higher temperature or moisture content in the lower troposphere) in distinguishing 100-year extreme precipitation events from more moderate extreme events. Similar results are found for the Oder catchment (see Supplementary Fig. A.11), where, in addition, also the 500 hPa ridge over the North Atlantic is slightly intensified during MEPEs. Furthermore, the lower-tropospheric moisture content is significantly reduced during MEPEs over several areas of central Europe in combination with reduced lower-tropospheric temperatures.

Not in all catchments are MEPEs characterised by intensified circulation anomalies in comparison to LEPEs. In order to demonstrate different intensification mechanisms, composite differences between MEPEs and LEPEs are shown in Fig. 2.8 for the Elbe catchment. MEPEs over this catchment are rather associated with a slight northeastward shift of the 500 hPa low towards

the east of the catchment instead of a clear intensification (Fig. 2.8a). Over the North Atlantic, the height of the 500 hPa surface is lower over Iceland and the ridge west of Ireland is slightly intensified during MEPEs. Similar results are found for sea-level pressure (Fig. 2.8b). The local sea-level-pressure minimum over eastern Europe is shifted northeastwards during MEPEs rather than being intensified compared to LEPEs. On a larger scale, sea-level-pressure values are generally lower over the northern part of the domain but higher in the southwest during MEPEs. On the contrary, as opposed to the Danube catchment, the lower-tropospheric temperature over large parts of eastern Europe is higher during MEPEs compared to LEPEs over the Elbe catchment, even though this difference is not statistically significant (Fig. 2.8c). The local cold anomaly over the Czech Republic and southern Poland is caused by the extreme precipitation event (e.g. due to cloud radiative cooling) and is not visible in the hours before the event (not shown). These generally higher temperatures go along with significantly increased lower-tropospheric moisture content, in particular in the region northeast of the sea-level-pressure minimum (Fig. 2.8d). This moisture can then be transported towards the Elbe catchment by the cyclonic circulation. In summary, more favourable thermodynamic conditions, in particular a higher atmospheric moisture content, thus distinguish MEPEs over the Elbe catchment. The circulation anomalies associated with these events are spatially shifted rather than intensified compared to LEPEs. Similar results are obtained for the Rhine catchment (see Supplementary Fig. A.12). MEPEs over the Rhine catchment are characterised by a southward shift of the mid-level and surface low-pressure anomalies in combination with a spatially large and significant intensification of an upper-level ridge over northern and eastern Europe. Additionally, temperature and lower-tropospheric moisture content are significantly higher during MEPEs over most of eastern Europe. In the Weser/Ems catchment, both dynamic and thermodynamic mechanisms play a role in the differences between MEPEs and LEPEs (see Supplementary Fig. A.13). The negative 500 hPa geopotential height anomaly is slightly enhanced, and the surface low is significantly intensified during MEPEs. Both temperature and lower-tropospheric moisture content are significantly higher over parts of eastern Europe, but conditions are even drier over large parts of central and western Europe.

Differences in geopotential height at 500 hPa as shown in Fig. 2.7a and Fig. 2.8a are an indicator of differences in the intensity of the upper-level low intensity as well as the general synoptic situation. However, differences in the wind that, for instance, transports moist air masses towards the catchment are more directly linked to the horizontal geopotential gradient. Supplementary Fig. A.14 shows the MEPE composites (left panels) and the differences to the LEPE composites (right panels) of the magnitude of the geopotential height gradient at 500 hPa for the Danube (upper panels) and Elbe (lower panels) catchments. The largest horizontal geopotential height gradients during MEPEs are found south/southeast of the centre of the upper-level cut-off low. Local maxima are also found north/northeast of its centre, near the respective river catchment (this applies to all catchments). In comparison with more moderate extreme events, MEPEs

show (mostly) significant intensified horizontal gradients over the eastern flank of the upper-level low centre. This is the case for all catchments, except for the Rhine (not shown). However, the intensification of the horizontal gradient extends more northward for events over the Elbe compared to the Danube catchment. The results for the Danube support the previous conclusion that the upper-level low is primarily more intense during MEPEs, but not dislocated, leading to an intensified horizontal gradient, particularly at its southern flank. However, for the Elbe catchment the upper-level low centre shifts towards Poland during MEPEs, which increases the horizontal geopotential height gradient over eastern Europe and thus intensifies the northward advection of warm and moist air masses. Most probably, this is the main reason for the increased temperature and specific humidity over northeastern Europe for MEPEs in the Elbe catchment (see Fig. 2.8c and 2.8d). For the Elbe catchment, the role of altered dynamical conditions during MEPEs is thus more subtle: while the intensity of the upper-level cut-off low is not substantially increased, a shift of the circulation pattern leads to increased southerly advection and thus more favourable thermodynamic conditions for extreme precipitation.

Finally, there is no significant difference in CAPE over central Europe between MEPEs and LEPEs (see Supplementary Fig. A.10b for the Danube) in all river catchments except for the Rhine, where CAPE is even reduced during MEPEs in some areas. This supports the assumption that convective instability is not a major discriminator of extreme precipitation in the large catchment areas of this study.

2.4.3 Cyclone development

The composite method to identify typical atmospheric patterns associated with extreme precipitation events is complemented by an event-based approach to objectively identify and track surface cyclones as described in Sect. 2.3.5. Cyclones are associated with both MEPEs and LEPEs at the day of the event, and tracks are connected backward in time until cyclone genesis. The positions of the surface cyclone centres associated with MEPEs are shown as coloured symbols in Fig. 2.6 and the cyclone frequency during MEPEs (taking all grid points within the outermost closed sea-level-pressure contour surrounding a sea-level minimum into account) in Fig. 2.9a. Most cyclones emerge downstream of the developing 500 hPa cut-off low (see colour shading in Fig. 2.6) on the day before or the day of the MEPEs. This area downstream of an upper-level positive potential vorticity anomaly is generally favourable for cyclogenesis (e.g. Hoskins et al., 1985). Most surface cyclones develop south of the Alps and move in parallel with the mid-tropospheric low along the Alps and towards the east or southeast of the Danube catchment. Such cyclone pathways are represented by the Vb type in the categorisation of van Bebber (1891). The cyclone frequency during MEPEs has a maximum southeast of the Danube catchment, with values around 80% over northern Croatia and western Hungary (see again Fig. 2.9a). The cyclone tracking results for MEPEs over the Elbe and Oder catchments are similar to the

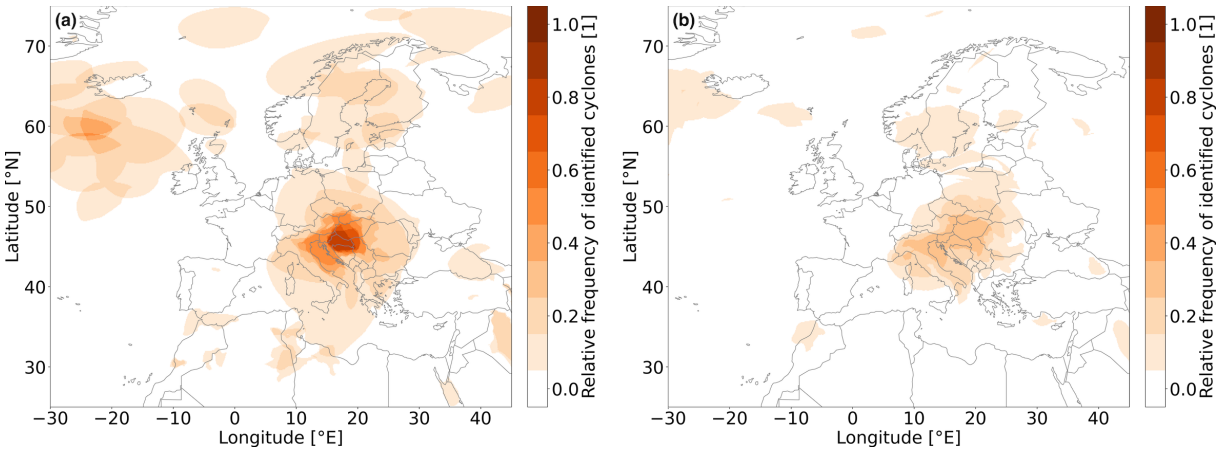

Figure 2.9: Cyclone frequency at 06:00 UTC on the day of **(a)** MEPEs and **(b)** LEPEs over the Danube catchment. All grid points within the outermost closed sea-level-pressure contour surrounding a sea-level minimum are taken into account for the calculation of this frequency, following previous studies (Pfahl, 2014; Wernli & Schwierz, 2006).

Catchments	Cyclone frequency				Mean minimum SLP	
	MEPEs		LEPEs		MEPEs (hPa)	LEPEs (hPa)
Rhine	11/13	(84.6%)	27/42	(64.3%)	999.0	1002.5
Weser/Ems	10/10	(100.0%)	20/29	(69.0%)	**992.4**	**999.6**
Elbe	10/11	(90.9%)	30/38	(79.0%)	995.3	996.6
Oder	12/13	(92.3%)	24/36	(66.7%)	**992.8**	**999.7**
Danube	11/13	(84.6%)	21/41	(51.2%)	995.8	999.5

Table 2.2: Absolute and relative cyclone frequencies as well as mean cyclone intensities, measured through the minimum sea-level pressure, of cyclones associated with MEPEs and LEPEs. Bold SLPs indicate significant differences on a significance level of 0.05.

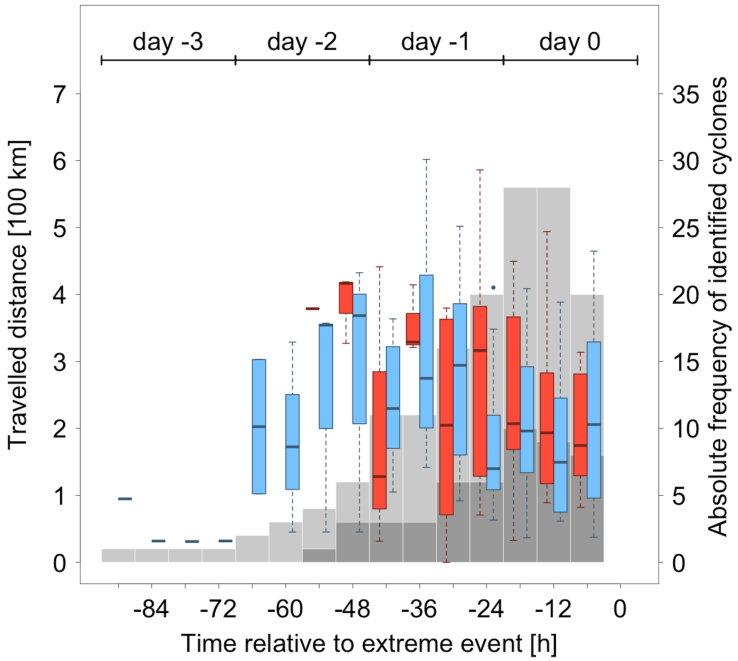

Figure 2.10: Distributions of travelled distances during 6-hourly time intervals of tracked cyclones during (red) MEPEs and (blue) LEPEs over the Danube catchment. The grey bars show the absolute cyclone counts at each time step for (dark grey) MEPEs and (light grey) LEPEs. The time on the x-axis is specified relative to the occurrence of the extreme event, and 0 hours corresponds to the end of the daily event.

Danube catchment, with cyclones also developing south of the Alps, but also over eastern Europe, and then moving northwards. Surface cyclones during MEPEs over the Rhine catchment rather develop north of the Alps or over the western Mediterranean and track northwards, while those associated with MEPEs over the Weser/Ems catchment mainly develop over southern and eastern Germany. Cyclones associated with LEPEs typically follow similar pathways as described for MEPEs, with only a few exceptions, in all river catchments (not shown). Nevertheless, relative cyclone frequencies during LEPEs are smaller than for MEPEs (see Table 2.2 and, for the Danube catchment, Fig. 2.9b), meaning that a smaller percentage of LEPE events is linked to a tracked surface cyclone. Moreover, also the cyclone intensity, measured here simply by the averaged minimum sea-level pressure, is enhanced for MEPEs compared to LEPEs (see again Table 2.2). These intensity differences are larger for the Weser/Ems, Oder and Danube catchments and even statistically significant for the former two, compared to the Rhine and Elbe. This is consistent with the result from the composite analysis that dynamical factors distinguish MEPEs from LEPEs in the former three catchments (see Sect. 2.4.2).

In addition to the cyclone pathway and intensity, its velocity may be an important factor for extreme precipitation, as slower-moving systems can lead to a larger precipitation accumulation at a specific location. In order to analyse cyclone velocities, Fig. 2.10 shows the travelled distances

of tracked cyclones in 6-hourly intervals for MEPEs (in red) and LEPEs (in blue). Only on the day of the events and the previous day can reasonable distributions be produced, as the number of identified cyclones is too low during earlier periods (see grey bars in Fig. 2.10). In general, cyclones tend to decelerate on the day of the event compared to the previous day, which is consistent with the hypothesis that slower-moving cyclones can enhance the precipitation amounts in the river catchments. However, comparing cyclone velocities between MEPEs and LEPEs during the day of the extreme events shows that there is a large scatter and no clear difference in the median velocities. Similar results are found for the other river catchments (not shown). Only for the Elbe and Oder catchments is there a slight tendency towards slower cyclones for MEPEs compared to LEPEs.

In summary, the results of the cyclone tracking analysis show that extreme precipitation events in the selected river catchments are associated with typical cyclone tracks from the south towards the east of the respective catchment and with a deceleration of the cyclones during the day of the event. MEPEs are linked to higher cyclone frequencies and also to more intense cyclones compared to LEPEs, in particular in the Oder, Danube and Weser/Ems catchments. However, the cyclones' translation velocities are similar for MEPEs and LEPEs and thus do not allow for distinguishing 100-year events from less extreme precipitation events.

2.5 Discussion and conclusion

The aim of this study has been to robustly investigate the atmospheric processes during 100-year precipitation events in large central European river catchments and their differences compared to less extreme events. A better understanding of these high-impact events may be instrumental to provide more accurate forecasts of river floods and reduce uncertainties in projections of their potential future changes. To perform such a robust process analysis, a large data set of model-generated daily precipitation fields is used, obtained from the ECMWF operational ensemble weather prediction system following a method introduced by Breivik et al. (2013). Statistical analyses show that the 10th forecast days from these simulations produce quasi-independent precipitation events, in particular with regard to extremes such as annual maxima, and that the intensity distribution of these simulated events lies within the uncertainties obtained from different observational data sets. With the help of extreme value theory, return values of 100-year and more moderate, 20- to 50-year extreme precipitation events are determined for each selected river catchment, and the events surpassing these return values are investigated with regard to the underlying atmospheric conditions.

An analysis of the temporal and spatial characteristics of the extreme precipitation events shows that most 100-year events occur during the extended summer June–September, with only a few

exceptions in May or October. This corresponds well with historical precipitation extremes (e.g. Grams et al., 2014; Ulbrich et al., 2003) and statistical analyses of rain gauge data (Fischer et al., 2018). More moderate precipitation extremes also peak during the summer season but may occur during winter in the Rhine and Weser/Ems catchments as well. The spatial distribution of precipitation during the extreme events is influenced by the topography of the catchments, in particular by the orographic effect of the Alps in the Danube and Rhine catchments.

In order to determine the characteristic atmospheric conditions associated with the 100-year precipitation events, a composite analysis is used in combination with a cyclone tracking algorithm. On the day before the events, an upper-level trough is typically located over western Europe, which slowly moves southeastwards in the direction of the Alps. Rossby wave breaking (cf. Portmann et al., 2021; Appenzeller et al., 1996) then leads to the formation of a cut-off low in the middle and upper troposphere that is visible as both a geopotential height and potential vorticity anomaly. Previous studies have also emphasised the importance of Rossby wave breaking for European precipitation extremes, in particular on the south side of the Alps (Barton et al., 2016; Martius et al., 2008). The resulting cut-off low can favour the formation of extreme precipitation through its influence on moisture transport, lower-tropospheric destabilisation and dynamical lifting (Schlemmer et al., 2010). The exact pathway and location of the forming cut-off, typically towards the southeast of the specific river catchment, determines where the heavy precipitation event occurs. During the day of the event, the upper-level cut-off low becomes quasi-stationary, also associated with the formation of high-pressure anomalies upstream over the North Atlantic and downstream over eastern Europe. Surface cyclogenesis regularly occurs east of the mid-tropospheric cut-off shortly before or during the extreme precipitation event. Cyclone pathways often, but not in all cases and for all catchments, resemble the classical Vb track (van Bebber, 1891), which has also been associated with many historical events (Hofstätter et al., 2018; Messmer et al., 2015; Grams et al., 2014; Bissolli et al., 2011; Mudelsee et al., 2004; Ulbrich et al., 2003). The involved cyclones are not necessarily very intense, consistent with previous findings (Pfahl & Wernli, 2012), but, in accordance with the upper-level anomalies, move slowly and thus lead to high precipitation accumulation in the catchment. The spatial configuration with a cyclone typically located to the southeast of the affected catchment is again consistent with similar configurations found for less extreme precipitation events (Pfahl, 2014). It leads to moisture transport from the south around the cyclone centres and then towards the catchment with northerly or northeasterly winds. This is especially relevant for the Danube and Rhine catchments, as a northerly flow towards the Alps enforces orographic precipitation enhancement. Previous case studies have shown that, during such situations, typically various moisture sources contribute to the precipitation, with evapotranspiration from the land surface often playing a dominant role (Krug et al., 2022; Grams et al., 2014; Winschall et al., 2014). The important role of moisture transport in particular for orographic precipitation associated with European floods has already been recognised in previous studies (Gvoždíková & Müller, 2021;

Froidevaux & Martius, 2016).

To identify the mechanisms that distinguish the very extreme, 100-year precipitation events (MEPEs), they are compared to a sample of less extreme events with return periods between 20 and 50 years (LEPEs). The general synoptic-scale patterns associated with LEPEs are similar to MEPEs, with an upper-level trough over western Europe on the day before the event that often develops into a cut-off low, going along with surface cyclogenesis slightly downstream. The specific differences between MEPEs and LEPEs depend on the river catchment. On the one hand, differences in dynamical processes are the most important for the Danube and Oder catchments. In particular, the cut-off low is intensified, surface cyclogenesis occurs more regularly and the surface cyclones are also more intense during MEPEs compared to LEPEs. This is expected to enhance moisture transport towards the catchments and dynamical forcing for ascent in the catchments, resulting in stronger precipitation. These results are in slight contrast to the findings of Pfahl and Wernli (2012), who did not detect differences in the intensity of cyclones associated with extreme precipitation in central Europe. This is likely due to the fact that they analysed less extreme events than those studied here. The difference in cyclone intensity thus appears to be a specific characteristic of very extreme, 100-year events. However, there are no clear differences between the translation velocities of cyclones associated with MEPEs and LEPEs. On the other hand, MEPEs in the Elbe and Rhine catchments differ from LEPEs mainly due to significantly higher temperature and lower-tropospheric moisture content over large areas east and northeast of the river catchments. No pronounced differences in the strength of cyclones and cut-off lows are found for these catchments. The enhanced precipitation during MEPEs can thus mainly be explained by higher moisture content in the air masses transported towards the catchments, which are associated with enhanced northward flow due to a shift in the upper-level circulation anomalies. Finally, in the Weser/Ems catchment both stronger circulation anomalies and higher moisture content distinguish MEPEs from LEPEs.

The approach used in this study, and, in particular, the analysis of extreme events in ECMWF ensemble prediction data, comes with a number of limitations. The first limitation is the limited time span of 12 years (2008-2019) from which the forecast data are taken. Due to this relatively short time span, there is also a limitation in the sampling of large-scale boundary conditions associated with the (multi-)decadal variability of the climate system. For instance, the full spectrum of the variability of the El Niño–Southern Oscillation and the Atlantic Multidecadal Oscillation is not sampled, and it might be possible that even more extreme or structurally different events occur under boundary conditions that are not represented in these 12 years. This should be analysed in future research based on coupled climate model ensemble data. Second, there might be a signature of anthropogenic forcing in the data set, leading to temporal inhomogeneities. Nevertheless, this study's analysis of the temporal homogeneity of the extreme events does not provide an indication of a trend due to anthropogenic climate warming. This is consistent with other studies showing that local/regional trends in extreme precipitation only

emerge over longer periods of time (e.g. Fischer et al., 2013). Third, although the statistical analysis has shown that the different ensemble members are rather independent on day 10 of the forecasts, there may still be some interdependence of extreme events occurring in different ensemble members initialised at the same day or on consecutive days, e.g. with regard to the synoptic-scale circulation. This would reduce the effective sample size of the composite and statistical significance analysis. Furthermore, the effective sample size of the entire data set may also be reduced if spatially extended extreme precipitation events lead to simultaneous MEPEs/LEPEs in several catchments. In this study's data set, however, the number of such (quasi-)simultaneous events in several ensemble members or catchments is relatively small.

In this study, the first systematic analysis is presented of very extreme 100-year large-scale precipitation events in central Europe that goes beyond case studies. As the observational record is too short, this study relies on simulated events, but a comparison to observations has shown that precipitation intensities are realistically represented in the applied ensemble prediction model. In future research, the approach may also be used for multi-day events, which have a high potential to cause flooding as described in Sect. 2.1, with the help of more recent ECMWF forecast data extending beyond lead times of 10 days. Additionally, the method may be applied to other regions, as the data set is available for the entire globe.

Chapter 3

Global estimates of 100-year return values of daily precipitation from ensemble weather prediction data

3.1 Introduction

Extreme precipitation is often associated with river floods, which are one of the most dangerous hazards for society and have caused high socioeconomic losses around the globe (Merz et al., 2021; Kron, 2015; Barredo, 2007; Douben, 2006). There are many historical examples of these events such as several flash floods due to a mesoscale convective system in South America in 2022 (Alcântara et al., 2023), an extreme flood event in central Europe in 2021 (Mohr et al., 2023) and a widespread flooding in Thailand during the monsoon season in 2011 (Gale & Saunders, 2013). River floods typically develop along one of two distinct pathways, either very quickly in form of a flash flood or as a slower increase of the runoff and water levels over several hours. On the one hand, flash floods, which often occur in smaller rivers, are associated with very high precipitation rates in a spatially limited domain, leading to a quickly developing peak discharge (Sene, 2016) that can threaten society along the river route, also downstream of the extreme precipitation event. On the other hand, larger-scale floods in larger rivers with a slower increase of water levels are typically caused by longer-lasting heavy precipitation over a wider area. A multitude of atmospheric drivers can contribute to the development of such extreme precipitation events and floods in different regions around the globe, such as convective cells, mesoscale convective systems, monsoonal lows or intense upper-level troughs or cut-off lows (Alcântara et al., 2023; Mohr et al., 2023; Gaume et al., 2016; Gale & Saunders, 2013). Latter is also discussed in Ch. 2.

In addition, orographic enhancement of precipitation can contribute to the development of floods in complex terrain.

The increase in global population, especially in high-risk areas, and the rise of the vulnerability of the society increases the risk of flood disasters (Kron, 2015). Moreover, climate simulations project that the frequency and intensity of extreme precipitation events is going to increase in a warmer climate (Pendergrass & Hartmann, 2014; Fischer et al., 2013; O'Gorman & Schneider, 2009), which is also associated with an increasing frequency of intense floods (see e.g. Alfieri et al., 2015). This, and a higher exposure of a growing proportion of the population to floods in a warmer climate, will drastically increase the flood risk on a global scale (Tellman et al., 2021; Alfieri et al., 2017; Jongman et al., 2012). In order to reduce or even prevent flood losses and damages, different kinds of flood protection measures have been developed. More recent extreme events have shown that flood damages have been reduced with the help of flood barrages compared to extreme precipitation that occurred several decades ago (see e.g. Merz et al., 2014; Bissolli et al., 2011), and that there is further potential to minimise flood losses in the future (Jongman et al., 2015). To this end, e.g., for the appropriate construction of dikes, it is crucial to precisely determine the precipitation amounts of potential extreme events that the protection measures should be able to withstand. In practical water management, such events are often denoted as "probable maximum precipitation" (World Meteorological Organization, 2009).

From a statistical point of view, this probable maximum precipitation can be quantified as the precipitation amount associated with extreme events with long return periods, typically on the order of 100 years, through extreme value statistics. To estimate such return values, long precipitation time series are required, which are conventionally obtained from observations. Although there are several observational data sets available with high quality and relatively high temporal and spatial resolution and coverage, this approach is affected by certain limitations (Rajulapati et al., 2020). First, the time series are often shorter than 100 years, which requires extrapolation to determine 100-year or larger return values and increases the associated statistical uncertainties. Second, if global coverage is desired, the uneven spatial distribution of rain gauges requires combining different data sources (e.g., rain gauge and satellite data), which can lead to spatial inhomogeneity in the estimated return values and associated uncertainties. Combining different data sets with diverging representations of extreme precipitation can also lead to inconsistencies on local scales (see e.g. Rajulapati et al., 2020). Third, precipitation trends, e.g., due to anthropogenic climate change, can compromise the extreme value statistics. Accordingly, Rajulapati et al. (2020) have shown that precipitation observations typically do not provide a consistent representation of extreme events and that 100-year return values differ significantly between observational data sets. Due to these limitations, previous studies often focused on extreme events with return periods of much less than 100 years (Rodrigues et al., 2020; Donat et al., 2013), for which observational time series are sufficient, and/or specific regions (Rodrigues et al., 2020;

Maraun et al., 2011). Alternatively, model simulations, for instance from weather prediction as in Ch. 2, seasonal forecasts (Kelder et al., 2020) or climate models (Mizuta & Endo, 2020) can provide long time series that allow for a statistically robust estimate also of 100-year return values. Nevertheless, these model-based estimates may of course suffer from other biases due to the imperfect representation of precipitation processes in the models.

In this study, the possibility is explored to use a model-generated data set from ensemble weather prediction for estimating 100-year return values of daily precipitation on a 1°x 1° grid covering the entire globe, extending the previous analysis that focused on European river catchments in Ch. 2. The equivalent length of the weather prediction data set is about 1200 years, that is much longer than the 100-year return period, promoting statistical robustness. Due to the daily accumulation, relatively large spatial scale, and limited model resolution, the studied extreme precipitation events are most relevant for larger-scale river floods and not so much for local flash floods triggered by convective precipitation. The main goal of this study is to compare these model-based 100-year return values to estimates from three different observational data sets and quantify their relative biases and statistical uncertainties. This may provide a basis for using the model-generated data set also for practical estimates of probable maximum precipitation, in particular in data-sparse regions.

The following Sect. 3.2 describes the ensemble weather prediction data as well as three observational data sets that are applied to evaluate the differences between the model-based and observation-based estimates of 100-year return values. In Sect. 3.3, the statistical methods to evaluate the ensemble prediction data and determine return values and confidence intervals are explained in detail. The resulting return values, their confidence intervals and differences to observational data sets are presented in Sect. 3.4. Finally, conclusions and a discussion of the main findings and limitations of this approach are provided in Sect. 3.5.

3.2 Data

In this study, ensemble weather prediction data are used to obtain a large data set of daily precipitation data on a global grid in order to estimate 100-year return values. The resulting estimates are compared to observational data sets obtained from rain gauge measurements and satellites for evaluating the differences between a model-based and an observational approach. All data sets are described in the following.

3.2.1 Ensemble prediction data

An archive of model output from operational forecasts of the ensemble prediction system (EPS) of the Integrated Forecasting System (IFS) by the European Centre for Medium-Range Weather Forecasts (ECMWF) is accessed in order to obtain a large set of simulated, but realistic, daily precipitation data. The IFS is used for all forecasting activities of the ECMWF and is a comprehensive earth system model that combines an atmospheric component with community models for other parts of the earth system (ECMWF, 2023e). More details regarding the IFS and the operational EPS forecasts are described in ECMWF (2023c). Using an operational weather prediction model has the advantage that the model is very well calibrated due to a comprehensive comparison to observations, even though observations of surface precipitation are not assimilated in the associated data assimilation scheme. Nevertheless, the EPS data may suffer from interdependence between the ensemble members, which is investigated in more detail in Sect. 3.3.1, and from temporal inhomogeneities due to updates of the prediction system. The latter as well as additional limitations of the application of ensemble weather prediction data for the approach in this study are discussed in more detail in Sect. 3.5.

Since March 2003, ensemble simulations of the operational weather prediction model are started twice a day, at 00:00 and 12:00 UTC, with forecasting times of at least 10 days. The ensemble contains 51 ensemble members. One member represents a controlled run without any perturbations while the other 50 members represent runs with slightly changed initial conditions between each other and with stochastic perturbations of the model physics. This results in 102 simulations per real day. More information about the workflow of the EPS can be found in Molteni et al. (1996).

The analyses in this study are based on daily precipitation sums, which are computed by adding up the large-scale and convective precipitation over 24 hours. From each simulation, the daily precipitation sum just of the 10th forecast day (accumulated precipitation between the forecast hours 216 and 240, same procedure for every initialisation time) is selected, instead of using all forecast days. This approach follows Ch. 2, in which a daily precipitation data set from the EPS is used to investigate the atmospheric conditions during extreme precipitation events over central Europe, and Breivik et al. (2013), who estimated return values of oceanic surface wave heights from EPS data. The basis of the approach is the assumption that, due to the advanced forecast time, the weather conditions on the 10th forecast day do not significantly correlate with the initial conditions of the specific simulation, such that the different realisations obtained from the ensemble members can be regarded as independent from each other. While the simulations of different ensemble members are strongly correlated to each other in the beginning, due to the dependence on the initial conditions, this correlation weakens with increasing forecast time. This decrease is particularly large for precipitation, compared to, e.g., geopotential height, due to its high temporal and spatial variability and its dependence on smaller-scale processes. In both Ch. 2

and Breivik et al. (2013), a comprehensive statistical analysis is performed to demonstrate the independence of the ensemble members on the 10th forecast day and to evaluate the statistics of daily precipitation and wave height in comparison to observational data. The data set used here is very similar to the data of Ch. 2, except that spatially averaged precipitation time series over central European river catchments are analysed in Ch. 2, while this study uses time series on a spatial grid of 1°x 1° spanning the entire globe. Therefore, just a short statistical evaluation of the ensemble prediction data (see Sect. 3.3.1), adapted to time series at individual grid point, is performed in this study, while it is referred to Ch. 2 for other, more detailed statistical analyses.

The IFS model was updated several times during the years 2003 and 2019, which may influence the simulated precipitation amounts as well as the forecast skill at advanced forecast times. In each new IFS model cycle, mainly small changes have been implemented to continuously improve the forecast skill over the years. Although no large improvements for a specific model cycle can be identified, there are some noteworthy updates that include a new formulation of the humidity analysis (Cycle 26r1), improved precipitation forecasts over Europe (Cycle 32r3) and improved near-coastal precipitation forecasts due to changes in cloud physics (Cycle 45r1). Details of all model cycle changes are described in ECMWF (2023d), while a full documentation of each individual model cycle is available from ECMWF (2023c). In Ch. 2, the influence of these model cycle updates on the daily precipitation time series have been evaluated. There, a systematic decrease of high precipitation percentiles (99th, 99.9th and 99.99th) is demonstrated, which corresponds to extreme precipitation events with large return periods, over central Europe within the first five years of the ensemble simulations (2003-2007). On the contrary, since 2008, the amplitude of these percentiles is rather constant, as discussed in more detail in Sect. 3.3.1. Hence, in order to avoid any temporal inconsistencies within the data set, only the ensemble simulations from the 1st of January 2008 until the 31st of December 2019 are used in this study, following Ch. 2. The restricted time period of 12 years of forecasts from the EPS archive in combination with 102 daily simulations provides a data set with an equivalent length of 1224 years of simulated but realistic daily precipitation events. The data are available on a regular lat–long grid with a changing resolution over time due to model updates. For a consistent analysis and comparison to observational data, they are re-gridded to a uniform resolution of 1°x 1° with the ECMWF interpolation scheme MIR (ECMWF, 2023f).

3.2.2 Observational data sets

One observational data set based on rain gauge measurements (REGEN) and two data sets based on a combination of satellite data and rain gauges (CHIRPS and PERSIANN) are used to compare daily 100-year precipitation return values and their confidence intervals from the EPS forecasts to observations. The observational data sets mainly differ in their covered region, the

type and amount of observations and the interpolation of the data to a regular lat–long grid. All observations are described in the following.

REGEN data

The Rainfall Estimates on a Gridded Network (REGEN) is a daily precipitation observation data set which uses quality controlled rain gauge measurements, spatially interpolated from several large observational precipitation archives, such as the Global Historical Climate Network Daily, hosted by the National Oceanic and Atmospheric Administration, and the Global Precipitation Climatology Centre, hosted by the Deutscher Wetterdienst. More information about this data set are presented in Contractor et al. (2020a). The spatial density of available rain gauges differs strongly between regions. Especially Africa and central Asia have a low station density compared to rather high station densities over North America, Europe and Australia. The data set also provides the standard deviation of the precipitation sums and the number of rain gauges, but in this study, only the daily precipitation sums (Version 1-2019) are used. The precipitation sums are based on around 135.000 stations and are available from the 1st of January 1950 until the 31th of December 2016 on a regular lat–long grid with a spatial resolution of 1°x 1° for all global land areas, except for Antarctica.

CHIRPS data

The Climate Hazards Group Infrared Precipitation with Stations (CHIRPS) data archive is a quasi-global, daily precipitation data set, hosted by the U.S. Geological Survey Earth Resources Observation and Science Center in collaboration with the Santa Barbara Climate Hazards Group at the University of California. The CHIRPS data result from a combination of quasi-global geostationary thermal infrared satellite observations from two sources of the National Oceanic and Atmospheric Administration, in situ precipitation observations obtained from a variety of national and regional meteorological services, the Tropical Rainfall Measuring Mission product from NASA, a monthly precipitation climatology and atmospheric model rainfall fields from NOAA. A more detailed description of the development workflow of the CHIRPS data can be found in Funk et al. (2014a). The data are available from the 1st of January 1981 until the 31th of December 2021 over land areas on a regular lat–long grid between 50°S and 50°N. In this study, the CHIRPS data (Version 2.0) with a spatial resolution of 0.25°x 0.25° are selected and interpolated (averaged over several 0.25° boxes) to a 1°x 1° grid for further analyses.

PERSIANN data

The Precipitation Estimation from Remotely Sensed Information using Artificial Neural Networks–Climate Data Record (PERSIANN-CDR), hosted by the Center for Hydrometeorology

and Remote Sensing at the University of California, are satellite based, daily precipitation observations. This data sets results from gridded satellite infrared data, obtained from a combination of several international geostationary satellites, in combination with an artificial neural network training using hourly precipitation data from the National Centers for Environmental Prediction stage IV. Additionally, the monthly product of the Global Precipitation Climatology Project is used for bias adjustments. Further details on this data set are described in Ashouri et al. (2015b). The daily precipitation sums of this data set (Version 1) are available from the 1st of January 1983 until the 31th of December 2021 on a regular lat–long grid between 60°S and 60°N with a spatial resolution of 0.25°x 0.25°. In this study, the data are interpolated to a 1°x 1° grid for further analyses. Missing values in the data set appear in cases when satellite data are not available and on dry days when no precipitation occurred (see Supplementary Fig. B.1). As an under-representation of dry days strongly influences the quantile distributions of the data (used for evaluations in Sect. 3.3.1), all missing values are set to 0 for further analyses, in order to improve the representation of the percentiles. However, this also leads to errors over areas that are regularly affected by non-availability of satellite data. Especially at around 50°N and 70°E as well as 50°S and 70°E this is most dominant, which is why these areas should be taken into account when interpreting the results from the PERSIANN observations.

3.3 Methodology

In this section, statistical analyses of the suitability of the EPS data for determining 100-year precipitation return values on a global grid are presented. Subsequently, the method to determine the return values and their confidence intervals is described.

3.3.1 Statistical evaluation of the ensemble prediction data

The suitability of the EPS data at the 10th forecast day has to be evaluated in order to consider these data as realistic and independent realisations of daily precipitation and to determine 100-year return values from this large data set. Following Ch. 2 and Breivik et al. (2013), it has to be evaluated if (1) the ensemble members can be considered as independent from each other, (2) each ensemble member properly represents the statistical distribution of daily precipitation compared to observations and (3) no significant trend of the high precipitation percentiles can be identified over time. These criteria are statistically evaluated and discussed in the following based on time series of daily precipitation sums on the 10th day of each forecast and at each global grid point. This spatial coverage is the main difference between this study and Ch. 2, in which time series of spatially averaged precipitation in several central European river catchments have been analysed.

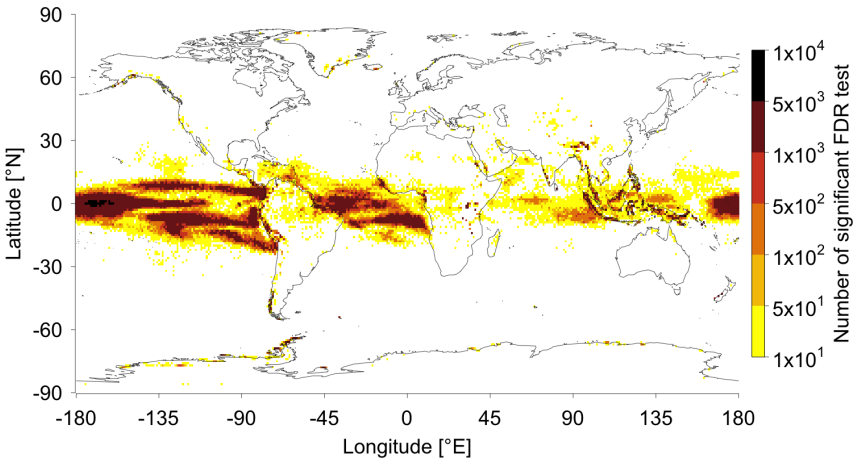

Figure 3.1: Number of statistical significant correlation coefficients per grid point, obtained from the FDR tests of Benjamini and Hochberg (1995), as described in Ventura et al. (2004), applied to multiple (5152) p values associated with the Pearson correlations between yearly maxima time series of individual ensemble members. Mind the logarithmic colour scale.

In order to evaluate the independence of the daily precipitation sums at the 10th forecast day between ensemble members, the statistical distribution of Spearman correlation coefficients between all possible ensemble member combinations (5151 in total) for time series of both all daily precipitation sums and annual maxima (which are used to determine the 100-year return values, see Sect. 3.3.2) have been analysed in Ch. 2. There, it is shown that the entire daily time series are weakly, but still significantly, correlated between the ensemble members (mean correlation around 0.19, similar for all river catchments). Time series of yearly maxima of daily precipitation sums are generally very weakly correlated as well (mean around 0), but there is almost no significant correlation identified, supporting the assumption that daily extreme precipitation is independent between ensemble members. Here, this correlation analysis is expanded to the global grid. Following Ch. 2, statistical significance with multiple correlation coefficients can be evaluated by applying the False Discovery Rate (FDR) test of Benjamini and Hochberg (1995), as described in Ventura et al. (2004), to an entire sample of p values, associated with the correlation coefficients of all ensemble member combinations at each grid point. Figure 3.1 shows the number of statistically significant correlation coefficients from the FDR test for time series of annual maximum daily precipitation at each global grid point. For most of the grid points, (almost) no significant correlations are found, especially poleward of 20°N and 20°S, supporting the hypothesis that annual maximum precipitation events are independent between ensemble members on a global scale. However, there are certain areas over the tropical oceans, the Maritime Continent and southeast Asia, where FDR tests show high numbers of significant correlation coefficients. In these regions, there is thus a high interdependence of extreme precipitation events in the ensemble members, and the EPS data set cannot be considered as equivalent to a time series of 1224 years in the analysis of 100-year return values. A likely reason for this interdepen-

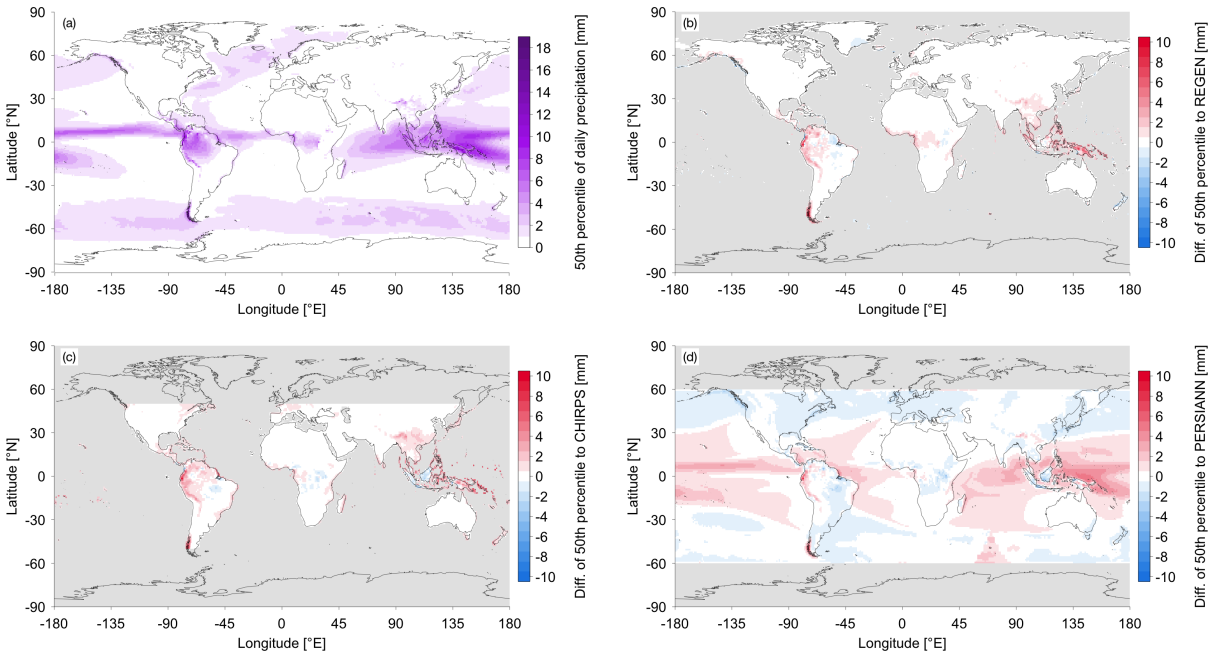

Figure 3.2: Global distribution of the 50th percentile of daily precipitation from **(a)** the EPS data and their difference to the observational data sets **(b)** REGEN, **(c)** CHIRPS and **(d)** PERSIANN. Areas where the observational data are not available are shown in light grey.

dence is the influence of internal climate modes with relatively long time scales, such as the El Niño-Southern Oscillation, on tropical precipitation events, which can lead to a synchronisation of annual maxima between ensemble members.

To evaluate the statistical distribution of daily precipitation, quantiles from the EPS data to three observational data sets (REGEN, ENSEMBLES daily gridded observational dataset for precipitation, temperature and sea level pressure in Europe (E-OBS) and Hydrometeorologische Rasterdaten (HYRAS)) are compared in Ch. 2 and a good agreement in the central European river catchments is found. For a similar analysis on the global scale, the 50th and 90th percentiles at each grid point is selected. Note that all days of a time series, including dry days, are considered for determining these percentiles (Pfleiderer et al., 2019). Figure 3.2 shows the 50th percentile (median) from the EPS data (taking all members together) in (a) and the differences to the observational data in (b-d). Higher median precipitation amounts of EPS data can generally be found over the oceans while the highest values lie within the tropics, in the area of the Intertropical Convergence Zone (ITCZ). Over the extratropical continents, due to a relatively high number of dry days, the median of daily precipitation is mostly below 1 mm. The differences of the 50th percentile to the REGEN and CHIRPS data set indicates a relatively good agreement over most continental regions (see Fig. 3.2b,c). Larger differences are obtained in the tropics, in particular over the northern part of South America, the Maritime Continent and part of southeast Asia, where the 50th percentile of the EPS data is up to 8 mm higher than for both observational

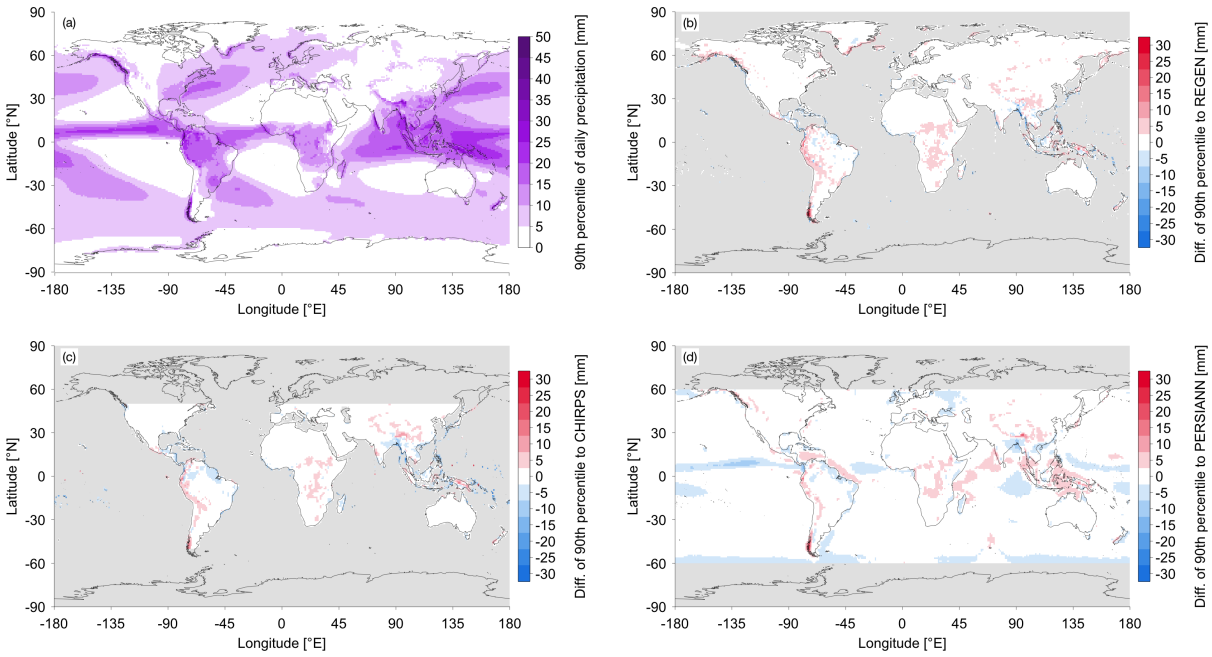

Figure 3.3: As Fig. 3.2, but for the 90th percentile.

data sets. The differences to the PERSIANN observations show a similar pattern over continental areas (see Fig. 3.2d), however, also revealing that the 50th percentile of the PERSIANN data is slightly higher (by 1 mm) over North and South America and Europe compared to the EPS data. Larger differences are found over the tropical and extratropical oceans with a higher median in the EPS data by 1 to 3 mm and up to 5 mm over the tropical West Pacific. Similar results are obtained for the 90th percentile (see Fig. 3.3). Most of the differences to the REGEN and CHIRPS observations (see Fig. 3.3b,c) are close to 0, however, larger differences are found over Africa, the west coast of South America (overestimation of up to 10 mm) and southeast Asia (under- and overestimation of up to 20 mm). The differences to the PERSIANN data show a very similar pattern over the continental areas (see Fig. 3.3d). Additionally, the differences over the oceans are also very small, except some minor over- and underestimations in the tropics by around 5 mm. All together, this analysis shows that the EPS data realistically represent daily precipitation statistics in most regions of the globe, with some larger biases over the tropics and a few high-altitude regions, e.g., in South America. In Ch. 2, the precipitation statistics between ensemble members have also been compared, but as no systematic differences are found, this analysis is not repeated here.

Stationarity of the time series is important for applying the extreme value analysis described in Sect. 3.3.2. To evaluate the stationarity of the EPS data, the Mann-Kendall test have been applied to several high percentiles and the yearly number of 100-year precipitation events for the years 2008 to 2019 in Ch. 2, and the yearly occurrences of such events in each individual catchment have also been compared to a Poisson distribution of independent events with a constant mean

rate. No indication of temporal non-stationarity in this period of 12 years has been found. Here, the same Mann-Kendall test is applied to the 99.9th percentile of daily precipitation (representing an almost 3-year precipitation event) at all global grid points (see Supplementary Fig. B.2). In order to evaluate the statistical significance of these multiple tests, again the FDR test is applied as introduced earlier. No significant trend is found for the EPS data. For the observational data sets, also due to the longer time series covering 39 years or more, some areas are associated with significant trends, rather evenly distributed over the globe (for REGEN, 8.4% of grid points with significant trends), over central Africa and central Asia (for CHIRPS, 2.4% of grid points with significant trends) or India and the Indian Ocean (for PERSIANN, 3.4% of grid points with significant trends). Nevertheless, trends are still not significant over the most part of the globe. In order to use a consistent methodology for all data sets and locations, thus, the stationarity assumption also for the observational time series is made.

In summary, the analyses show that, in most regions, daily precipitation obtained from different members of the ECMWF EPS can be considered as statistically independent. Exceptions are some areas over the tropical oceans and Maritime Continent (see again Fig. 3.1). Additionally, the model data realistically represent different quantiles of daily precipitation in comparison to three observational data sets (see Figs. 3.2 and 3.3), again with the exception of a few regions mostly in the tropics. Finally, there is no indication of non-stationarity in the data set over the time frame analysed here. Thus, the EPS data are considered to be suitable for a global analysis of 100-year return values of daily precipitation.

3.3.2 Determination of return values and confidence intervals

To determine 100-year return values of daily precipitation and their confidence intervals at each grid point, the daily precipitation sums from all ensemble members are used to build long time series. The block maximum approach from extreme value statistics is applied (see Coles et al., 2001) with yearly blocks, which results in 1224 block maxima at each location. The yearly block size is large enough to fulfil the Fisher-Tippett theorem, such that a generalised extreme value distribution (GEV) is fitted to the block maxima by the maximum likelihood approach. To obtain the best fit of the GEV, the location (μ), scale (σ) and shape (ξ) parameters are estimated. Following Stephenson (2002), the return value v can be computed from these estimated parameters by the following equation:

$$\begin{aligned} v &= \mu + \sigma \cdot \frac{(x^{\xi} - 1)}{\xi} \\ x &= \frac{-1}{log(1 - \frac{1}{p})} \end{aligned} \tag{3.1}$$

in which the specific return period in years in denoted by p. The confidence intervals of the return values are obtained through bootstrap resampling (see Coles et al., 2001). From the original set of block maxima, a new set of maxima is drawn with replacement. Then, the GEV is fitted to the new set of block maxima and the return value is again determined from Eq. (3.1). This procedure is repeated 1000 times, leading to 1000 different return values from which the 0.025 and 0.975 quantiles are used as confidence intervals.

At some grid points with very low precipitation amounts during the entire year (e.g., over the Sahara Desert), the best fit of the GEV yields very high estimates of the shape parameter ξ (up to 3). This results in extraordinary high return values compared to neighbouring grid points with low return values. Papalexiou and Koutsoyiannis (2013) analysed estimated shape parameters from GEV fits for over 15.000 globally distributed observational records, using yearly maxima of daily precipitation as block maxima as well. Even for rather short time series of at most 10 years, which are often associated with higher shape parameters than longer time series, the shape parameters all lie between -0.6 and 0.6, independent of their location. However, almost no time series of their observational data set are located in very dry regions such as the Sahara Desert. In order to prevent unrealistic high or low return values but still allow shape parameters outside the range of -0.6 and 0.6 for areas that are typically not covered by observations, grid points with estimated shape parameters below -1 or above 1 and scale parameters below -70 or above 70 are excluded from the analyses in this study.

3.4 Results

In this section, the estimated 100-year return values of daily precipitation and their confidence intervals are presented. Estimates from the EPS data are compared to the observational estimates based on REGEN, CHIRPS and PERSIANN.

3.4.1 Return values

Global estimates of 100-year return values of daily precipitation from the EPS data set are shown in Fig. 3.4a. Generally, higher return values can be found in tropics and parts of the subtropics, while return values decrease towards the poles. The return values range from 0.98 mm over Antarctica up to 985.36 mm over the Arabian Sea, near the southeast coast of the Arabian Peninsula. The area of the Arabian Sea generally shows the highest return values, ranging from 600 mm to 900 mm, followed by parts of India, the Himalayas, southeast Asia and the ITCZ regions of the Atlantic and Pacific Ocean with return values of 400 mm to 600 mm. Return values of about 300 mm are found for most other parts of the tropical and subtropical oceans, the northern part of South America, the region south of the Sahel and northern parts of Australia.

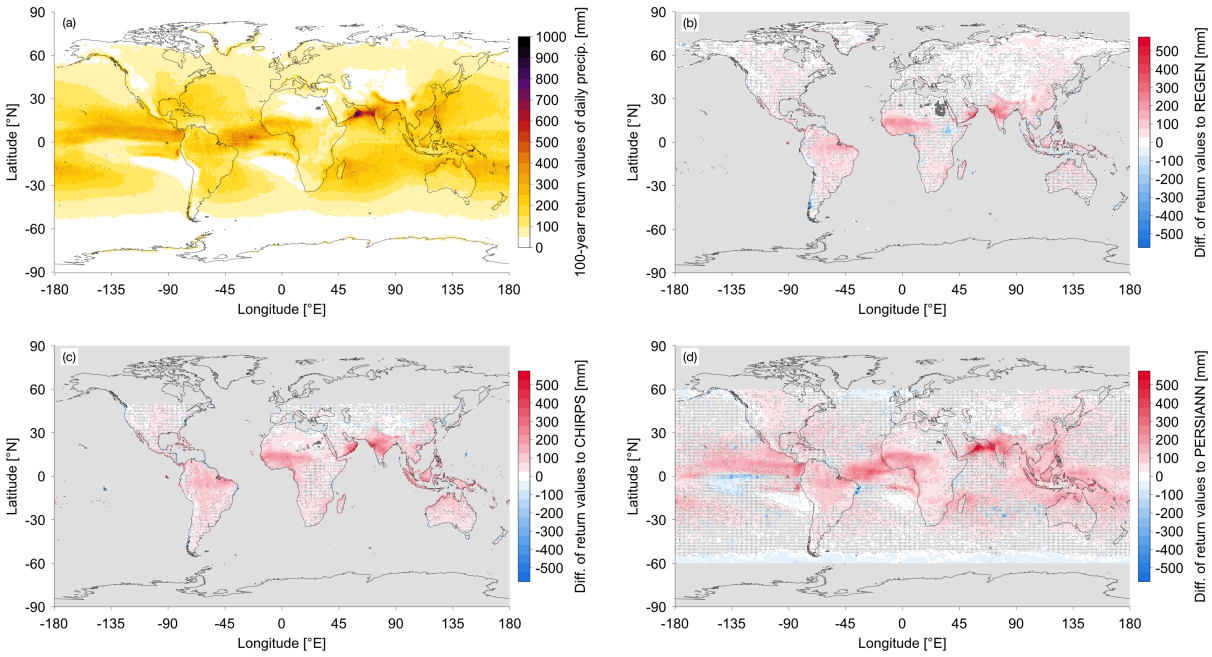

Figure 3.4: **(a)** Global distribution of 100-year return values of daily precipitation, estimated from EPS data, and their difference to the observational estimates from **(b)** REGEN, **(c)** CHIRPS and **(d)** PERSIANN. Areas where the observational data are not available are shown in light grey. Dark grey shading indicates grid points for which the GEV parameters are outside the allowed range and thus no return values can be estimated. Stippling in **(b)**-**(d)** shows where the confidence interval of the EPS data overlaps with the confidence interval from the specific observational data set.

North America, Europe and northern Asia are associated with return values of around 100 mm, while a 100-year event over most regions poleward of 60°N and 60°S does not exceed 50 mm. Typical dry regions such as the Sahara Desert and the Tibetan Plateau are also associated with very low 100-year return values.

A 100-year daily precipitation event over the southeast coast of the Arabian Peninsula would exceed the local annual mean precipitation by a factor of seven or higher (see Fig. 3.5). Very high exceedances of the annual mean can also be found over certain oceanic regions near the west coasts of Africa, North and South America and over regions with low return values such as the Sahara Desert and the Taklamakan Desert. A 100-year extreme event over Australia would contribute about 20% to 60% (depending on the region) to the annual mean, while this percentage typically ranges around 10% for most of the other continental areas such as North and South America, Europe, central and southern Africa and Asia.

A comparison with the observational data set REGEN shows generally higher EPS estimates over large parts of the globe and very large differences in several tropical and subtropical regions (Fig. 3.4b). The 100-year return values from the EPS data are clearly higher over the southeast

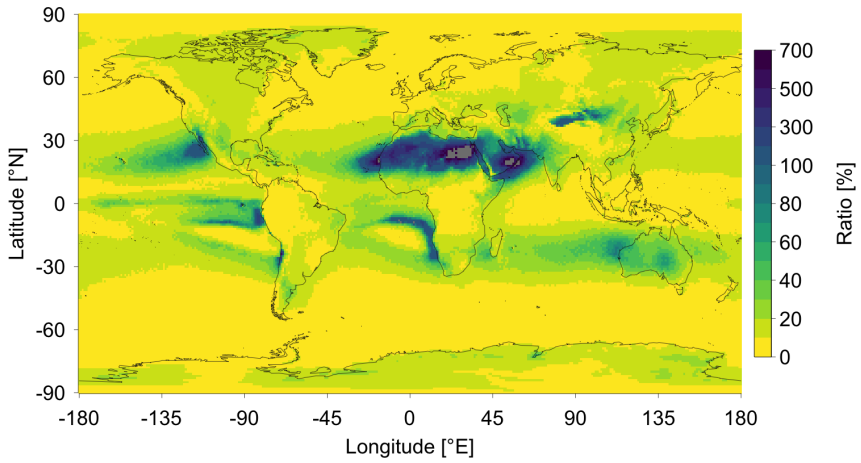

Figure 3.5: Ratio between the precipitation amount of a 100-year event of daily precipitation and the annual mean precipitation from the EPS data in %. The annual mean precipitation is averaged over all ensemble members and over the years 2008 to 2019. Mind the non-linear colour scale. Values above 700% are shown in grey.

coast of the Arabian Peninsula (by 300-500 mm), India (by 100-400 mm), western Africa (by 100-300 mm) and over the Amazon (by 100-200 mm). Additionally, the confidence intervals of the EPS data do not overlap with the REGEN data in these regions, the differences are thus statistically significant. Over other parts of South America, the southern half of Africa, southeast Asia and Australia, the EPS estimates are about 50-100 mm higher, but the confidence intervals overlap in parts of these areas. Most other regions do not show large differences in the estimated return values. However, especially over parts of Chile, the Abyssinia Plateau in east Africa and over some coastal areas in southeast Asia, the EPS data are associated with lower return values than the REGEN data (no overlap of confidence intervals). Overall, the confidence intervals of EPS and REGEN return value estimates overlap at 50.4% of the grid boxes. The differences of EPS return values to the CHIRPS and PERSIANN observational estimates (Figs. 3.4c,d) are very similar to each other. The confidence intervals of EPS and CHIRPS overlap at 45.1% of the grid boxes, and for EPS and PERSIANN this overlap is 55.9%. Furthermore, the CHIRPS and PERSIANN results are mostly consistent with the differences to the REGEN estimates described above. However, the strongly negative differences over Chile and the Abyssinia Plateau do not occur for the CHIRPS and PERSIANN data. Additionally, the positive differences over the Arabian Peninsula, India, southeast Asia and Australia are even larger. In the comparison with PERSIANN, also oceanic regions can be considered. In particular in the ITCZ region, around Madagascar and over the eastern Indian and western Pacific Ocean, the EPS data produce higher return values than PERSIANN. There are also some negative differences over the tropical Pacific, the most eastern tip of the Brazilian coast and for most areas poleward of 50°N and 50°S. It should be kept in mind here that, over parts of the tropical oceans, the EPS estimates are less trustworthy than in other regions due to methodological issues associated with interdependence between the ensemble members (see again Sect. 3.3.1).

3.4.2 Confidence intervals

Confidence intervals (CIs) on a 95% level are determined for each return value estimate. To compare the confidence interval ranges (that is, the difference between upper and lower bounds) between data sets, on the one hand, in Fig. 3.6 they are shown relative to the corresponding return value estimate, as higher return values are typically associated with larger confidence intervals. In this way, the relative uncertainty of the 100-year return values is quantified. On the other hand, Fig. 3.7 shows the absolute confidence interval ranges, quantifying the absolute uncertainties.

The largest relative uncertainties are found in tropical and subtropical regions. Especially over the Sahara Desert, the southeastern part of the Arabian Peninsula and some areas over the tropical Pacific and Atlantic Ocean, the relative CIs range from 30% to 80% (see Fig. 3.6a). However, there is no clear pattern that higher CI ranges predominantly occur over regions with particularly high or low return values. For instance, high relative uncertainties are found in the dry Sahara Desert, but also over the wet Arabian Sea. Over most other parts of the tropics and subtropics, the range of the CIs lies between 10% and 30%. Poleward of 30°N and 30°S, the relative CI ranges are typically around 10%. As mentioned before, higher return values are associated with higher CIs, as shown by the absolute values in Fig. 3.7a. The tropics and several subtropical areas have the highest absolute CI ranges, especially over the Arabian Sea (up to 400 mm) and the tropical Pacific and Atlantic (100 to 300 mm). Absolute CIs over North America, Europe and northern Asia, typically lie around 10 mm.

The differences of the relative CI ranges between the EPS and REGEN data sets are shown in Fig. 3.6b. Over almost all continental areas, the relative uncertainties are reduced in the EPS data compared to CHIRPS, with typical differences on the order of 50-100 p.p.. Over specific regions such as the west coast of South America, the Sahara Desert, the Arabian Peninsula and Greenland, this decrease is even larger (-200 to -800 p.p.), while the CIs mainly overlap with each other in these regions. A slight increase in the relative uncertainty by around 10 p.p. is found for some grid points over the Amazon, west Africa, India and China. In terms of absolute CI ranges (Fig. 3.7b), the uncertainty is reduced in the EPS data compared to REGEN by up to 300 mm over southeast Asia and Australia and around 50 mm over North America and Europe. Note that this corresponds to a reduction by at least a factor of two, that is a substantially reduced uncertainty, in most regions. There are a few more extended (compared to the relative CI ranges) areas of larger absolute uncertainties in the EPS data over the Amazon, west Africa and India with increases of 20 to 100 mm. These are also regions where the CIs do not overlap.

Similar results are found for both relative and absolute uncertainties taking the CHIRPS data for comparison. The relative CI range is smaller in the EPS data over almost all regions (Fig. 3.6c), and the magnitude of this reduction is typically even larger (around -100 p.p.) than for REGEN, except for the Sahara Desert. Differences in the absolute uncertainty compared to CHIRPS are

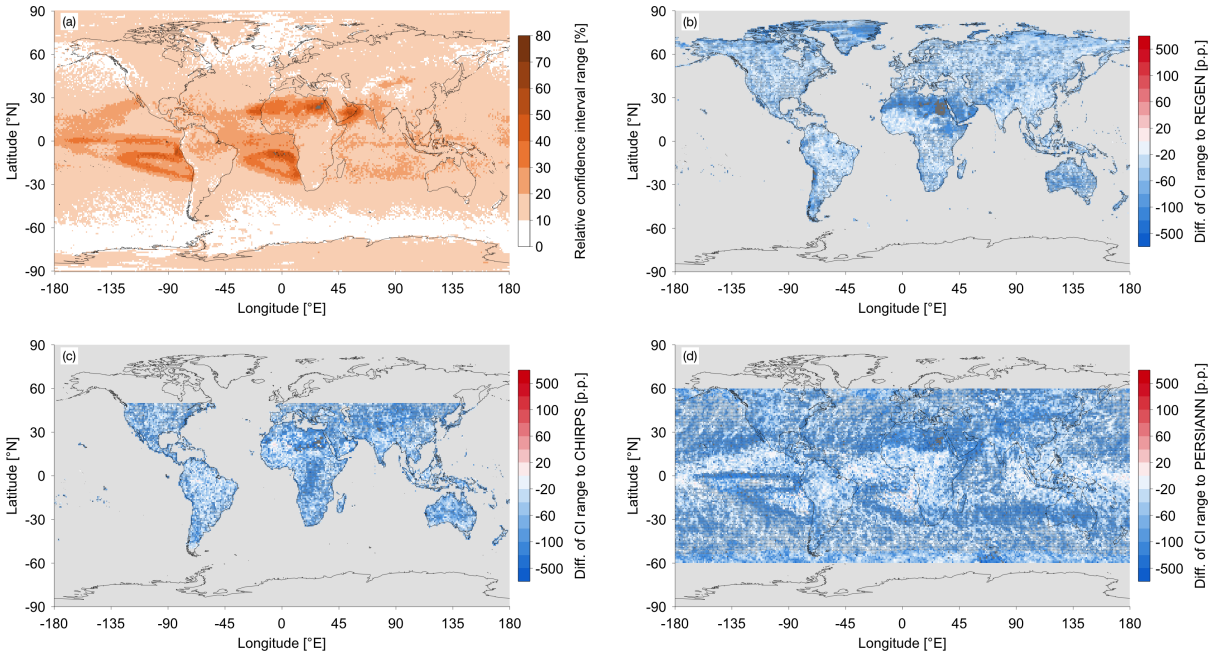

Figure 3.6: **(a)** Global distribution of the relative range of confidence intervals on a 95% level, relative to the associated return values, and their differences to the observational estimates from **(b)** REGEN, **(c)** CHIRPS and **(d)** PERSIANN. Areas where the observational data are not available are shown in light grey. Dark grey shading indicates grid points for which the GEV parameters are outside the allowed range and thus no return values can be estimated. Stippling in **(b)**-**(d)** shows where the confidence interval of the EPS data overlaps with the confidence interval from the specific observational data set. Mind the non-linear colour scales. In **(b)**-**(d)**, only values between -700 and 700 p.p. are displayed.

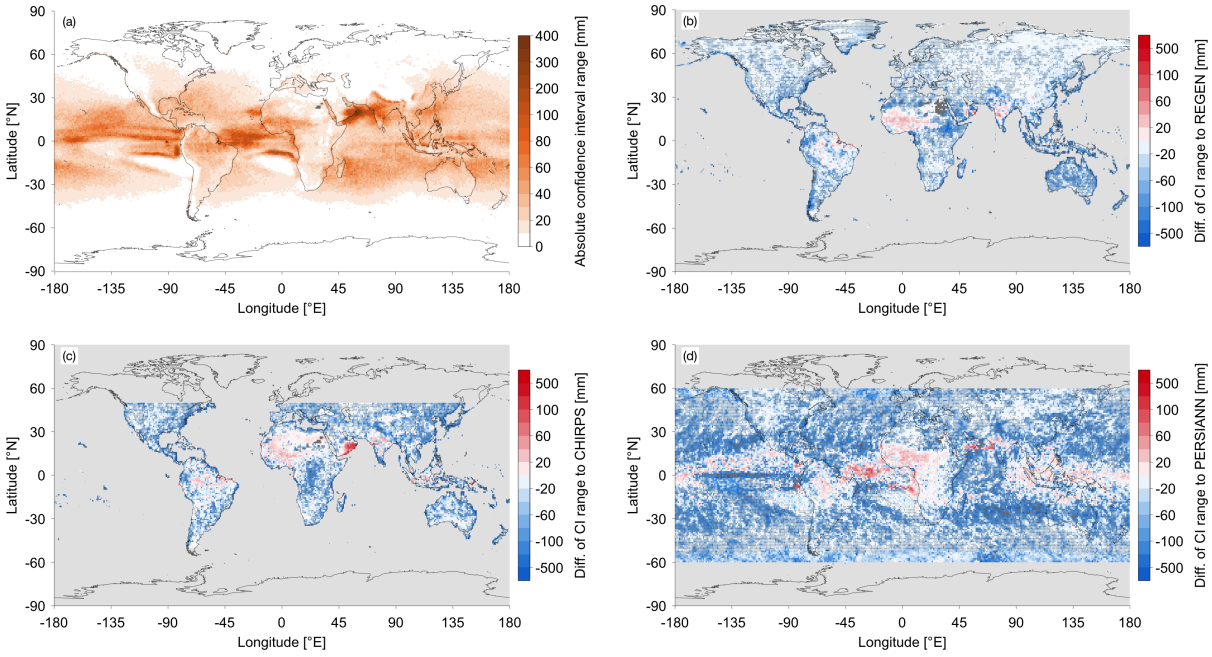

Figure 3.7: As Fig. 3.6, but for the absolute range of confidence intervals in mm.

again similar as for REGEN, but with a more enhanced and broader increase in the southeast of the Arabian Peninsula of up to 400 mm (Fig. 3.7c). Finally, the uncertainty in EPS is also reduced compared to PERSIANN, with similar patterns over the continents as for REGEN and CHIRPS (Fig. 3.6d). In addition, a reduction of relative CI ranges with a similar magnitude (around -100 p.p.) is also found over most oceanic regions, where CIs still overlap in the extratropics, but less so in the tropics. Some of these tropical regions with significant differences between the EPS and PERSIANN estimates of 100-year return values are associated with a larger absolute uncertainty in the EPS data by around 50 mm and up to 300 mm over the tropical Atlantic (Fig. 3.7d). Note that such a co-occurring increase of absolute uncertainty and decrease in relative uncertainty is linked to substantially higher return value estimates in the EPS data.

3.5 Discussion and conclusion

The aim of this study has been to determine 100-year return values of daily precipitation and their confidence intervals (CIs) on a global scale from a large data set of model-generated events and to evaluate the differences to three observational data sets (REGEN, CHIRPS and PERSIANN). A quantification of such extreme return values is crucial for properly setting up flood protection measures and, hence, reduce flood risks, also because such extreme events are expected to occur more frequently in a warmer climate. The large set of simulated global daily precipitation fields has been obtained from operational ensemble weather prediction data by the ECMWF, following the approach of Ch. 2 and Breivik et al. (2013). The statistical analyses of this study show that, when using the 10th forecast days from these simulations, annual precipitation maxima are independent between the different ensemble members in most regions, except for the tropical oceans and the Maritime Continent, where the results are thus less trustworthy. Biases in the climatological distribution of precipitation with respect to the observational data sets, evaluated through the 50th and 90th percentile, are also relatively small in most regions. Additionally, there is no significant trend in the occurrence of intense precipitation over the 12 years at all grid points, and the EPS data can thus be considered as stationary in time. With the help of extreme value statistics, 100-year return values and the associated confidence intervals on a 95% level are determined and compared to estimates from the observational data sets.

Based on these EPS data, the largest 100-year return values of daily precipitation occur in the tropics with a maximum around 950 mm (absolute CI range of 400 mm) over the Arabian Sea near the coast of the Arabian Peninsula. The return values decrease towards the poles with a minimum only slightly above 0 mm over parts of Antarctica. Over India, the Himalayas and the tropical Pacific and Atlantic, 100-year events are associated with precipitation amounts around 500 mm (absolute CI range around 200 mm), while for Australia, Africa, South America and the subtropical oceans they typically amount to about 200 mm (absolute CI range around 50 mm).

The return values over North America, Europe and central Asia lie mostly between 50 and 100 mm (absolute CI range of 10 mm). Over continental areas, a 100-year event would typically amount to about 10-20% of annual mean precipitation (20-50% for Australia), but in dry regions such as the Sahara Desert and Arabian Peninsula the estimated 100-year return value even exceed the annual mean precipitation by a factor of up to 7. The 100-year return values from the EPS data are in general agreement with other studies of multi-year precipitation extremes. For instance, Rodrigues et al. (2020) determined 10-year return values for Brazil and found slightly lower values and a local maximum of 200 mm further towards the east coast. Gründemann et al. (2023) studied 100-year return values over global land areas based on several statistical approaches and a data set obtained from a combination of satellite observations, reanalyses and gauge data. They found similar spatial patterns as documented here, but lower return values over, for instance, the Sahel, the east coast of the Arabian Peninsula and parts of India. Also the comparison with the observational data sets in this study indicates systematically higher return values in the EPS data set over most of the globe. In many regions, in particular in the extratropics, the confidence intervals of EPS and observational estimates still overlap. Larger, also statistically significant differences are obtained in some tropical regions where the EPS method is less robust due to interdependence of ensemble members and/or general biases in the precipitation climatology, but also over other areas where the data set performs well in the statistical evaluation, such as parts of northeastern South America, western tropical Africa, India and eastern China. This might be due to model deficiencies, e.g., in the representation of convective precipitation in the tropics, but may also point to a systematic underestimation of very extreme daily precipitation events in observations due to the relatively short time series and thus limited sampling. Such a potential underestimation might have important consequences for practical applications and should be considered in estimates of "probable maximum precipitation" for designing flood protection measures.

The relative uncertainty of the 100-year return values is quantified through relative confidence interval ranges, which typically lie within 10-30% for most of the regions, but can be higher than 50% over the Sahara Desert, the Arabian Peninsula and parts of the tropical and subtropical Pacific and Atlantic. An important result is that these relative uncertainties, and in most regions also the absolute CI ranges, are substantially reduced in the EPS data compared to observational estimates. This reduction is typically on the order of 50-100 p.p., but can locally amount to up to 600 p.p., e.g., over the Sahara Desert and the Arabian Peninsula. The systematic and substantial reduction of statistical uncertainty is due to the much longer time series and is the main advantage of the model-generated EPS data.

The approach in this study to estimate 100-year precipitation return values from EPS data has several limitations, as also discussed in Ch. 2. First, the model-generated precipitation data may be affected by model biases and the imperfect representation of specific processes in the model. Such biases are assumed to be particularly large for small-scale, convective precipitation events,

which is one reason why this study focuses on larger-scale events on a 1°x 1° grid. Second, the time span of the forecast data is limited to 12 years (2008-2019) which comes along with a limited sampling of large-scale boundary conditions. Therefore, not the entire range of (multi-)decadal variability of the climate system is reproduced in the data set. Third, there is a certain influence of anthropogenic forcing in the data set in specific regions, as mentioned in Sect. 3.3.1, which can lead to temporal inhomogeneities. However, the trend analyses shows that this is mainly restricted to a few areas over tropical and subtropical oceans. Fourth, the method does not work well in regions where the ensemble members are not independent from each other, which is mainly the tropical oceans and the Maritime Continent.

In future research, the approach used here may be applied for events with different return periods and also to other weather prediction ensemble data set, which may help clarifying the reasons for the systematically higher return values in the EPS data compared to observations. Finally, large initial condition ensemble simulations with climate models may be used to investigate the influence of climate warming on 100-year precipitation events.

Chapter 4

How do very extreme daily precipitation events over central European river catchments change in a warmer climate?

4.1 Introduction

Central European river catchments have regularly been affected by flooding events in the last few decades. The Rhine flood in June 2021, the Berlin metropolitan flood in June 2017 and the central European flood in June 2013, during which several river catchments were affected, are just a few outstanding events. They resulted in devastating damages to the socioeconomic system, especially in highly populated areas. During the Rhine flood in 2021, several people lost their lives or got injured, several buildings and small villages were destroyed and properties were not available for a long time (Korswagen et al., 2022; Schüttrumpf et al., 2022), as a result of spatially extended precipitation above 200 mm and peak discharges of about 1000-1300 m^3/s at the Altenahr gauge (Lehmkuhl et al., 2022; Kreienkamp et al., 2021). The flooding event in 2017 resulted in total losses of around EUR 60 million, which made this event the costliest natural hazard over the Berlin metropolitan area between 2002 and 2017 (Caldas-Alvarez et al., 2022). Several basements were flooded and infrastructure was disrupted due to large-scale inundation from precipitation amounts of up to 196 mm in 24 hours over the Berlin metropolitan area (Caldas-Alvarez et al., 2022). Although previous improvements in flood protection reduced the socioeconomic losses during the central European flood in 2013, still record-breaking water levels of 12.75 m were measured by several gauges in the German city Passau (Merz et al., 2014). As

these flooding events are often associated with large-scale extreme precipitation in the vicinity of the flooding, early and precise forecasts of such extreme precipitation are crucial for predicting flooding events and producing reliable warnings to the society.

In order to improve the forecasts of extreme precipitation events and reduce potential risks for the society, an accurate understanding of the atmospheric processes is of high importance. Based on previous studies, extreme precipitation events over central Europe are often associated with quasi-stationary mid-latitude cyclones that last for one up to a few days (Mohr et al., 2023; Caldas-Alvarez et al., 2022; Grams et al., 2014; Ulbrich et al., 2003). Such surface cyclones are often linked to upper-level troughs or cut-off lows over western or central Europe (Caldas-Alvarez et al., 2022; Lehmkuhl et al., 2022), and are also particularly strong when an upper-level cut-off low is identified (Hofstätter et al., 2018). Intensified extreme precipitation is typically associated with an intensification of the surface cyclone as a result of intensified advection of moist air and lifting processes (Messmer et al., 2015). Additionally, they regularly originate from "Vb" weather situations, in which surface cyclones develop over the western Mediterranean and move northeastward towards central Europe (van Bebber, 1891). However, just 23% of Vb events are linked to extreme precipitation over central Europe (Messmer et al., 2015), showing that just the existence of a Vb event can not only explain most events. As mentioned before, the quasi-stationarity of the surface cyclone is also important as a slow propagation can lead to a higher total amount over the target area. Blöschl et al. (2013) have shown that the stationarity can be increased by the presence of a blocking anticyclone over the North Atlantic and/or over western Russia, as it was the case during the flooding event over central Europe in 2013. In addition, orographically induced lifting of air masses along mountains can increase the precipitation amount even more (Grams et al., 2014; Blöschl et al., 2013; Ulbrich et al., 2003). All the previously mentioned atmospheric characteristics are related to large-scale (partly meso-scale) dynamical processes. However, thermodynamic processes do also play an important role. Historical extreme precipitation events over central Europe show a very high frequency during the summer season, which is also found for extreme precipitation events with even higher return periods (up to 100 years), obtained from ensemble weather prediction data of Ch. 2. The higher temperatures facilitate the evaporation of moisture into the atmosphere from several water sources such as the North Atlantic and Mediterranean (Blöschl et al., 2013; Ulbrich et al., 2003) as well as from continental areas such as central and eastern Europe (Caldas-Alvarez et al., 2022; Grams et al., 2014). Therefore, the combination of dynamic and thermodynamic processes is necessary for a holistic analysis of extreme precipitation events.

Observational records show that precipitation extremes intensified and increased in frequency within the last decades, confirming also results from multi-model simulations a few decades ago (Myhre et al., 2019; Fischer & Knutti, 2016, 2014; Madsen et al., 2014). The importance of estimating changes in the intensity of extreme precipitation events with global warming may also be increasing within the next decades as previous studies have shown that extreme precipitation

in future climate projections increase in their intensity and frequency (Gründemann et al., 2022; Myhre et al., 2019; Ban et al., 2015; Muller et al., 2011; O'Gorman & Schneider, 2009), also for large parts of central Europe (Nissen & Ulbrich, 2017; Madsen et al., 2014; Collins et al., 2013; Feldmann et al., 2013). For example, Collins et al. (2013) analysed multi-model CMIP5 projections for the end of the century and found that extreme precipitation over central Europe significantly increases by about 10-15% for 5-day annual maximum precipitation and 2.5-5.0%/K for 20-year return values, although the seasonal mean precipitation shows both in- and decreases (depending on the season), often within the range of internal variability. With an intensification of extreme precipitation, flood intensities also increase (Tabari, 2020). A better understanding of the underlying processes that lead to these intensified precipitation events in a warmer climate is, hence, indispensable. Previous studies have shown that changes of extreme precipitation can be decomposed into dynamic (change of atmospheric motion) and thermodynamic (change in atmospheric moisture content) contributions (Pfahl et al., 2017; Emori & Brown, 2005). Pfahl et al. (2017) decomposed daily extreme precipitation from global climate-model simulations and showed that thermodynamic contributions would globally lead to a homogeneous increase of about 3-9%/K. At least for the extratropics, this is overall in line with the expected precipitation intensification from the Clausius-Clapeyron equation of about 6-7%/K (Ban et al., 2015; O'Gorman, 2015; Emori & Brown, 2005), relating the change in saturation vapour pressure to the surface temperature. As warmer air masses can contain more water vapour, the precipitation intensity is also expected to increase at that rate, because more atmospheric moisture can precipitate. Hence, the thermodynamic contribution is rather well understood but the dynamic contribution modifies the extreme precipitation on a regional scale, either by amplifying or weakening the increases from the thermodynamic contribution (Tandon et al., 2018; Emori & Brown, 2005), by regionally about 10%/K or more (Pfahl et al., 2017). In addition, the dynamical influence is particularly large over orographically complex terrain (O'Gorman, 2015), which is partly the case in central Europe. Taking all these results into account, changes in extreme precipitation on a regional scale depend on both thermodynamic and dynamic contributions.

Previous analyses of future changes in European precipitation extremes have two main limitations. Firstly, most studies focused on events with return periods on the order of one year, although the strongest impacts are typically caused by rarer events (see Ch. 1). Exceptions (such as Collins et al. (2013)) used a purely statistical approach. And secondly, the analysis of processes leading to changes in European precipitation extremes is mostly based on scaling analysis (linking precipitation changes to changes in temperature) or on a decomposition into thermodynamic and dynamic contributions (Tandon et al., 2018; Pfahl et al., 2017; Emori & Brown, 2005), but a detailed analysis of the underlying changes in the atmospheric circulation is currently missing, in particular for high impact events with multi-annual return periods. Therefore, this study focuses on the changes of atmospheric characteristics of daily precipitation events over five major central European river catchments with return periods of at least 10 years, which may

potentially result in severe flooding, between the historical and a projected warmer climate state. In order to perform such a robust analysis, ensemble climate simulations are used to generate a large set of daily weather situations in a quasi-stationary climate, resulting in a time series with an equivalent length of about 350 years (per climate state, which is represented by a 10-year time slice). An analysis of 100-year precipitation events would be more consistent with the previous analyses of Chs. 2 and 3, however, the number of 100-year events in the ensemble climate simulations is much smaller than the number of 100-year events from Ch. 2 (see Table 4.1). Therefore, no robust results can be obtained for changes in the characteristics of these events between the historical and a warmer climate, so that the return period for the extreme events is reduced to 10 years. The suitability of the ensemble climate simulations is statistically evaluated following the evaluations of Ch. 2. Several extreme precipitation events with return periods of at least 10 years are identified by extreme value statistics and the results from Ch. 2 are used to evaluate the realistic representation of extreme events in the historical climate simulations. Then, changes of the atmospheric characteristics of the extreme precipitation events between the two climate states are systematically analysed and classified into dynamic and thermodynamic processes, following previous studies with a similar concept (Pfahl et al., 2017), but without explicitly using their scaling methodology.

Section 4.2 describes the ensemble climate simulations that are used to analyse characteristical differences of 10-year precipitation events between the historical and a warmer climate. This is followed by methodological aspects such as the processing of these ensemble data and the identification of extreme events. In Sect. 4.3, temporal and spatial changes as well as atmospheric characteristics, classified into dynamic and thermodynamic processes, of these extreme events between both climate states are presented. Finally, Sect. 4.4 provides conclusions and a discussion of the most important findings in this study and its limitations.

4.2 Data & methodology

This section provides information about the ensemble climate simulations for historical runs and future projections from the Community Earth System Model Large Ensemble (CESM-LE), followed by the methodological approaches for the definition of the central European river catchments, the statistical evaluation of the ensemble climate simulations and the determination of 10-year precipitation events.

4.2.1 CESM-LE climate simulations

In order to robustly analyse the changes in characteristics of 10-year daily precipitation events over central European river catchments in a warmer climate, a large pool of daily weather

Catchments	10-year (CESM)	100-year (CESM)	100-year (EPS)
Rhine	51	3	13
Weser/Ems	45	3	10
Elbe	44	2	11
Oder	44	3	13
Danube	41	2	13

Table 4.1: Number of daily extreme precipitation events in the historical CESM-LE simulations and the EPS data for all river catchments.

conditions for both the historical and a warmer climate is generated by using ensemble climate simulations from the CESM-LE. The CESM-LE is a fully coupled, community, global climate model that provides state-of-the-art simulations of the Earth's past, present and future climate states (Kay et al., 2015). The large ensemble consists of 35 ensemble members, which are slightly disturbed in their initial conditions (stochastic air temperature perturbation on the order of 10^{-14}K). The historical runs are based on historical forcing from 1920 to 2005 (Lamarque et al., 2010), while the future projections are based on the representative concentration pathway 8.5 external forcing (RCP8.5) from 2006 to 2100 (Meinshausen et al., 2011), an emission scenario with a linear increase of the global emissions until the end of the current century. This external forcing of RCP8.5 leads to an increase of the global surface temperature of approximately 5 K by the year 2100 (for all ensemble members). More details on the CESM-LE can be found in Kay et al. (2015). In this study, 6-hourly output of simulations over 11 years (for the historical climate, 1990-2000) and 10 years (for a warmer climate, 2091-2100) with a spatial resolution of approximately 0.94° in latitude and 1.25° in longitude are evaluated. Simulations for these two time slices have been re-run at ETH Zurich, based on restart files from the original CESM-LE runs, in order to provide more comprehensive output data.

4.2.2 River catchments

As in Sect. 2.3.1, five major central European river catchments are again selected for this analysis, representing the rivers Rhine, Elbe, Oder, the upper and most western part of the Danube as well as the two rivers Weser and Ems (denoted as Weser/Ems) as one catchment. This enables a comparison between the historical CESM-LE simulations and the EPS data of Ch. 2. However, as the spatial resolution of the CESM-LE simulations is slightly different to the EPS data (see Sect. 2.2.1), the selection of the catchment borders is slightly adapted and shown in Fig. 4.1. Again, the grid points are allocated to a specific river catchment according to the river basin map by the Waterways and Shipping Administration of Germany, shown in Wasserstraßen- und Schifffahrtsverwaltung des Bundes (2022). Most of the area of each river catchment overlap with the catchments from the EPS data, indicated by the dashed grey lines, except for some minor areas around the catchment borders. Still, this does not particularly affect the selection and analysis of extreme precipitation events as most of the precipitation typically occur over

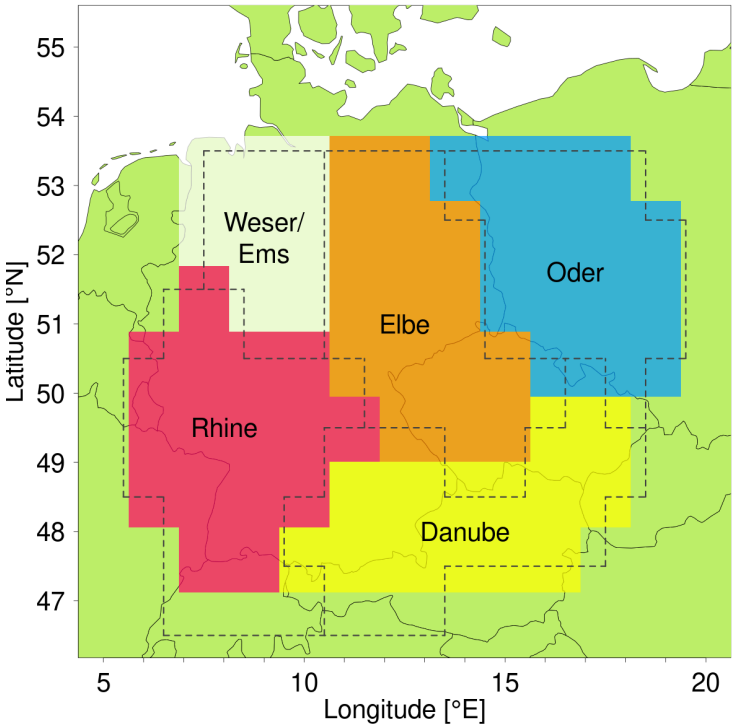

Figure 4.1: River catchments of the rivers Rhine; Elbe; Oder; Danube; and the combination of the rivers Weser and Ems, denoted Weser/Ems, based on a 0.94°x 1.25° lat–long grid over central Europe. For comparison, the catchment borders from the EPS data (see Sect. 2.3.1) are marked by dashed grey lines.

the catchment's centre (see Fig. 2.3a). Again, time series of daily precipitation for each river catchment are arranged by averaging all grid points of the associated river catchment at each time step and attaching these time series of each ensemble member to one complete time series, as described in Sect. 2.3.1.

4.2.3 Statistical evaluation of the CESM-LE simulations

In order to evaluate the suitability of the CESM-LE simulations for the analysis and comparison of typical characteristics of 10-year precipitation events between the historical and a warmer climate, several statistical properties are examined following the statistical evaluation of Ch. 2. For simplicity, the figures are just shown for the Danube catchment. However, the figures for all other river catchments are shown in the Appendix and particularly different results are mentioned in the text.

The basic requirement for taking all daily precipitation data from the CESM-LE simulations (for one time slice) into account is the independence of the ensemble members. A statistical evaluation of the independence of the ensemble members is presented in Fig. 4.2a, showing the statistical distribution of Spearman correlation coefficients between all possible ensemble member

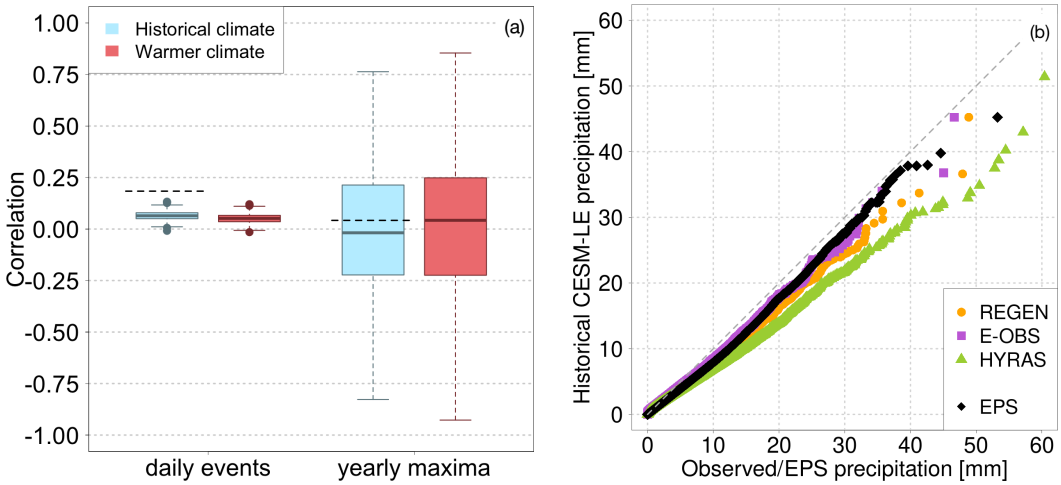

Figure 4.2: Statistical evaluation of daily precipitation data from CESM-LE climate simulations for the Danube catchment. **(a)** Distribution of Spearman correlation coefficients between (left) daily precipitation time series and (right) annual maximum daily precipitation for every combination of ensemble members (595 in total) in the (blue) historical and a (red) warmer climate. The box indicates the 25th and 75th percentile, while the whiskers extend to the most outer point, which is not more than 1.5 times the interquartile range from the box. Dashed black lines indicate the median of the correlation coefficient distribution of the EPS data as in Fig. 2.2a. **(b)** Quantile–quantile plots of daily precipitation between the historical CESM-LE simulations (vertical axis) and four data sets (REGEN, HYRAS, E-OBS and EPS; horizontal axis). Changes in simulated precipitation (vertical axis) for HYRAS observations are due to the reduced area with HYRAS coverage (only grid points with at least 90% HYRAS coverage are taken into account).

combinations (595 in total) of (left) entire time series (taking all daily precipitation into account) and (right) annual maxima (as representative of extreme events), for the historical (blue) and a warmer (red) climate. Low (high) correlations show a high (low) independence between the ensemble members. The correlation coefficients for the two left box plots (representative of entire time series of ensemble members) range from -0.01 to 0.15 with mean values around 0.07 (historical climate) and 0.05 (warmer climate). For comparison, dashed black lines indicate the median of the distribution of correlation coefficients from the EPS data as in Fig. 2.2a. The very low correlations show a high independence between all ensemble members and are particularly lower than the correlation median computed from the EPS data, which is expected since the CESM-LE runs have been initialised several decades before the analysed period, while it is only nine days for the EPS data. Still, in order to analyse extreme precipitation events, not entire time series are used but the most extreme events, here annual maxima. Therefore, the two right box plots in Fig. 4.2a show the distribution of correlation coefficients for time series, which consist of the annual maxima (11 for historical and 10 for warmer climate) of each ensemble member. Most of the correlations vary around 0 and are again slightly lower than the correlation median from the EPS data. However, there is a large spread of the values from

-0.9 to +0.85. As in Sect. 2.3.2, the false discovery rate test of Benjamini and Hochberg (1995), as described in Ventura et al. (2004), is applied to all p values associated with the individual correlation coefficients between the annual maxima in order to evaluate the statistical significance of multiple correlation coefficients. According to this test, no significant correlations are found for the historical climate and just 3 are found for the warmer climate (Rhine: 2, Weser/Ems: 1). These low numbers of significant correlations coefficients for extreme precipitation events in combination with the very low correlations between entire time series demonstrate the statistical independence of extreme precipitation events between the ensemble members.

A second criterion for the usability of the climate simulations in a warmer climate is a realistic representation of observed precipitation statistics in the historical climate. This is evaluated by comparing the quantile distributions of daily precipitation between the historical CESM-LE simulations (taking all members together) and four different data sets, three observational data sets (REGEN, HYRAS and E-OBS; all described in Sect. 2.2.2) and the EPS data. This is performed with quantile-quantile plots (Q–Q plots) and is shown in Fig. 4.2b. Two quantile distributions are the same when the associated Q–Q plot lies on the diagonal. For the Danube catchment, this is just the case for daily precipitation between 0 and 5 mm. The historical CESM-LE simulations slightly underestimate higher daily precipitation than 5 mm, especially in comparison to the REGEN and HYRAS observations. Still, the differences to the EPS data are the lowest. Such larger differences between model-based and observation-based data sets were also found in the statistical evaluation of the EPS data in Fig. 2.2b, which was justified with the influence of the relative complex topography of the Alps in the Danube catchment. This is also the case here as the Q–Q plots for all other river catchments match quite well with the diagonal for most precipitation intensities (see Fig. C.1 in the Appendix). However, the underestimation of the EPS data compared to HYRAS data of Fig. 4.2b is not quite comparable to the underestimation in Fig. 2.2b of Ch. 2 as the definition of the grid boxes has changed in this study (see Fig. 4.1). All together, this analysis shows that observational precipitation statistics predominantly match with the historical CESM-LE simulations but a small underestimation of daily precipitation over the Danube is taken into account for further analyses, also for analyses in a warmer climate.

The statistical evaluation shows that the daily precipitation events from individual ensemble members of the CESM-LE simulations can be considered as statistically independent (see Fig. 4.2a) as entire time series show very small correlations and (almost) no significant correlations can be found for extreme events. Historical CESM-LE simulations represent observed precipitation statistics relatively well (see Fig. C.1 in the Appendix), although areas with complex terrain (Danube catchment) show a slightly larger disagreement (see Fig. 4.2b). Additionally, there are no systematic differences between the ensemble members for both climate states (not shown) as the model physics are identical and just the initial conditions are perturbed. Taking all this into account, the CESM-LE simulations are considered to be suitable for an analysis of changes of

Catchments	RV & CI (mm, hist.)	RV & CI (mm, warm.)
Rhine	26.43 (25.41, 27.45)	29.63 (28.44, 30.73)
Weser/Ems	29.89 (28.61, 31.21)	34.96 (33.39, 36.52)
Elbe	26.75 (25.58, 27.79)	30.12 (28.73, 31.50)
Oder	28.56 (27.18, 29.91)	30.38 (28.94, 31.74)
Danube	28.56 (27.34, 29.28)	33.98 (32.64, 35.43)

Table 4.2: Return values (RV) and confidence intervals (CI) of 10-year daily precipitation in the historical and a warmer climate over different river catchments, obtained from the procedure in Sect. 4.2.4.

10-year precipitation event characteristics in a warmer climate.

4.2.4 Determination of extreme precipitation events

In order to determine return values with a specific return period and select the associated extreme precipitation events for further analyses from the CESM-LE simulations, the daily precipitation data from all ensemble members are combined as a very large time series for each of the time slices. The block maxima approach from extreme value statistics is applied to these time series (see Coles et al., 2001). Block maxima are determined from yearly time periods. This results in 385 (historical climate) and 350 (warmer climate) block maxima which are both large enough to fulfil the Fisher-Tippett theorem, so that a generalised extreme value distribution (GEV) can be fitted to all block maxima of a certain time slice by using the maximum likelihood approach. The location, scale and shape parameters are estimated in order to get the best fit of the extreme value distribution. With these estimates, the return values can then be computed by Eq. 2.1 as described in Sect. 2.3.3. Confidence intervals are obtained by using the bootstrap resampling method (see Coles et al., 2001). Block maxima are drawn with replacement from the original set and handled as a new set of block maxima, to which the GEV is again fitted and the return value is computed by Eq. 2.1. This is repeated 1000 times, resulting in 1000 slightly different return values, from which the 0.025 and 0.975 quantiles represent the confidence intervals. The resulting 10-year return values and associated confidence intervals are presented in Table 4.2 and discussed in Sect. 4.3.2. All daily precipitation events over a specific river catchment with precipitation amounts above the 10-year return value are selected for further analyses.

Using this approach to select extreme precipitation events can include cases in which events occur simultaneously, but just in different ensemble members, or as consecutive events, even within the same ensemble member. This is important to detect as such cases decrease the effective sample size of the composites and, hence, influence the results. The identified 10-year precipitation events from the CESM-LE simulations do not show any case of simultaneous events in both time slices and all river catchments. Additionally, there are also just very few cases of consecutive events with an average of 2.6 cases (Rhine: 1, Weser/Ems: 1, Elbe: 6, Oder: 3, Danube: 2) in the

historical and 0.8 cases (Rhine: 1, Weser/Ems: 1, Elbe: 0, Oder: 2, Danube: 0) in the warmer climate. Given the high total numbers of 10-year precipitation events in all river catchments, as presented in Table 4.1, a reduction of the effective sample size due to simultaneous or consecutive events does not play a major role.

4.3 Results

This section starts with a validation of circulation conditions associated with central European precipitation extremes from historical CESM-LE simulations with the EPS data. As these conditions are reasonably well represented in the historical simulations, the CESM-LE model is used to study future changes in the intensity and the spatial and temporal distribution of the extreme precipitation events as well as future changes in their underlying processes, which are classified into dynamic and thermodynamic processes. In the following, extreme precipitation events with a return period of at least 10 years are denoted as the most extreme precipitation events (MEPEs).

4.3.1 Validation of historical CESM-LE simulations for future projections

An analysis of changes in atmospheric characteristics of 100-year precipitation events in a warmer climate from CESM-LE simulations would allow a proper comparison to the results of Ch. 2 from the EPS data. However, the time series of the CESM-LE simulations are rather small with about 350 years of daily precipitation events, leading to around 3 events per time slice and river catchment (see Table 4.1). As this sample size is too low for performing a robust analysis, the return period is reduced to 10 years. In order to evaluate such changes, the historical CESM-LE simulations are validated by the EPS data. This validation is performed by comparing the monthly distributions and the circulation conditions of 10-year precipitation events from the historical CESM-LE simulations with the 100-year precipitation events from the EPS data. In order to obtain a first idea whether specific differences are associated with the different event intensity or linked to differences between the models, also the differences of atmospheric characteristics of 100-year precipitation events between the historical CESM-LE simulations and the EPS data are taken into account, in spite of the small sample size of CESM-LE. This model validation is presented in the following by a comparison of composites of the geopotential height at 500 hPa and the sea level pressure. Composites are constructed by averaging the fields of an atmospheric variable at a certain time step over all selected events of a specific catchment. This highlights the general structures that are common for all or most of the events.

Figure 4.3 shows the seasonal distribution of the 10-year events from CESM-LE simulations in comparison to the seasonality of 100-year EPS events. The monthly distribution and the max-

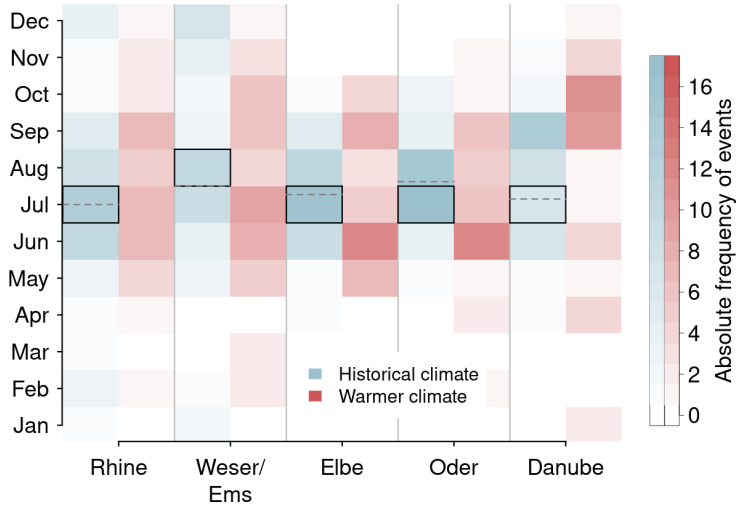

Figure 4.3: Monthly distribution of 10-year precipitation events from CESM-LE simulations of (blue) the historical and (red) a warmer climate for all five river catchments. The month with the highest 100-year precipitation event frequency and the median of the monthly distribution from the EPS data are marked by a grey box and a grey dashed line, respectively.

imum frequency match very well between 10-year events from historical CESM-LE simulations and 100-year events from EPS data (see blue and grey boxes and dashed grey lines in Fig. 4.3). Although events with different return values are compared, no large differences in the temporal occurrence of events can be found, except for the Danube with a slight temporal displacement. An evaluation of atmospheric characteristics is performed by comparing the composites of the geopotential height at 500 hPa in combination with the sea level pressure for 10-year events in historical CESM-LE simulations with 100-year events from EPS data, shown for all river catchments in Fig. 4.4.

When comparing the figures for the Elbe, Oder and Danube catchment, many similarities of the atmospheric configuration are found in both the mid- and lower-troposphere. For each composite, a cut-off low at 500 hPa and a sea level pressure minimum slightly downstream are found. There are just minor differences in the historical CESM-LE simulations compared to the EPS data, such as a slightly more western location and weaker intensity of the upper-level cut-off low, a less pronounced or weaker ridge over eastern Europe and a decreased intensity (around 5 hPa) of the surface cyclone near the river catchment. These weaker intensities of the circulation anomalies may be associated with the less extreme events, but also the larger sample size in CESM-LE simulations, which may lead to a smoothing of the composites. A comparison of 100-year events between the historical CESM-LE simulations and EPS data additionally provides information on whether the slightly changed characteristics arise from model differences or differences due to the event intensity. Such a comparison is presented in Fig. C.2 in the Appendix. Although the composites of 100-year events from the historical CESM-LE simulations only comprise 2-3

events per composite (see Table 4.1), the intensity of the surface cyclone is very similar to the EPS data for all three river catchments. Therefore, the results illustrate that there are no distinct differences in the atmospheric configuration of extreme precipitation events between historical CESM-LE simulations and EPS data in these catchments and that lower intensities of surface cyclones are likely associated with the differences in event intensity (return period) and sample size.

However, larger differences are found for the Rhine and Weser/Ems catchment (see Fig. 4.4a-d). Although the configuration near the surface is quite similar between 10-year events from historical CESM-LE simulations and 100-year events from EPS data over the Rhine catchment, no upper-level cut-off low is found in CESM-LE simulations. For the Rhine catchment, an upper-level trough is located over central Europe but, still, with a similar intensity and location of the centre. Additionally, there is no large ridge over eastern Europe. This is, however, not the case for the 100-year events from the historical CESM-LE simulations (see Fig. C.2a). For 100-year events, an upper-level cut-off low over central Europe can be found but with a weaker intensity, just like the surface cyclone. The atmospheric configuration in the mid-troposphere for 10-year events in historical CESM-LE simulations over the Weser/Ems catchment is completely different from the 100-year events from EPS data and mainly represent westerly winds over Europe. Just the location of the surface cyclone is quite similar but with a lower intensity. Taking the composite of 100-year events from historical CESM-LE simulations into account (see Fig. C.2c), a similar pattern of the location and intensity of an upper-level cut-off low, a surface cyclone and a ridge over eastern Europe can again be found. Therefore, the results show that there are no distinct differences of the atmospheric configuration of extreme precipitation events with return periods of 100 years between historical CESM-LE simulations and EPS data (but note again the small sample size in CESM-LE simulations). However, the characteristics of 10-year and 100-year events differ the most over the Weser/Ems catchment.

The results of this section demonstrate the overall agreement of the atmospheric configurations of 10-year precipitation events from historical CESM-LE simulations and 100-year precipitation events from the EPS data in most of the catchments. Differences rather arise from the choice of a lower return period for events from historical CESM-LE simulations instead of model differences, consistently showing slightly weaker intensities of the upper-level cut-off low and the surface cyclone in CESM-LE simulations. These differences in the atmospheric configuration are rather small for events over the Rhine, Elbe, Oder and Danube catchment, which highlights that CESM-LE simulations provide realistic representations of extreme precipitation events. Based on the relatively small differences of the circulation conditions between 10-year CESM-LE events and 100-year EPS events, the following results on future changes in 10-year CESM-LE events may be regarded as representative (at least qualitatively) also for extreme events of even larger intensities. However, results for the Weser/Ems catchment should be interpreted with care as the differences in the atmospheric configuration are particularly large, especially in the mid-troposphere.

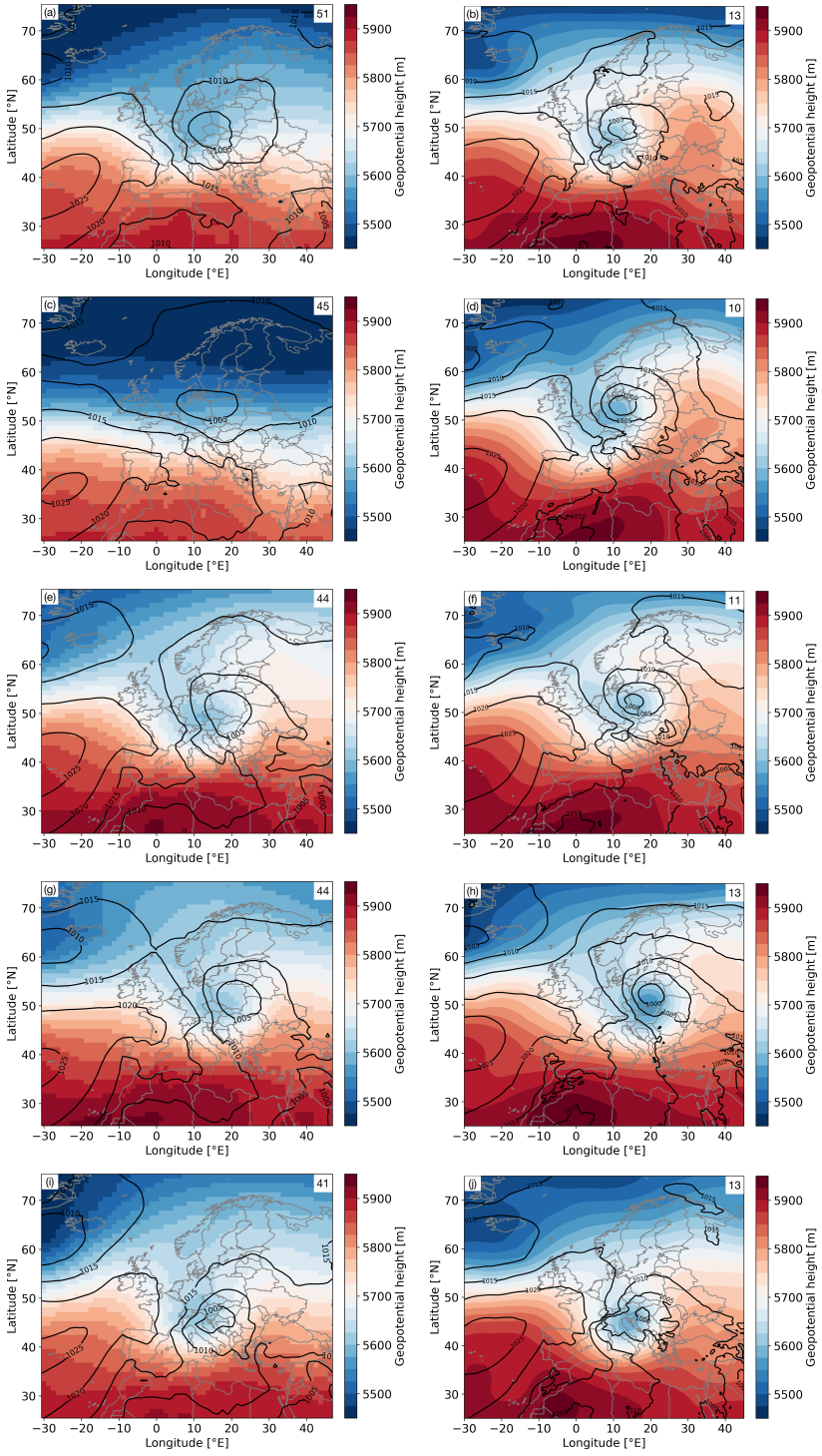

Figure 4.4: Composites of geopotential height at 500 hPa (colour shading) and sea level pressure (contours) 12 hours after the start of daily extreme precipitation over the **(a,b)** Rhine, **(c,d)** Weser/Ems, **(e,f)** Elbe, **(g,h)** Oder and **(i,j)** Danube catchment for **(left)** 10-year events from historical CESM-LE simulations and for **(right)** 100-year events from EPS data. The number of events per composite is provided in the top right corner.

All together, circulation conditions associated with central European precipitation extremes are reasonably well represented in historical CESM-LE simulations so that future changes in the intensity and frequency of these events and the underlying processes can be studied with this model.

4.3.2 Spatial and temporal changes

The daily precipitation intensity of MEPEs generally increases in a warmer climate for all river catchments. This is presented more explicitly in Table 4.2 with a comparison of 10-year return values of daily precipitation and their confidence intervals between the historical and projected CESM-LE simulations. The return values typically range between 26 and 30 mm for the historical climate and between 29 and 35 mm for a warmer climate. This is associated with increases of about 2 to 5 mm, while smaller changes can be found over the Oder (1.82 mm, 1.15%/K), Rhine (3.20 mm, 2.45%/K) and Elbe (3.37 mm, 2.34%/K) catchment and higher changes over the Weser/Ems (5.07 mm, 3.73%/K) and Danube (5.42 mm, 3.80%/K) catchment. In addition, the confidence intervals are just overlapping for the Oder catchment. However, the intensification of the daily precipitation during MEPEs in a warmer climate is not homogeneous in space, which can be seen in Fig. 4.5a in more detail for the Danube catchment. Although the mean increase is 5.42 mm, this is the result of even higher precipitation amounts over the eastern part of the catchment (above 10 mm) in combination with smaller changes (and even decreases) over the western part. Such spatial inhomogeneities of changes in precipitation intensity are also found for all other river catchments, however, with different locations of the highest increases (see left panels of Fig. C.3 in the Appendix).

As explained in Sect. 4.1, it is expected that the precipitation intensity increases by a rate of about 6-7%/K in a warmer climate just because of the thermodynamic increase of saturation humidity expressed by the Clausius-Clapeyron (CC) equation. In order to evaluate the rate of precipitation increases in Fig. 4.5a with the CC rate, Fig. 4.5b shows the relative precipitation increase with regard to the magnitude of warming (between the two climate states) for the area of the extreme precipitation over the Danube catchment. In this thesis, the warming is quantified by the local annual mean temperature increase at the grid point where the precipitation change is evaluated. The precipitation increases over the eastern part of the catchment occur with a rate of about 5.0-7.5%/K which is very similar to the CC rate. However, there are also increases in the vicinity of the catchment with higher rates of above 10%/K. Over these areas, precipitation may not just be intensified by the thermodynamic increase of the atmospheric moisture content but also by certain dynamical processes. Similar results can be found for the other river catchments (see right panels of Fig. C.3 in the Appendix), where precipitation increases within each catchment occur with a similar rate to the CC rate but increases in the vicinity of each catchment can reach values above 10%/K. Still, not every part of each catchment is associated with precipitation

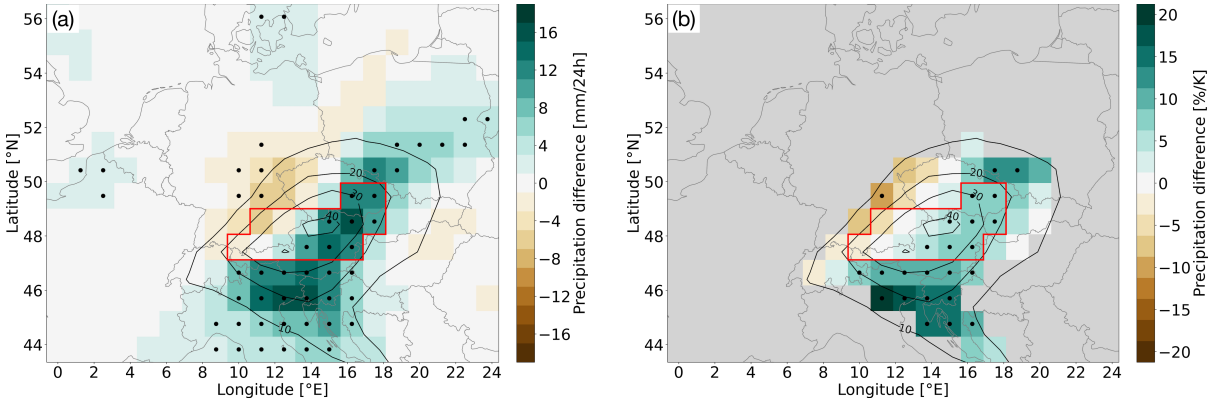

Figure 4.5: Composite difference of the accumulated precipitation amount of 10-year precipitation events over the Danube catchment, indicated by the red box, from CESM-LE simulations between a warmer and the historical climate expressed as **(a)** absolute changes (in mm/24h) and **(b)** relative changes with regard to the magnitude of local warming (in %/K) for grid points with at least 10 mm/24h in the historical composite (other grid points marked in grey). Positive (negative) values represent higher (lower) amounts in a warmer climate. Significant differences are marked by black dots. The composite from the historical simulations is shown as black contours (contour interval of 10 mm/24h).

increases. Thus, the precipitation increase over an entire river catchment, averaged over all grid points of that catchment, is lower than the expected CC rate of 6-7%/K. This is also shown in the previous paragraph for all five river catchments.

Another interesting aspect is the evaluation of possible changes in the temporal occurrence of MEPEs between the historical and a warmer climate. This is analysed by comparing the monthly distributions of the events, presented in Fig. 4.3 for all river catchments. In the historical climate, MEPEs typically occur in the warmest months, ranging from May to October with a peak frequency between June and August. However, a few events can also occur in other seasons (e.g. winter) over the Rhine and Weser/Ems catchment. Similar results were also found for the extreme precipitation events from the EPS data (see Fig. 2.4). In the warmer climate, the highest frequency of MEPEs is still found in the warmest months, except for the Danube catchment. However, the distributions broaden so that events in spring and autumn become relatively more frequent. Larger differences are found for the Danube catchment, in which the maximum occurrence of events shifts towards the autumn season with the highest frequencies in September and October. Overall, events are still most frequent in the warmer months but have a higher chance to occur in all seasons, in contrast to the distributions in the historical climate.

4.3.3 Dynamical characteristics

The spatial analysis of changes in total accumulated precipitation during 10-year precipitation events between the historical and a warmer climate (see Sect. 4.3.2) showed increases over specific

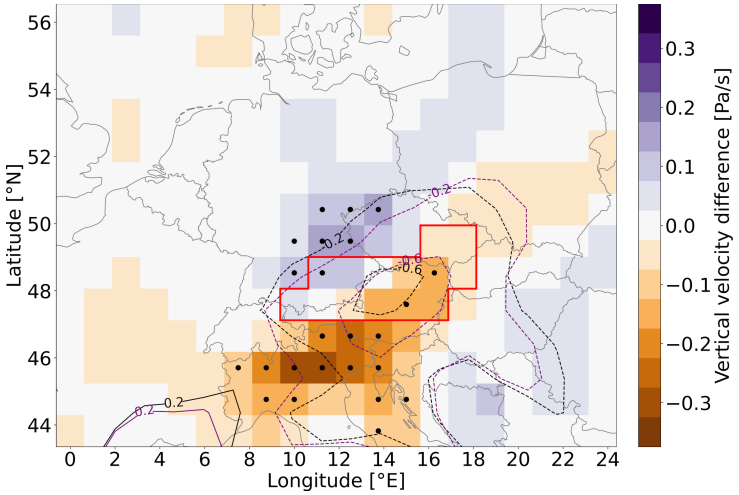

Figure 4.6: Composite difference of the vertical velocity at 700 hPa of 10-year precipitation events over the Danube catchment, indicated by the red box, from CESM-LE simulations between a warmer and the historical climate. Positive (negative) values represent a weakening (intensification) of the ascent in a warmer climate. Significant changes are marked by black dots. The composite from the historical (warmer) simulations is shown as black (purple) contours (contour interval of 0.4 Pa/s).

areas of each river catchment in a warmer climate. This is caused by changes in atmospheric characteristics during these extreme precipitation events. Previous studies have shown that changes in extreme precipitation can be decomposed into dynamical and thermodynamical contributions (Pfahl et al., 2017; O'Gorman, 2015; Allen & Ingram, 2002). This is why, in this study, changes in dynamic and thermodynamic factors that may lead to extreme precipitation changes are separately analysed. While this section focuses on changes in the dynamical characteristics such as the upper-level cut-off low, the surface cyclone and the resulting flow patterns, the following section takes thermodynamic aspects such as the temperature and specific humidity distributions into account.

The changes of the accumulated precipitation over the Danube catchment in Fig. 4.5 are associated with changes in the vertical velocity at 700 hPa, which are presented in Fig. 4.6. Areas with an increase of the precipitation in a warmer climate are linked to an intensification of the ascent (negative values), while decreases are linked to a weakening ascent (positive values). Additionally, several changes are statistically significant so that dynamical processes are supposed to be important for explaining the precipitation changes. Similar results are also found for the Rhine, Weser/Ems and Elbe catchment with significant changes over a few parts (see Fig. C.4 in the Appendix). However, there are no significant changes of the vertical velocity for the Oder catchment, indicating that changes in dynamical characteristics may not be most important there.

Differences in the geopotential height at 500 hPa and the sea level pressure can provide infor-

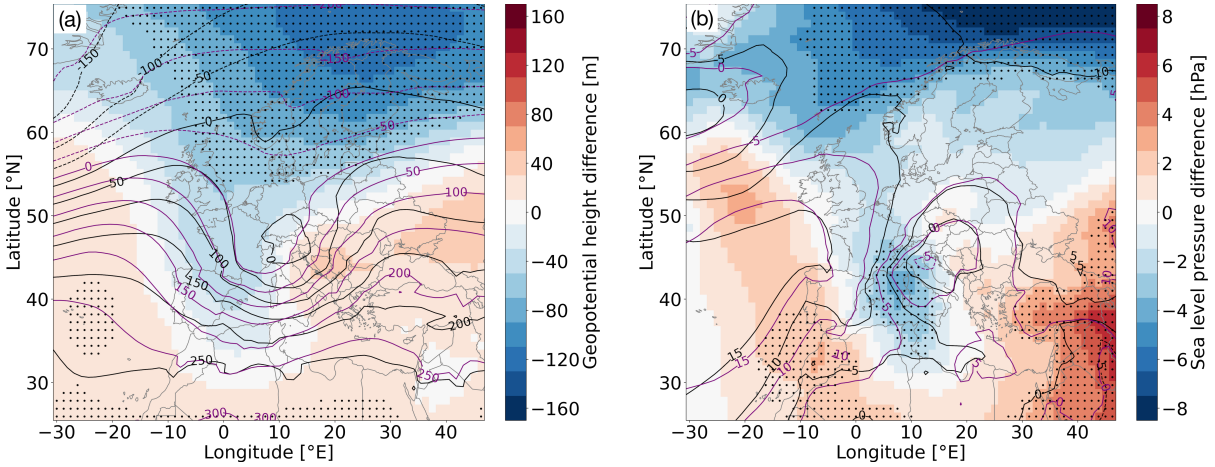

Figure 4.7: Composite difference of **(a)** geopotential height at 500 hPa and **(b)** sea level pressure of 10-year precipitation events over the Danube catchment from CESM-LE simulations between a warmer and the historical climate. Positive (negative) values represent higher (lower) geopotential height and sea level pressure, respectively, in a warmer climate. Significant differences are marked by black dots. The composite from the historical (warmer) simulations is shown as black (purple) contours (contour interval of 50 m and 5 hPa, respectively).

mation about potential reasons for the altered vertical velocity patterns. To construct these composites, the mean value in the catchment area is subtracted from the respective field (geopotential height or sea level pressure) in order to better evaluate the changes in location and intensity of troughs and ridges. Otherwise, most differences arise from a general increases of the geopotential height due to higher temperatures in a warmer climate. Such differences with regard to the historical climate are presented in Fig. 4.7 for the Danube catchment. The geopotential height at 500 hPa slightly decreases over western Europe and increases over eastern Europe (see Fig. 4.7a). This weak westward shift of the upper-level cut-off low or trough can also be seen by comparing the single composites (shown as individual contours). This shift can explain the significantly increased ascent south of the Alps in a warmer climate (see Fig. 4.6) as the flow at 500 hPa has a larger component perpendicular to the Alpine ridge from the south, whereas it is more parallel to the Alps in the historical climate. However, the upper-level trough over Europe in a warmer climate is not significantly intensified, just a large area of lower geopotential height over northern Europe. Also, there is just a slight intensification of the ridge over the North Atlantic and eastern Europe which can be a potential indicator for a more stationary trough in a warmer climate.

The sea level pressure composites for the historical and a warmer climate show similar patterns as well (see Fig. 4.7b). Significantly lower pressure is found over the northern Mediterranean which is associated with the westward shift of the upper-level trough and increasing ascent over this region. The sea level pressure minimum is slightly lower and also shifted towards northern

Italy, which can be associated with the increased precipitation south of the Alps. However, this is not directly related to the precipitation over the river catchment itself. Instead, the precipitation increase in the eastern part of the catchment (see Fig. 4.5) might be linked to the slight eastward extension of the area of low sea level pressure in the warmer climate. Also, there is slightly higher pressure in a warmer climate over the North Atlantic and parts of eastern Europe which might contribute to a reduced propagation velocity of the surface cyclone and, therefore, an increase of the precipitation amount.

Dynamical differences of events over the Rhine and Elbe catchment show similar patterns (see Figs. C.5a,b and C.7a,b in the Appendix). The upper-level cut-off lows at 500 hPa are slightly shifted westwards and are not intensified, explaining the slight westward shift of the precipitation distribution during the events. Additionally, the upper-level ridges over eastern Europe are intensified (partly significant) for both catchments, possibly increasing the stationarity of the surface cyclone and, hence, the precipitation amount. Changes near the surface are also quite similar with higher pressure northeast and lower pressure southwest of each catchment, although less pronounced for the Elbe catchment. There are almost no changes in the dynamical configuration (mid-tropospheric and at the surface) of events between the historical and a warmer climate for the Oder catchment (see Fig. C.8a,b in the Appendix), confirming that changes in the precipitation intensity do not predominantly arise from changes in the dynamical configuration. There is just a small westward shift of the upper-level cut-off low at 500 hPa, explaining the slight spatial shift of the precipitation distribution. For the Weser/Ems catchment, a strong and significant intensification of an upper-level ridge over eastern Europe and slightly over the eastern North Atlantic is found, associated with significantly higher surface pressure over these regions as well. However, this result is mainly influenced by the upper-level conditions of the historical composite, representing just westerly conditions over entire Europe.

4.3.4 Thermodynamic characteristics

The contribution of thermodynamic changes to the precipitation increases in a warmer climate is evaluated through changes in temperature and specific humidity, especially in the lower troposphere where the bulk of the atmospheric moisture content is located. Due to the general climate warming, higher temperatures are expected also during the extreme precipitation events. The lower-tropospheric temperature at 700 hPa for events over the Danube catchment, presented in Fig. 4.8a, increases over most European regions. However, this increase is smaller than the global mean temperature increase of about 5 K due to the shift of the monthly distribution resulting in less events in summer and more events in spring and autumn (see Fig. 4.3). However, there is not just an evenly distributed increase of the temperature but a significant intensification of the horizontal temperature gradient over central Europe with relatively higher temperatures over eastern Europe and relatively lower temperatures over western Europe. In addition, this points

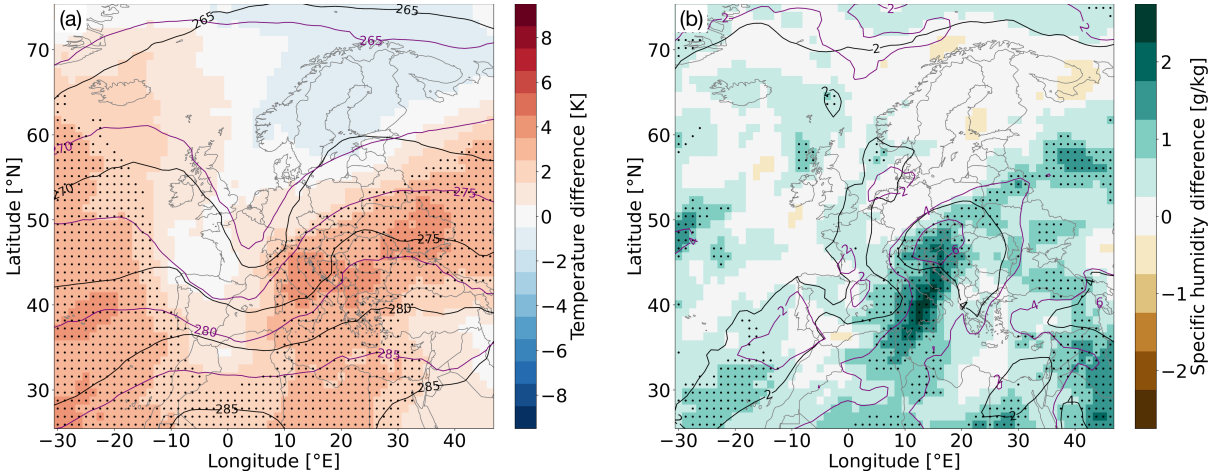

Figure 4.8: Composite difference of **(a)** temperature and **(b)** specific humidity at 700 hPa of 10-year precipitation events over the Danube catchment from CESM-LE simulations between a warmer and the historical climate. Positive (negative) values represent higher (lower) specific humidity and temperature, respectively, in a warmer climate. Significant differences are marked by black dots. The composite from the historical (warmer) simulations is shown as black (purple) contours (contour interval of 2 g/kg and 5 K, respectively).

to a stronger meridional temperature advection associated with the upper-level cut-off low and the surface cyclone.

A temperature increase is often connected to a higher moisture content in these regions as a warmer atmosphere can contain more moisture. As expected, the lower-tropospheric temperature increase over eastern Europe is associated with an increase of the lower-tropospheric moisture content over a similar area (see Fig. 4.8b for specific humidity at 700 hPa). This increase is statistically significant in several regions and particularly large south and southeast of the centre of the surface cyclone as well as over Italy and corresponding areas of the Mediterranean. However, there are no clear differences of the atmospheric moisture content over western Europe where the temperature does not substantially increase either.

Although the largest increases of both lower-tropospheric temperature and specific humidity are not directly located over the specific river catchment but rather further southeast, they may still influence the precipitation intensification. When taking the dynamical characteristics into account, the higher moisture content is advected with a southwesterly flow towards the river catchment (see Fig. 4.7 for dynamical situation). It can be summarised that the precipitation increase over the eastern (and slightly southern) part of the Danube catchment can be explained by an intensified ascent of air masses and increased lower-tropospheric moisture. In contrast, the western part is associated with a weakening of ascent and just a minor increase of moisture content, leading to the slight decrease of the precipitation intensity.

Similarities are found for changes in the thermodynamic characteristics for all other river catch-

ments (see Figs. C.5c,d and C.6c,d and C.7c,d and C.8c,d in the Appendix). For these catchments, there is an overall significant increase of the temperature at 700 hPa over Europe. Again, an intensification of the temperature dipole with higher temperatures over eastern Europe is found for all three catchments, just as for the Danube. While the overall temperature increase and dipole intensification is highest for the Weser/Ems and Rhine, weaker changes can be seen for the Elbe and Oder. However, for all these catchments, the lower troposphere contains significantly more moisture over large parts of Europe, especially over the specific river catchment and its vicinity. These results show further that the thermodynamic characteristics generally are an important contribution to the precipitation intensification for all river catchments.

4.4 Discussion and conclusion

The aim of this study is to analyse changes in 10-year precipitation events over central European river catchments from ensemble climate simulations between the historical and a projected warmer climate. Dynamic and thermodynamic factors that may lead to extreme precipitation events are separately analysed in order to properly understand potential changes of atmospheric mechanisms in a warmer climate. This is crucial as extreme precipitation events can result in high socioeconomic losses and are projected to intensify and occur more frequently in previous climate simulation studies (Gründemann et al., 2022; Myhre et al., 2019; Ban et al., 2015). In order to perform this analysis, a large set of daily precipitation fields with a quasi-stationary climate is obtained from ensemble climate simulations from the Community Earth System Model Large Ensemble (CESM-LE), following the approach from Ch. 2. Statistical evaluations show that annual maxima of daily precipitation are independent between the ensemble members and that the intensity distribution of historical CESM-LE simulations matches with observational data sets and the ensemble prediction (EPS) data of Ch. 2 generally well, with some larger disagreement for the orographically complex Danube catchment. 10-year precipitation events are identified with the help of extreme value statistics and typical atmospheric conditions of these events from historical climate simulations are validated with the EPS data. As these conditions are reasonably well represented in the CESM-LE simulations, a robust analysis of climatological changes of 10-year precipitation events is performed. Although an analysis of 100-year events would be more consistent with the studies in Chs. 2 and 3, no robust results can be obtained for them due to the low number of 100-year events in the climate simulations.

A short analysis of changes in the spatial and temporal characteristics of 10-year precipitation events reveal that these events generally intensify by about 2-5 mm/24h (depending on the catchment). The precipitation increases are, however, not evenly distributed over the entire catchment. Such a general increase of the precipitation amount in a warmer climate was also found in previous climate simulation studies (Gründemann et al., 2022; Myhre et al., 2019; Ban

et al., 2015; Collins et al., 2013). Local increases of the accumulated precipitation amount of about 8-16 mm/24h are significant and often lie around 5-10%/K, which was expected from the Clausius-Clapeyron equation and is also shown in Ban et al. (2015), O'Gorman (2015), and Emori and Brown (2005). Still, differences may appear due to the quantification of the warming. For that, the local annual mean temperature increase at a specific grid point is used here, while the global mean temperature increase or the local temperature increase during extreme events (for the scaling of O'Gorman and Schneider (2009)) are used in other studies. Here, the results show that the extreme precipitation events in a warmer climate still occur most frequently within an extended summer season from May to September. This is quite similar to the temporal distribution of historical extreme events (Grams et al., 2014; Ulbrich et al., 2003) and extreme events from ensemble weather prediction data as shown in Ch. 2. However, the distributions of all river catchments have broadened so that events can also regularly occur in the spring and autumn season. Just for the Danube, the peak of the temporal distribution has been shifted towards the autumn season.

Previous studies of Tandon et al. (2018), Pfahl et al. (2017), and Emori and Brown (2005) have decomposed changes of extreme precipitation into a dynamic and thermodynamic contribution. Based on that, changes of dynamic and thermodynamic processes are separately evaluated here but not as explicitly as in these studies. Over the Danube, Rhine, Elbe and Weser/Ems catchment, significant increases (decreases) of the upward vertical velocity at 700 hPa over regions with increased (decreased) precipitation intensity are found, indicating that the dynamical processes play an important role for explaining the precipitation increase. Over these catchments, except Weser/Ems, the upper-level trough or cut-off low at 500 hPa is not significantly intensified but slightly shifted westwards, explaining the westward shift of the precipitation increase over at least the Rhine and Elbe. For Weser/Ems, a development of an upper-level trough is found, conditioned by westerlies over Europe in the historical CESM-LE composite. Additionally, a slight intensification (partly significant) of the upper-level ridge over eastern Europe is identified for all these catchments, typically associated with an increase of the stationarity of the cut-off low as the propagation is decelerated. Near the surface, significantly lower pressure is simulated over the northern Mediterranean. Also, significantly higher surface pressure for the Weser/Ems catchment is found over the British Isles and western Russia. The surface cyclone near each specific river catchment did, however, not particularly intensify for any catchment, except slightly for the Danube catchment. Also, the slight eastward extension of the area with low pressure for the Danube is a possible indicator for the eastward shift of the precipitation increase. For the Oder catchment, neither significant changes of the vertical velocity nor particularly large changes in the upper- and lower-tropospheric configuration are found. This indicates that the contribution of dynamical processes to the precipitation increase is rather small, although this contribution is clearly more important even in contiguous river catchments such as Elbe and Danube.

As mentioned before, a significant thermodynamic contribution to the precipitation intensification is expected from the Clausius-Clapeyron equation. The lower-tropospheric temperature at 700 hPa during the precipitation extremes is generally increased over all parts of Europe, except for the Danube. For the Danube cases, the temperature increase over Europe is smaller than for the other catchments due to the shift of the monthly distribution, resulting is less events in the summer season. For all catchments, an intensified horizontal temperature gradient over central Europe is found, resulting in relatively higher values over eastern Europe and relatively lower values over western Europe. Given the specific upper-level and surface conditions, this points to a stronger meridional temperature advection for all catchments, which can be a possible indicator for increased precipitation. The overall significantly higher temperatures over Europe also induce higher lower-tropospheric (at 700 hPa) moisture content over most regions but especially in the vicinity of the specific river catchment, which are typically advected to that catchment by dynamical processes. This leads to a higher amount of precipitable water over the catchment and is, hence, an important factor in explaining the precipitation increases. For the Oder catchment, the change of the horizontal temperature gradient and moisture content in the lower troposphere is the lowest compared to all other catchments, explaining also the lowest changes in precipitation intensity for the Oder.

This approach of using ensemble climate simulations for an evaluation of climatological changes of extreme precipitation events has the limitation that, although historical simulations were validated with realistic ensemble weather prediction data from Ch. 2, climate simulations with a spatial resolution of about 1° do not adequately represent the entire range of atmospheric characteristics and processes of extreme precipitation events.

In future research, this approach can be adapted to other river catchments, as the climate simulations are globally available, or extended to precipitation events with higher return periods under the condition that longer simulations and/or a higher number of ensemble members are available in order to expand the number of daily precipitation fields. Taking other variables such as the vertically integrated water vapour and the water vapour transport into account can also increase the robustness of the results. Additionally, the decomposition of dynamic and thermodynamic factors can be evaluated more explicitly by using the scaling of O'Gorman and Schneider (2009). Finally, multi-day events can be analysed with this approach as well, which also have a high potential of triggering severe flooding events.

Chapter 5

Discussion and conclusion of most important thesis findings

The overarching aim of this thesis has been to robustly analyse atmospheric mechanisms of daily extreme precipitation events over central Europe with return periods on the order of 100 years, to robustly determine the associated return value estimates, even on a global scale, and to study future changes in such central European events due to climate warming. Such extreme precipitation events are known to regularly trigger devastating flooding events in central European river catchments with high socioeconomic losses (Caldas-Alvarez et al., 2022; Korswagen et al., 2022; Grams et al., 2014; Merz et al., 2014; Ulbrich et al., 2003) and an improved understanding of the underlying processes may contribute to more accurate forecasts of such events. As several previous climate simulation studies have shown, extreme precipitation will intensify and occur more frequently within the extratropics in a warmer climate (Gründemann et al., 2022; Myhre et al., 2019; Fischer & Knutti, 2014; Madsen et al., 2014), increasing the risk of high-impact river floods, especially in vulnerable areas, in the future (Tellman et al., 2021; Alfieri et al., 2017). Additionally, there is a high demand of precise estimates of return values of the associated precipitation extremes as flood protection measures strongly rely on them for adequate preparations. This is especially the case for specific regions of the world that are not covered by reliable and long observational time series, resulting in a high uncertainty of estimated return values.

In order to perform robust analyses of such extreme events and return values, long time series of daily precipitation are needed that are multiple times longer than the required return period of 100 years. Although observational time series usually cover up to about 100 years, such a length is too short for robust process analyses. Also, such long observational time series are not available for all regions of the world and may partly be not quite reliable. Therefore, this thesis uses ensemble simulations in order to generate a large set of model-generated daily precipitation

fields. The resulting data set can be considered as an equivalent time series of several hundreds of years and is, thus, considerably longer than conventional observational time series. However, a statistical evaluation prior to the analysis is needed to confirm the suitability of the data set. This thesis uses such an ensemble simulation approach in order to answer the three research questions that are mentioned in Ch. 1 and are discussed in the following. As explained in Ch. 4, the process analysis regarding the third research question has changed to an analysis of 10-year events, although an analysis of 100-year events would be more consistent with the other research questions. However, no robust results can be obtained for 100-year events due to the smaller sample size of the ensemble climate simulations.

Research question 1:
What distinguishes 100-year daily precipitation extremes over central European river catchments from more moderate extreme events?

For this research question, investigated in Ch. 2, robust process analyses of 100-year precipitation events over central European river catchments are performed and differences to less extreme events are identified by using a large data set of daily precipitation fields, obtained from the 10th forecast days of operational ensemble predictions by the ECMWF, following the approach of Breivik et al. (2013). Statistical evaluations show that the precipitation fields, and especially the extreme events, can be considered as independent events and that the individual ensemble members realistically reproduce precipitation distributions of observational data. With extreme value statistics, specific return values are estimated and events exceeding these values are systematically analysed. An analysis of 100-year events is performed in the beginning in order to better evaluate the differences to more moderate extreme events.

100-year events show high frequencies within the extended summer from June to September (for all catchments), which corresponds well with historical extreme events (e.g. Caldas-Alvarez et al., 2022; Grams et al., 2014; Ulbrich et al., 2003) and statistical analyses (Fischer et al., 2018). These events are typically associated with a quasi-stationary upper-level cut-off low over central Europe, originated from Rossby wave breaking (cf. Portmann et al., 2021; Appenzeller et al., 1996) of a trough over western Europe the day before the event, in combination with a surface cyclone southeast of the specific catchment. Surface cyclogenesis often occurs east of the upper-level cut-off low and cyclone pathways typically resemble the "Vb" track of van Bebber (1891) as also seen in historical events (e.g. Hofstätter et al., 2018; Bissolli et al., 2011; Mudelsee et al., 2004). All these configurations facilitate the transport of lower-tropospheric moisture from the south towards the specific catchment, probably evaporated especially from continental areas (cf. Krug et al., 2022; Grams et al., 2014; Winschall et al., 2014).

This analysis is consistent with previous studies regarding several aspects, confirming the specific

atmospheric mechanisms in a robust way. Based on that, robust differences to less extreme events are analysed. The monthly occurrences and general synoptic-scale patterns from less extreme events are quite similar to the 100-year events but specific differences to distinguish these events depend on the catchment, even when they are located next to each other. On the one hand, differences in dynamical processes such as an intensified upper-level cut-off low, more frequent surface cyclogenesis and intensified surface cyclones are most important for the Danube and Oder catchment, without significant differences in lower-tropospheric temperature and moisture content. These different dynamical configurations are expected to enhance the moisture transport to the catchment and the ascent within the catchment. On the other hand, 100-year and less extreme events in the Elbe and Rhine catchment mainly differ due to significantly higher lower-tropospheric temperature and moisture content east of the catchments, explaining intensified precipitation by higher moisture transport towards the catchments. Differences in upper-level cut-off low and surface cyclone intensity are not found for these catchments.

Research question 2:
How reliable are global estimates of 100-year return values of daily precipitation from ensemble weather prediction data in comparison to observational data sets?

To answer this research questions, analysed in detail in Ch. 3, operational ensemble weather prediction data from the ECMWF at the 10th forecast day are used to obtain a large set of global daily precipitation fields in order to robustly estimate 100-year return values and their confidence intervals on a global scale and evaluate the differences to the observational data sets REGEN, CHIRPS and PERSIANN, following the approach used in Ch. 2 for the first research question. Again, statistical evaluations show that the data set realistically represent intensity distributions for almost all regions. However, precipitation extremes between the ensemble members are not independent for tropical oceans and the Maritime Continent, where results are, thus, less trustworthy. Still, the ensemble data can overall be considered as suitable in terms of representing daily precipitation characteristics. With extreme value statistics, 100-year return values and the associated confidence intervals on a 95% level are estimated for both the ensemble prediction data and the observational data. Differences between the data sets are evaluated by the return values and the absolute and relative confidence intervals.

The largest 100-year return values of daily precipitation from the ensemble data are found in most parts of the tropics with values up to 950 mm over the Arabian Sea, followed by values around 500 mm over India and the tropical Pacific and Atlantic, about 200 mm over Australia, Africa and South America, and 50 to 100 mm over North America, Europe and central Asia, generally decreasing towards the poles. These estimates are in general agreement with other studies of multi-year precipitation extremes (e.g. Gründemann et al., 2023; Rodrigues et al., 2020). In comparison to observational data, the ensemble data indicate systematically higher

return values over most parts of the globe. While the confidence intervals between the data sets still overlap in many regions, in particular in the extratropics, large statistically significant differences are obtained in parts of northeastern South America, western tropical Africa, India and eastern China. These large differences can be either explained by model deficiencies, e.g., in the representation of convective precipitation or by a systematic underestimation of very extreme daily precipitation in observational data due to the shorter time series and, thus, limited sampling. The relative confidence intervals of the ensemble prediction data typically lie within 10-30% for most regions but can also be higher than 50% over the Sahara Desert, the Arabian Peninsula and parts of tropical oceans. These relative uncertainties, in most regions also the absolute ranges, are substantially reduced in the ensemble data compared to all observational estimates, typically on the order of 50-100 p.p. and up to 600 p.p. over some tropical regions. Therefore, this systematic and substantial reduction of statistical uncertainty due to the much longer time series of the ensemble data mainly enables more reliable and precise estimates of 100-year return values on a global scale.

Research question 3:
How do very extreme daily precipitation events over central European river catchments change in a warmer climate?

This research question is answered by using a large set of daily precipitation events in a quasi-stationary climate from ensemble climate simulations of the CESM-LE in order to robustly analyse climatological changes in 10-year precipitation events over central European river catchments between the historical and a projected warmer climate. This analysis is performed in Ch. 4 and follows again the approach used in Ch. 2 for the first research question. Here, statistical evaluations show that the ensemble climate simulations are overall suitable for a robust analysis with such an approach. 10-year precipitation events are identified with extreme value statistics and circulation conditions from historical simulations are validated with the ensemble data from Ch. 2. As these conditions are reasonably well represented in the historical simulations, a robust analysis is performed by separately analysing dynamic and thermodynamic factors that may lead to these extreme events, based on the idea of studies from Tandon et al. (2018), Pfahl et al. (2017), and Emori and Brown (2005), who decomposed changes into dynamic and thermodynamic contributions.

Prior to the separate analysis of dynamic and thermodynamic factors, projected future changes in spatial and temporal characteristics of these extreme events are evaluated. The analysis reveals that 10-year events generally intensify by about 2-5 mm/24h in a warmer climate (depending on the catchment), which was also found in previous studies (Gründemann et al., 2022; Myhre et al., 2019; Ban et al., 2015; Collins et al., 2013). Local increases of about 8-16 mm/24h are significant and often lie around 5-10%/K, which is expected from the Clausius-Clapeyron relation and is

also shown in Ban et al. (2015), O'Gorman (2015), and Emori and Brown (2005). Additionally, the monthly distributions have broadened so that 10-year precipitation events can also regularly occur in spring and autumn. For the Danube, the peak of that distribution has even been shifted towards the autumn season.

Over all catchments, except for the Oder, significant future changes of the lower-tropospheric vertical velocity at 700 hPa over regions with changed precipitation intensity are found, indicating that dynamical processes are important for explaining the precipitation changes. For most of these catchments, the upper-level trough or cut-off low at 500 hPa is just slightly shifted westwards, but has a similar intensity as in present-day climate, explaining the strongest precipitation increase in the western parts of the Rhine and Elbe, in combination with a slight, but partly significant, intensification of the upper-level ridge over eastern Europe, which is typically associated with an increase in the stationarity of the low. Near the surface, only small changes are found for all catchments, except significantly lower pressure over the northern Mediterranean. However, there is no particular intensification of the surface cyclone near the specific catchment but a slight eastward extension of low pressure east of the Danube catchment, which is a possible indicator for the strongest precipitation increase in the eastern part. Changes of dynamical processes for the Oder are rather small as also no large changes in the atmospheric configuration are found.

For all catchments, except for the Danube, the lower-tropospheric temperature at 700 hPa during 10-year precipitation events significantly increases over all parts of Europe, which is slightly expected from the external forcing of RCP8.5 in the future projections. For the Danube, this increase is smaller due to the shift of the monthly distribution of events towards the autumn. Still, an intensified horizontal temperature gradient over central Europe is found for all catchments, which points to a stronger meridional temperature advection during the events. In addition, these higher temperatures go along with higher lower-tropospheric moisture content over most regions but especially in the vicinity of the specific catchment, which is an important factor for explaining the precipitation increase. All together, both dynamic and thermodynamic processes are important for explaining precipitation changes in a warmer climate, indicating that less pronounced changes in one of these processes can result in smaller precipitation changes (see Oder catchment as an example).

Taking the results of all studies in this thesis into account, the benefit of using ensemble simulations for robust analyses of extreme precipitation events becomes apparent. Firstly, atmospheric characteristics of these events can be analysed robustly from ensemble weather prediction data as several events are evaluated. This allows systematic conclusions of certain processes in contrast to single event analyses. Secondly, data from ensemble weather predictions can be considered as a valid alternative to observational data sets also for quantitative estimates of return values as uncertainties of return value estimates are significantly and substantially reduced, even on a global scale. With that, flood protection measures in all parts of the world can be improved. Finally, explicit and robust changes of atmospheric configurations associated with the historical and a warmer climate are obtained from ensemble climate simulations, which helps in understanding the changes of extreme event processes in a warmer climate. With that, preparations for more intense events in the future can be improved.

All this has been analysed by using ensemble simulations as a large data set of daily precipitation events, evaluated as statistically suitable for a robust analysis. However, this approach still comes with a few limitations. Firstly, as the ensemble weather prediction data from the ECMWF are taken from a limited time span of 12 years (2008-2019), just a limited sampling of (multi-)decadal variability modes (e.g. El Niño–Southern Oscillation) of the climate system is represented, which might influence the intensity and structure of extreme precipitation events. Secondly, although the statistical evaluations show rather independent events on the 10th forecast day between the ensemble members, some interdependence in the synoptic-scale circulation may still occur for events on consecutive days, slightly reducing the effective sample size in statistical and composite analyses. Thirdly, this approach does also not work well in regions where the ensemble members are not independent from each other, which is the case for some tropical regions from the analysis in Ch. 3. Fourthly, the sample size of extreme events can be a limiting factor for a robust analysis. This is especially the case for ensemble climate simulations, as extreme events with return periods of 10 years are analysed in Ch. 4 due to the too small sample size of 100-year event. Finally, the model-generated precipitation data in both ensemble weather prediction data and ensemble climate simulations may be affected by imperfect representation of specific processes in the model, e.g. small-scale convection, which is why the focus in this thesis is on large-scale events.

In future research, the approaches in this thesis may also be applied to other regions or catchments and to multi-day events, which also have a high potential to cause flooding events. Also, events with higher return periods can be analysed under the condition that longer simulations and/or more ensemble members are available for an expanded data set. Data from other ensemble weather predictions or ensemble climate simulations can be analysed in order to evaluate the influence of the choice of specific data sets. Finally, concerning the process analyses, other variables such as vertically integrated water vapour can be taken into account to increase the robustness of certain results.

References

Alcântara, E., J. A. Marengo, J. Mantovani, L. R. Londe, R. L. Y. San, E. Park, Y. N. Lin, J. Wang, T. Mendes, A. P. Cunha, L. Pampuch, M. Seluchi, S. Simões, L. A. Cuartas, D. Goncalves, K. Massi, R. Alvalá, O. Moraes, C. S. Filho, R. Mendes, and C. Nobre (2023). "Deadly disasters in Southeastern South America: flash floods and landslides of February 2022 in Petrópolis, Rio de Janeiro". In: *Natural Hazards and Earth System Sciences* 23.3, pp. 1157–1175. DOI: 10.5194/nhess-23-1157-2023.

Alfieri, L., P. Burek, L. Feyen, and G. Forzieri (2015). "Global warming increases the frequency of river floods in Europe". In: *Hydrology and Earth System Sciences* 19.5, pp. 2247–2260. DOI: 10.5194/hess-19-2247-2015.

Alfieri, L., B. Bisselink, F. Dottori, G. Naumann, A. de Roo, P. Salamon, K. Wyser, and L. Feyen (2017). "Global projections of river flood risk in a warmer world". In: *Earth's Future* 5.2, pp. 171–182. DOI: 10.1002/2016EF000485.

Allen, M. R. and W. J. Ingram (2002). "Constraints on future changes in climate and the hydrologic cycle". In: *Nature* 419.6903, pp. 224–232. DOI: 10.1038/nature01092.

Appenzeller, C. H., H. C. Davies, and W. A. Norton (1996). "Fragmentation of stratospheric intrusions". In: *Journal of Geophysical Research* 101.D1, pp. 1435–1456. DOI: 10.1029/95JD02674.

Ashouri, H., K.-L. Hsu, S. Sorooshian, D. K. Braithwaite, K. R. Knapp, L. D. Cecil, B. R. Nelson, and O. P. Prat (2015a). *Index of /data/precipitation-persiann/access, National Centers for Environmental Information [data set]*. last access: 22 July 2023. URL: https://www.ncei.noaa.gov/data/precipitation-persiann/access/.

— (2015b). "PERSIANN-CDR: Daily precipitation climate data record from multisatellite observations for hydrological and climate studies". In: *Bulletin of the American Meteorological Society* 96.1, pp. 69–83. DOI: 10.1175/BAMS-D-13-00068.1.

Ban, N., J. Schmidli, and C. Schär (2015). "Heavy precipitation in a changing climate: Does short-term summer precipitation increase faster?" In: *Geophysical Research Letters* 42.4, pp. 1165–1172. DOI: 10.1002/2014GL062588.

Barredo, J. I. (2007). "Major flood disasters in Europe: 1950–2005". In: *Natural Hazards* 42.1, pp. 125–148. DOI: 10.1007/s11069-006-9065-2.

Barton, Y., P. Giannakaki, H. von Waldow, C. Chevalier, S. Pfahl, and O. Martius (2016). "Clustering of regional-scale extreme precipitation events in southern Switzerland". In: *Monthly Weather Review* 144.1, pp. 347–369. DOI: 10.1175/MWR-D-15-0205.1.

Benjamini, Y. and Y. Hochberg (1995). "Controlling the false discovery rate: a practical and powerful approach to multiple testing". In: *Journal of the Royal Statistical Society* 57.1, pp. 289–300. DOI: 10.1111/j.2517-6161.1995.tb02031.x.

Bissolli, P., K. Friedrich, J. Rapp, and M. Ziese (2011). "Flooding in eastern central Europe in May 2010–reasons, evolution and climatological assessment". In: *Weather* 66.6, pp. 147–153. DOI: 10.1002/wea.759.

Blöschl, G., T. Nester, J. Komma, J. Parajka, and R. A. P. Perdigão (2013). "The June 2013 flood in the Upper Danube Basin, and comparisons with the 2002, 1954 and 1899 floods". In: *Hydrology and Earth System Sciences* 17.12, pp. 5197–5212. DOI: 10.5194/hess-17-5197-2013.

Breivik, Ø., O. J. Aarnes, J.-R. Bidlot, A. Carrasco, and Ø. Saetra (2013). "Wave extremes in the northeast Atlantic from ensemble forecasts". In: *Journal of Climate* 26.19, pp. 7525–7540. DOI: 10.1175/JCLI-D-12-00738.1.

Caldas-Alvarez, A., M. Augenstein, G. Ayzel, K. Barfus, R. Cherian, L. Dillenardt, F. Fauer, H. Feldmann, M. Heistermann, A. Karwat, F. Kaspar, H. Kreibich, E. E. Lucio-Eceiza, E. P. Meredith, S. Mohr, D. Niermann, S. Pfahl, F. Ruff, H. W. Rust, L. Schoppa, T. Schwitalla, S. Steidl, A. H. Thieken, J. S. Tradowsky, V. Wulfmeyer, and J. Quaas (2022). "Meteorological, impact and climate perspectives of the 29 June 2017 heavy precipitation event in the Berlin metropolitan area". In: *Natural Hazards and Earth System Sciences* 22.11, pp. 3701–3724. DOI: 10.5194/nhess-22-3701-2022.

Coles, S., J. Bawa, L. Trenner, and P. Dorazio (2001). *An introduction to statistical modeling of extreme values*. Vol. 208. London: Springer. DOI: 10.1007/978-1-4471-3675-0.

Collins, M., R. Knutti, J. Arblaster, J.-L. Dufresne, T. Fichefet, P. Friedlingstein, X. Gao, W. J. J. Gutowski, T. Johns, G. Krinner, M. Shongwe, C. Tebaldi, A. J. Weaver, and M. Wehner (2013). "Long-term climate change: projections, commitments and irreversibility". In: *Climate Change 2013 - The Physical Science Basis: Contribution of Working Group I to the Fifth Assessment Report of the Intergovernmental Panel on Climate Change*. Cambridge, UK: Cambridge University Press, pp. 1029–1136.

Contractor, S., M. G. Donat, L. V. Alexander, M. Ziese, A. Meyer-Christoffer, U. Schneider, E. Rustemeier, A. Becker, I. Durre, and R. S. Vose (2020a). "Rainfall Estimates on a Gridded Network (REGEN)–a global land-based gridded dataset of daily precipitation from 1950 to 2016". In: *Hydrology and Earth System Sciences* 24.2, pp. 919–943. DOI: 10.5194/hess-24-919-2020.

— (2020b). *Rainfall Estimates on a Gridded Network based on all station data v1-2019, National Computational Infrastructure [data set]*. last access: 22 July 2023. DOI: 10.25914/5ca4c380b0d44.

Cornes, R. C., G. van der Schrier, E. J. M. van den Besselaar, and P. D. Jones (2018a). "An ensemble version of the E-OBS temperature and precipitation data sets". In: *Journal of Geophysical Research* 123.17, pp. 9391–9409. DOI: 10.1029/2017JD028200.

— (2018b). *E-OBS gridded dataset, ECA&D [data set]*. last access: 22 July 2023. URL: https://www.ecad.eu/download/ensembles/download.php.

Donat, M. G., L. V. Alexander, H. Yang, I. Durre, R. Vose, R. J. H. Dunn, K. M. Willett, E. Aguilar, M. Brunet, J. Caesar, B. Hewitson, C. Jack, A. M. G. Klein Tank, A. C. Kruger, J. Marengo, T. C. Peterson, M. Renom, C. Oria Rojas, M. Rusticucci, J. Salinger, A. S. Elrayah, S. S. Sekele, A. K. Srivastava, B. Trewin, C. Villarroel, L. A. Vincent, P. Zhai, X. Zhang, and S. Kitching (2013). "Updated analyses of temperature and precipitation extreme indices since the beginning of the twentieth century: The HadEX2 dataset". In: *Journal of Geophysical Research* 118.5, pp. 2098–2118. DOI: 10.1002/jgrd.50150.

Douben, K.-J. (2006). "Characteristics of river floods and flooding: a global overview, 1985–2003". In: *Irrigation and Drainage* 55.S1, S9–S21. DOI: 10.1002/ird.239.

ECMWF (2023a). *Archive Catalogue - Control forecast, ECMWF [data set]*. last access: 22 July 2023. URL: https://apps.ecmwf.int/archive-catalogue/?type=cf&class=od&stream=enfo&expver=1.
— (2023b). *Archive Catalogue - Perturbed forecast, ECMWF [data set]*. last access: 22 July 2023. URL: https://apps.ecmwf.int/archive-catalogue/?type=pf&class=od&stream=enfo&expver=1.
— (2023c). *IFS documentation*. last access: 22 July 2023. URL: https://www.ecmwf.int/en/publications/ifs-documentation.
— (2023d). *Integrated Forecasting System*. last access: 22 July 2023. URL: https://www.ecmwf.int/en/forecasts/documentation-and-support/changes-ecmwf-model.
— (2023e). *Modelling and Prediction*. last access: 22 July 2023. URL: https://www.ecmwf.int/en/research/modelling-and-prediction.
— (2023f). *The new ECMWF interpolation package MIR*. last access: 22 July 2023. URL: https://www.ecmwf.int/en/newsletter/152/computing/new-ecmwf-interpolation-package-mir.
Emori, S. and S. J. Brown (2005). "Dynamic and thermodynamic changes in mean and extreme precipitation under changed climate". In: *Geophysical Research Letters* 32.17. DOI: 10.1029/2005GL023272.
Engel, H. (1997). "The flood events of 1993/1994 and 1995 in the Rhine River basin". In: *Destructive Water: Water-caused Natural Disasters, their Abatement and Control*. Vol. 239. Wallingford, UK: IAHS Press, pp. 21–32.
Engel, H. (2004). "The flood event 2002 in the Elbe river basin, causes of the flood, its course, statistical assessment and flood damages". In: *La Houille Blanche* 90.6, pp. 33–36. DOI: 10.1051/lhb:200406003.
Feldmann, H., G. Schädler, H.-J. Panitz, and C. Kottmeier (2013). "Near future changes of extreme precipitation over complex terrain in Central Europe derived from high resolution RCM ensemble simulations". In: *International Journal of Climatology* 33.8, pp. 1964–1977. DOI: 10.1002/joc.3564.
Fischer, E. M., U. Beyerle, and R. Knutti (2013). "Robust spatially aggregated projections of climate extremes". In: *Nature Climate Change* 3.12, pp. 1033–1038. DOI: 10.1038/nclimate2051.
Fischer, E. M. and R. Knutti (2014). "Detection of spatially aggregated changes in temperature and precipitation extremes". In: *Geophysical Research Letters* 41.2, pp. 547–554. DOI: 10.1002/2013GL058499.
— (2016). "Observed heavy precipitation increase confirms theory and early models". In: *Nature Climate Change* 6.11, pp. 986–991. DOI: 10.1038/nclimate3110.
Fischer, M., H. W. Rust, and U. Ulbrich (2018). "Seasonal Cycle in German Daily Precipitation Extremes". In: *Meteorologische Zeitschrift* 27.1, pp. 3–13. DOI: 10.1127/metz/2017/0845.
Flaounas, E., L. Aragão, L. Bernini, S. Dafis, B. Doiteau, H. Flocas, S. L. Gray, A. Karwat, J. Kouroutzoglou, P. Lionello, F. Pantillon, C. Pasquero, P. Patlakas, M. A. Picornell, F. Porcù, M. D. K. Priestley, M. Reale, M. Roberts, H. Saaroni, D. Sandler, E. Scoccimarro, M. Sprenger, and B. Ziv (2023). "A composite approach to produce reference datasets for extratropical cyclone tracks: Application to Mediterranean cyclones". In: *Weather and Climate Dynamics Discussion [preprint]*. in review. DOI: 10.5194/wcd-2022-63.
Froidevaux, P. and O. Martius (2016). "Exceptional integrated vapour transport toward orography: an important precursor to severe floods in Switzerland". In: *Quarterly Journal of the Royal Meteorological Society* 142.698, pp. 1997–2012. DOI: 10.1002/qj.2793.

Funk, C. C., P. J. Peterson, M. F. Landsfeld, D. H. Pedreros, J. P. Verdin, J. D. Rowland, B. E. Romero, G. J. Husak, J. C. Michaelsen, and A. P. Verdin (2014a). "A quasi-global precipitation time series for drought monitoring". In: *U.S. Geological Survey Data Series* 832.4, pp. 1–12. DOI: 10.3133/ds832.

— (2014b). *Index of /products/CHIRPS-2.0/global_ daily/netcdf/p25, University of California at Santa Barbara [data set]*. last access: 22 July 2023. URL: https://data.chc.ucsb.edu/products/CHIRPS-2.0/global_daily/netcdf/p25/.

Gale, E. L. and M. A. Saunders (2013). "The 2011 Thailand flood: climate causes and return periods". In: *Weather* 68.9, pp. 233–237. DOI: 10.1002/wea.2133.

Gaume, E., M. Borga, M. C. Llassat, S. Maouche, M. Lang, and M. Diakakis (2016). "Mediterranean extreme floods and flash floods". In: *The Mediterranean Region under Climate Change. A Scientific Update*. IRD Editions, pp. 133–144. URL: https://hal.science/hal-01465740.

Grams, C. M., H. Binder, S. Pfahl, N. Piaget, and H. Wernli (2014). "Atmospheric processes triggering the central European floods in June 2013". In: *Natural Hazards and Earth System Sciences* 14.7, pp. 1691–1702. DOI: 10.5194/nhess-14-1691-2014.

Grams, C. M., H. Wernli, M. Böttcher, J. Čampa, U. Corsmeier, S. C. Jones, J. H. Keller, C.-J. Lenz, and L. Wiegand (2011). "The key role of diabatic processes in modifying the upper-tropospheric wave guide: a North Atlantic case-study". In: *Quarterly Journal of the Royal Meteorological Society* 137.661, pp. 2174–2193. DOI: 10.1002/qj.891.

Gründemann, G. J., E. Zorzetto, H. E. Beck, M. Schleiss, N. van de Giesen, M. Marani, and R. J. van der Ent (2023). "Extreme precipitation return levels for multiple durations on a global scale". In: *Journal of Hydrology* 621. DOI: 10.1016/j.jhydrol.2023.129558.

Gründemann, G. J., N. van de Giesen, L. Brunner, and R. J. van der Ent (2022). "Rarest rainfall events will see the greatest relative increase in magnitude under future climate change". In: *Communications Earth & Environment* 3.1, p. 235. DOI: 10.1038/s43247-022-00558-8.

Gvoždíková, B. and M. Müller (2021). "Moisture fluxes conducive to central European extreme precipitation events". In: *Atmospheric Research* 248, p. 105182. DOI: 10.1016/j.atmosres.2020.105182.

Hammond, M. J., A. S. Chen, S. Djordjević, D. Butler, and O. Mark (2015). "Urban flood impact assessment: A state-of-the-art review". In: *Urban Water Journal* 12.1, pp. 14–29. DOI: 10.1080/1573062X.2013.857421.

Hofstätter, M., A. Lexer, M. Homann, and G. Blöschl (2018). "Large-scale heavy precipitation over central Europe and the role of atmospheric cyclone track types". In: *International Journal of Climatology* 38.S1, e497–e517. DOI: 10.1002/joc.5386.

Hoskins, B. J., M. E. McIntyre, and A. W. Robertson (1985). "On the use and significance of isentropic potential vorticity maps". In: *Quarterly Journal of the Royal Meteorological Society* 111.470, pp. 877–946. DOI: 10.1002/qj.49711147002.

James, P., A. Stohl, N. Spichtinger, S. Eckhardt, and C. Forster (2004). "Climatological aspects of the extreme European rainfall of August 2002 and a trajectory method for estimating the associated evaporative source regions". In: *Natural Hazards and Earth System Sciences* 4.5/6, pp. 733–746. DOI: 10.5194/nhess-4-733-2004.

Jongman, B., P. J. Ward, and J. C. J. H. Aerts (2012). "Global exposure to river and coastal flooding: Long term trends and changes". In: *Global Environmental Change* 22.4, pp. 823–835. DOI: 10.1016/j.gloenvcha.2012.07.004.

Jongman, B., H. C. Winsemius, J. C. J. H. Aerts, E. Coughlan de Perez, M. K. van Aalst, W. Kron, and P. J. Ward (2015). "Declining vulnerability to river floods and the global benefits

of adaptation". In: *Proceedings of the National Academy of Sciences* 112.18, E2271–E2280. DOI: 10.1073/pnas.1414439112.

Kappeler, M. (2017). *15 Jahre Jahrhundertflut in Dresden*. last access: 22 July 2023. URL: https://www.dnn.de/lokales/dresden/15-jahre-jahrhundertflut-in-dresden-XD5UYXPBK3A6MONDYC6MHYXGYA.html.

Kay, J. E., C. Deser, A. Phillips, A. Mai, C. Hannay, G. Strand, J. M. Arblaster, S. C. Bates, G. Danabasoglu, J. Edwards, M. Holland, P. Kushner, J.-F. Lamarque, D. Lawrence, K. Lindsay, A. Middleton, E. Munoz, R. Neale, K. Oleson, L. Polvani, and M. Vertenstein (2015). "The Community Earth System Model (CESM) large ensemble project: A community resource for studying climate change in the presence of internal climate variability". In: *Bulletin of the American Meteorological Society* 96.8, pp. 1333–1349. DOI: 10.1175/BAMS-D-13-00255.1.

Kelder, T., M. Müller, L. J. Slater, T. I. Marjoribanks, R. L. Wilby, C. Prudhomme, P. Bohlinger, L. Ferranti, and T. Nipen (2020). "Using UNSEEN trends to detect decadal changes in 100-year precipitation extremes". In: *npj Climate and Atmospheric Science* 3.47. DOI: 10.1038/s41612-020-00149-4.

Kenyon, J. and G. C. Hegerl (2010). "Influence of modes of climate variability on global precipitation extremes". In: *Journal of Climate* 23.23, pp. 6248–6262. DOI: 10.1175/2010JCLI3617.1.

Korswagen, P. A., S. Harish, J. Oetjen, and D. Wüthrich (2022). "Post-flood field survey of the Ahr Valley (Germany): building damages and hydraulic aspects". In: DOI: 10.4233/uuid:3cafd772-facd-4e3a-8b1a-cee978562ff1.

Kreibich, H., P. Bubeck, M. Kunz, H. Mahlke, S. Parolai, B. Khazai, J. Daniell, T. Lakes, and K. Schröter (2014). "A review of multiple natural hazards and risks in Germany". In: *Natural Hazards* 74.3, pp. 2279–2304. DOI: 10.1007/s11069-014-1265-6.

Kreienkamp, F., S. Y. Philip, J. S. Tradowsky, S. F. Kew, P. Lorenz, J. Arrighi, A. Belleflamme, T. Bettmann, S. Caluwaerts, S. C. Chan, A. Ciavarella, L. de Cruz, H. de Vries, N. Demuth, A. Ferrone, E. M. Fischer, H. J. Fowler, K. Goergen, D. Heinrich, Y. Henrichs, G. Lenderink, F. Kaspar, E. Nilson, F. E. L. Otto, F. Ragone, S. I. Seneviratne, R. K. Singh, A. Skålevåg, P. Termonia, L. Thalheimer, M. van Aalst, J. van den Bergh, H. van de Vyver, S. Vannitsem, G. J. van Oldenborgh, B. van Schaeybroeck, R. Vautard, D. Vonk, and N. Wanders (2021). "Rapid attribution of heavy rainfall events leading to the severe flooding in Western Europe during July 2021". In: *World Weather Attribution*, pp. 1–51.

Kron, W. (2015). "Flood disasters–a global perspective". In: *Water Policy* 17.S1, pp. 6–24. DOI: 10.2166/wp.2015.001.

Krug, A., F. Aemisegger, M. Sprenger, and B. Ahrens (2022). "Moisture sources of heavy precipitation in Central Europe in synoptic situations with Vb-cyclones". In: *Climate Dynamics* 59.11–12, pp. 3227–3245. DOI: 10.1007/s00382-022-06256-7.

Kundzewicz, Z. W., U. Ulbrich, T. Brücher, D. Graczyk, A. Krüger, G. C. Leckebusch, L. Menzel, I. Pińskwar, M. Radziejewski, and M. Szwed (2005). "Summer floods in Central Europe – Climate Change Track?" In: *Natural Hazards* 36, pp. 165–189. DOI: 10.1007/s11069-004-4547-6.

Lamarque, J.-F., T. C. Bond, V. Eyring, C. Granier, A. Heil, Z. Klimont, D. Lee, C. Liousse, A. Mieville, B. Owen, M. G. Schultz, D. Shindell, S. J. Smith, E. Stehfest, J. van Aardenne, O. R. Cooper, M. Kainuma, N. Mahowald, J. R. McConnell, V. Naik, K. Riahi, and D. P. van Vuuren (2010). "Historical (1850–2000) gridded anthropogenic and biomass burning emissions of reactive gases and aerosols: methodology and application". In: *Atmospheric Chemistry and Physics* 10.15, pp. 7017–7039. DOI: 10.5194/acp-10-7017-2010.

Lehmkuhl, F., H. Schüttrumpf, J. Schwarzbauer, C. Brüll, M. Dietze, P. Letmathe, C. Völker, and H. Hollert (2022). "Assessment of the 2021 summer flood in Central Europe". In: *Environmental Sciences Europe* 34.1, p. 107. DOI: 10.1186/s12302-022-00685-1.

Madsen, H., D. Lawrence, M. Lang, M. Martinkova, and T. Kjeldsen (2014). "Review of trend analysis and climate change projections of extreme precipitation and floods in Europe". In: *Journal of Hydrology* 519, pp. 3634–3650. DOI: 10.1016/j.jhydrol.2014.11.003.

Magnusson, L., J.-R. Bidlot, S. T. K. Lang, A. Thorpe, N. Wedi, and M. Yamaguchi (2014). "Evaluation of medium-range forecasts for Hurricane Sandy". In: *Monthly Weather Review* 142.5, pp. 1962–1981. DOI: 10.1175/MWR-D-13-00228.1.

Magnusson, L. and E. Källén (2013). "Factors influencing skill improvements in the ECMWF forecasting system". In: *Monthly Weather Review* 141.9, pp. 3142–3153. DOI: 10.1175/MWR-D-12-00318.1.

Maraun, D., T. J. Osborn, and H. W. Rust (2011). "The influence of synoptic airflow on UK daily precipitation extremes. Part I: Observed spatio-temporal relationships". In: *Climate Dynamics* 36.1, pp. 261–275. DOI: 10.1007/s00382-009-0710-9.

Martius, O., C. Schwierz, and H. C. Davies (2008). "Far-upstream precursors of heavy precipitation events on the Alpine south-side". In: *Quarterly Journal of the Royal Meteorological Society* 134.631, pp. 417–428. DOI: 10.1002/qj.229.

Meinshausen, M., S. J. Smith, K. Calvin, J. S. Daniel, M. L. T. Kainuma, J.-F. Lamarque, K. Matsumoto, S. A. Montzka, S. C. B. Raper, K. Riahi, A. Thomson, G. J. M. Velders, and D. P. P. van Vuuren (2011). "The RCP greenhouse gas concentrations and their extensions from 1765 to 2300". In: *Climatic change* 109, pp. 213–241. DOI: 10.1007/s10584-011-0156-z.

Merz, B., G. Blöschl, S. Vorogushyn, F. Dottori, J. C. J. H. Aerts, P. Bates, M. Bertola, M. Kemter, H. Kreibich, U. Lall, and E. Macdonald (2021). "Causes, impacts and patterns of disastrous river floods". In: *Nature Reviews Earth & Environment* 2.9, pp. 592–609. DOI: 10.1038/s43017-021-00195-3.

Merz, B., F. Elmer, M. Kunz, B. Mühr, K. Schröter, and S. Uhlemann-Elmer (2014). "The extreme flood in June 2013 in Germany". In: *La Houille Blanche* 1, pp. 5–10. DOI: 10.1051/lhb/2014001.

Messmer, M., J. J. Gómez-Navarro, and C. C. Raible (2015). "Climatology of Vb cyclones, physical mechanisms and their impact on extreme precipitation over Central Europe". In: *Earth System Dynamics* 6.2, pp. 541–553. DOI: 10.5194/esd-6-541-2015.

Mizuta, R. and H. Endo (2020). "Projected changes in extreme precipitation in a 60-km AGCM large ensemble and their dependence on return periods". In: *Geophysical Research Letters* 47.13, e2019GL086855. DOI: 10.1029/2019GL086855.

Mohr, S., U. Ehret, M. Kunz, P. Ludwig, A. Caldas-Alvarez, J. E. Daniell, F. Ehmele, H. Feldmann, M. J. Franca, C. Gattke, M. Hundhausen, P. Knippertz, K. Küpfer, B. Mühr, J. G. Pinto, J. Quinting, A. M. Schäfer, M. Scheibel, F. Seidel, and C. Wisotzky (2023). "A multi-disciplinary analysis of the exceptional flood event of July 2021 in central Europe–Part 1: Event description and analysis". In: *Natural Hazards and Earth System Sciences* 23.2, pp. 525–551.

Molteni, F., R. Buizza, T. N. Palmer, and T. Petroliagis (1996). "The ECMWF ensemble prediction system: Methodology and validation". In: *Quarterly Journal of the Royal Meteorological Society* 122.529, pp. 73–119. DOI: 10.1002/qj.49712252905.

Mudelsee, M., M. Börngen, G. Tetzlaff, and U. Grünewald (2004). "Extreme floods in central Europe over the past 500 years: Role of cyclone pathway "Zugstrasse Vb"". In: *Journal of Geophysical Research* 109.D23. DOI: 10.1029/2004JD005034.

Mueller, M. (2003). "Damages of the Elbe flood 2002 in Germany-a review". In: *EGS-AGU-EUG Joint Assembly* (Apr. 6–11, 2003). Vol. 5. Nice, France: Geophysical Research Abstracts, p. 12992.

Muller, C. J., P. A. O'Gorman, and L. E. Back (2011). "Intensification of precipitation extremes with warming in a cloud-resolving model". In: *Journal of Climate* 24.11, pp. 2784–2800. DOI: 10.1175/2011JCLI3876.1.

Munich Re (1999). "Naturkatastrophen in Deutschland: Schadenerfahrungen und Schadenpotentiale". In: *Publication of the Munich Re*.

— (2022). *Hurricanes, cold waves, tornadoes: Weather disasters in USA dominate natural disaster losses in 2021*. last access: 6 April 2022. URL: https://www.munichre.com/en/company/media-relations/media-information-and-corporate-news/media-information/2022/natural-disaster-losses-2021.html.

Myhre, G., K. Alterskjær, C. W. Stjern, Ø. Hodnebrog, L. Marelle, B. H. Samset, J. Sillmann, N. Schaller, E. Fischer, M. Schulz, and A. Stohl (2019). "Frequency of extreme precipitation increases extensively with event rareness under global warming". In: *Scientific reports* 9.1, p. 16063. DOI: 10.1038/s41598-019-52277-4.

Neu, U., M. G. Akperov, N. Bellenbaum, R. Benestad, R. Blender, R. Caballero, A. Cocozza, H. F. Dacre, Y. Feng, K. Fraedrich, J. Grieger, S. Gulev, J. Hanley, T. Hewson, M. Inatsu, K. Keay, S. F. Kew, I. Kindem, G. C. Leckebusch, M. L. R. Liberato, P. Lionello, I. I. Mokhov, J. G. Pinto, C. C. Raible, M. Reale, I. Rudeva, M. Schuster, I. Simmonds, M. Sinclair, M. Sprenger, N. D. Tilinina, I. F. Trigo, S. Ulbrich, U. Ulbrich, X. L. Wang, and H. Wernli (2013). "IMILAST: A community effort to intercompare extratropical cyclone detection and tracking algorithms". In: *Bulletin of the American Meteorological Society* 94.4, pp. 529–547. DOI: 10.1175/BAMS-D-11-00154.1.

Nissen, K. M. and U. Ulbrich (2017). "Increasing frequencies and changing characteristics of heavy precipitation events threatening infrastructure in Europe under climate change". In: *Natural Hazards and Earth System Sciences* 17.7, pp. 1177–1190. DOI: 10.5194/nhess-17-1177-2017.

O'Gorman, P. A. and T. Schneider (2009). "The physical basis for increases in precipitation extremes in simulations of 21st-century climate change". In: *Proceedings of the National Academy of Sciences* 106.35, pp. 14773–14777. DOI: 10.1073/pnas.0907610106.

O'Gorman, P. A. (2015). "Precipitation extremes under climate change". In: *Current Climate Change Reports* 1, pp. 49–59. DOI: 10.1007/s40641-015-0009-3.

O'Gorman, P. A. and T. Schneider (2009). "Scaling of precipitation extremes over a wide range of climates simulated with an idealized GCM". In: *Journal of Climate* 22.21, pp. 5676–5685. DOI: 10.1175/2009JCLI2701.1.

Osinski, R., P. Lorenz, T. Kruschke, M. Voigt, U. Ulbrich, G. C. Leckebusch, E. Faust, T. Hofherr, and D. Majewski (2016). "An approach to build an event set of European windstorms based on ECMWF EPS". In: *Natural Hazards and Earth System Sciences* 16.1, pp. 255–268. DOI: 10.5194/nhess-16-255-2016.

Papalexiou, S. M. and D. Koutsoyiannis (2013). "Battle of extreme value distributions: A global survey on extreme daily rainfall". In: *Water Resources Research* 49.1, pp. 187–201. DOI: 10.1029/2012WR012557.

Pendergrass, A. G. and D. L. Hartmann (2014). "Changes in the distribution of rain frequency and intensity in response to global warming". In: *Journal of Climate* 27.22, pp. 8372–8383. DOI: 10.1175/JCLI-D-14-00183.1.

Pfahl, S. (2014). "Characterising the relationship between weather extremes in Europe and synoptic circulation features". In: *Natural Hazards and Earth System Sciences* 14.6, pp. 1461–1475. DOI: 10.5194/nhess-14-1461-2014.

Pfahl, S., P. A. O'Gorman, and E. M. Fischer (2017). "Understanding the regional pattern of projected future changes in extreme precipitation". In: *Nature Climate Change* 7.6, pp. 423–427. DOI: 10.1038/nclimate3287.

Pfahl, S. and H. Wernli (2012). "Quantifying the relevance of cyclones for precipitation extremes". In: *Journal of Climate* 25.19, pp. 6770–6780. DOI: 10.1175/JCLI-D-11-00705.1.

Pfleiderer, P., C.-F. Schleussner, K. Kornhuber, and D. Coumou (2019). "Summer weather becomes more persistent in a 2°C world". In: *Nature Climate Change* 9.9, pp. 666–671. DOI: 10.1038/s41558-019-0555-0.

Portmann, R., M. Sprenger, and H. Wernli (2021). "The three-dimensional life cycles of potential vorticity cutoffs: A global and selected regional climatologies in ERA-Interim (1979–2018)". In: *Weather and Climate Dynamics* 2.2, pp. 507–534. DOI: 10.5194/wcd-2-507-2021.

Rajulapati, C. R., S. M. Papalexiou, M. P. Clark, S. Razavi, G. Tang, and J. W. Pomeroy (2020). "Assessment of extremes in global precipitation products: How reliable are they?" In: *Journal of Hydrometeorology* 21.12, pp. 2855–2873. DOI: 10.1175/JHM-D-20-0040.1.

Rauthe, M., H. Steiner, U. Riediger, A. Mazurkiewicz, and A. Gratzki (2013a). "A Central European precipitation climatology–Part I: Generation and validation of a high-resolution gridded daily data set (HYRAS)". In: *Meteorologische Zeitschrift* 22.3, pp. 235–256. DOI: 10.1127/0941-2948/2013/0436.

— (2013b). *HYRAS gridded data (daily), Deutscher Wetterdienst [data set]*. last access: 22 July 2023. URL: https://gdk.gdi-de.org/geonetwork/srv/api/%20records/de.dwd.hydromet.hyras.daily.info.status.

Rodrigues, D. T., W. A. Gonçalves, M. H. C. Spyrides, C. M. Santos e Silva, and D. O. de Souza (2020). "Spatial distribution of the level of return of extreme precipitation events in Northeast Brazil". In: *International Journal of Climatology* 40.12, pp. 5098–5113. DOI: 10.1002/joc.6507.

Schlemmer, L., O. Martius, M. Sprenger, C. Schwierz, and A. Twitchett (2010). "Disentangling the forcing mechanisms of a heavy precipitation event along the Alpine south side using potential vorticity inversion". In: *Monthly Weather Review* 138.6, pp. 2336–2353. DOI: 10.1175/2009MWR3202.1.

Schüttrumpf, H., J. Birkmann, C. Brüll, L. Burghardt, G. Johann, E. Klopries, F. Lehmkuhl, A. Schüttrumpf, and S. Wolf (2022). "Herausforderungen an den Wiederaufbau nach dem Katastrophenhochwasser 2021 in der Eifel". In: *Nachhaltigkeit im Wasserbau - Umwelt, Transport, Energie. Dresdner Wasserbauliche Mitteilungen 68*. Dresden, Germany: Technische Universität Dresden, Institut für Wasserbau und technische Hydromechanik, pp. 5–16.

Sene, K. (2016). "Flash floods". In: *Hydrometeorology*. Cham: Springer, pp. 273–312. DOI: 10.1007/978-3-319-23546-2_9.

Sillmann, J., V. V. Kharin, X. Zhang, F. W. Zwiers, and D. Bronaugh (2013). "Climate extremes indices in the CMIP5 multimodel ensemble: Part 1. Model evaluation in the present climate". In: *Journal of Geophysical Research* 118.4, pp. 1716–1733. DOI: 10.1002/jgrd.50203.

Sodemann, H., H. Wernli, and C. Schwierz (2009). "Sources of water vapour contributing to the Elbe flood in August 2002—A tagging study in a mesoscale model". In: *Quarterly Journal of the Royal Meteorological Society* 135.638, pp. 205–223. DOI: 10.1002/qj.374.

Sprenger, M., G. Fragkoulidis, H. Binder, M. Croci-Maspoli, P. Graf, C. M. Grams, P. Knippertz, E. Madonna, S. Schemm, B. Škerlak, and H. Wernli (2017). "Global climatologies of

Eulerian and Lagrangian flow features based on ERA-Interim". In: *Bulletin of the American Meteorological Society* 98.8, pp. 1739–1748. DOI: 10.1175/BAMS-D-15-00299.1.

Statista (2022). *Teuerste Naturkatastrophen für die weltweite Versicherungswirtschaft im Jahr 2021 nach Gesamtschaden und versichertem Schaden*. last access: 6 April 2022. URL: https://de.statista.com/statistik/daten/studie/195502.

Stephenson, A. G. (2002). "evd: Extreme Value Distributions". In: *R News* 2.2. last access: 22 July 2023, pp. 31–32. URL: https://CRAN.R-project.org/doc/Rnews/.

Szalińska, W., I. Otop, and T. Tokarczyk (2014). "Precipitation extremes during flooding in the Odra River Basin in May-June 2010". In: *Meteorology, Hydrology and Water Management* 2.1, pp. 13–20.

Tabari, H. (2020). "Climate change impact on flood and extreme precipitation increases with water availability". In: *Scientific reports* 10.1, p. 13768. DOI: 10.1038/s41598-020-70816-2.

Tandon, N. F., X. Zhang, and A. H. Sobel (2018). "Understanding the dynamics of future changes in extreme precipitation intensity". In: *Geophysical Research Letters* 45.6, pp. 2870–2878. DOI: 10.1002/2017GL076361.

Tellman, B., J. A. Sullivan, C. Kuhn, A. J. Kettner, C. S. Doyle, G. R. Brakenridge, T. A. Erickson, and D. A. Slayback (2021). "Satellite imaging reveals increased proportion of population exposed to floods". In: *Nature* 596.7870, pp. 80–86. DOI: 10.1038/s41586-021-03695-w.

Ulbrich, U., T. Brücher, A. H. Fink, G. C. Leckebusch, A. Krüger, and J. G. Pinto (2003). "The central European floods of August 2002: Part 2-Synoptic causes and considerations with respect to climatic change". In: *Weather* 58.11, pp. 434–442. DOI: 10.1256/wea.61.03B.

van Bebber, W. J. (1891). *Die Zugstrassen der barometrischen Minima nach den Bahnenkarten der deutschen Seewarte für den Zeitraum 1875-1890*. 8, pp. 361–366.

Ventura, V., C. J. Paciorek, and J. S. Risbey (2004). "Controlling the proportion of falsely rejected hypotheses when conducting multiple tests with climatological data". In: *Journal of Climate* 17.22, pp. 4343–4356. DOI: 10.1175/3199.1.

Wasserstraßen- und Schifffahrtsverwaltung des Bundes (2022). *Gewässereinzugsgebiete Deutschland (WMS)*. last access: 14 January 2022. URL: https://www.gdws.wsv.bund.de/DE/service/karten/02_Geodatendienste_Geoanwendungen/01_Geodatendienste_NEU/Geodatendienste_node.html.

Weigel, A. (2017). *Wie geht es den Deggendorfern heute?* last access: 22 July 2023. URL: https://www.spiegel.de/panorama/deggendorf-wie-geht-es-den-menschen-nach-dem-hochwasser-von-2013-heute-a-1159592.html.

Wernli, H. and C. Schwierz (2006). "Surface cyclones in the ERA-40 dataset (1958–2001). Part I: Novel identification method and global climatology". In: *Journal of the Atmospheric Sciences* 63.10, pp. 2486–2507. DOI: 10.1175/JAS3766.1.

Winschall, A., S. Pfahl, H. Sodemann, and H. Wernli (2014). "Comparison of Eulerian and Lagrangian moisture source diagnostics–the flood event in eastern Europe in May 2010". In: *Atmospheric Chemistry and Physics* 14.13, pp. 6605–6619. DOI: 10.5194/acp-14-6605-2014.

World Meteorological Organization (2009). *Manual on estimation of probable maximum precipitation (PMP)*. Vol. 1045. Geneva: World Meteorological Organization, 258 pp.

Appendix A

Appendix of Chapter 2

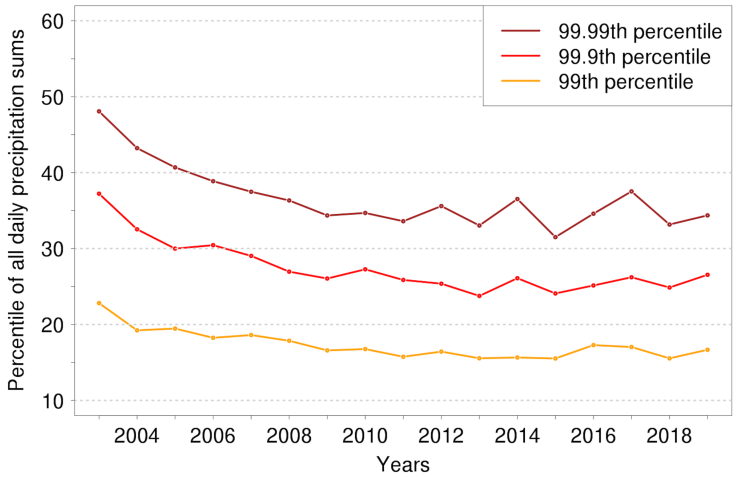

Figure A.1: Yearly distribution of the 99th, 99.9th and 99.99th percentile of the daily accumulated precipitation amounts over the Danube catchment. All percentiles decrease from 2003 until about 2008.

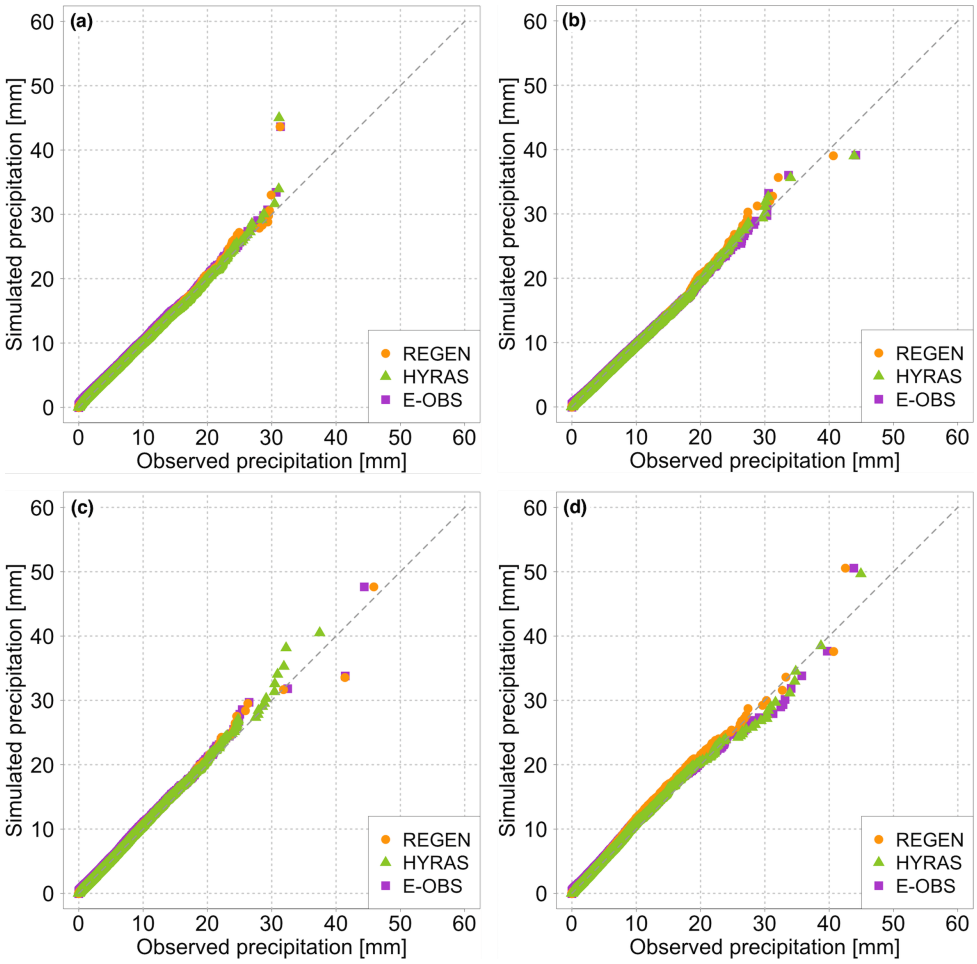

Figure A.2: Same as in Fig. 2.2b, but for events over the **(a)** Rhine, **(b)** Weser/Ems, **(c)** Elbe and **(d)** Oder catchment.

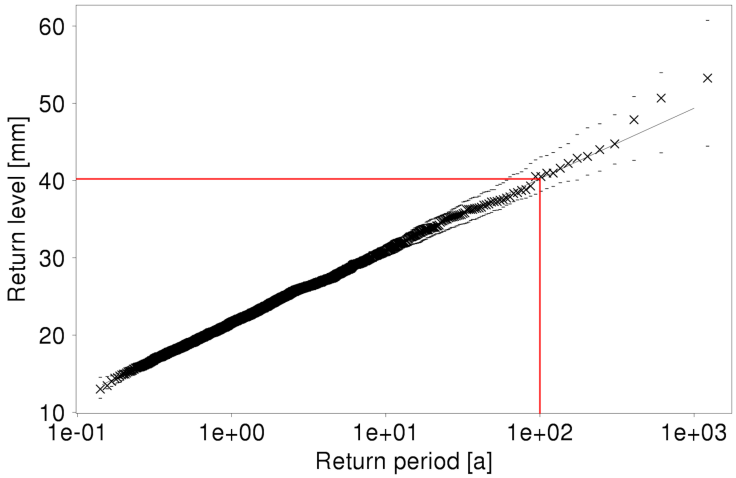

Figure A.3: Return level plot from the generalised extreme value distribution, based on yearly precipitation maxima from the ensemble prediction data for the Danube catchment. The red lines mark the return level of a 100-year precipitation event.

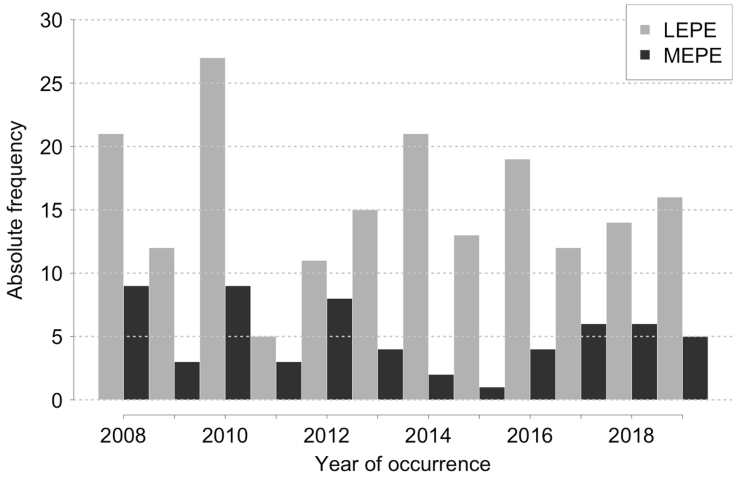

Figure A.4: Yearly distribution of all MEPEs and LEPEs over all catchments combined.

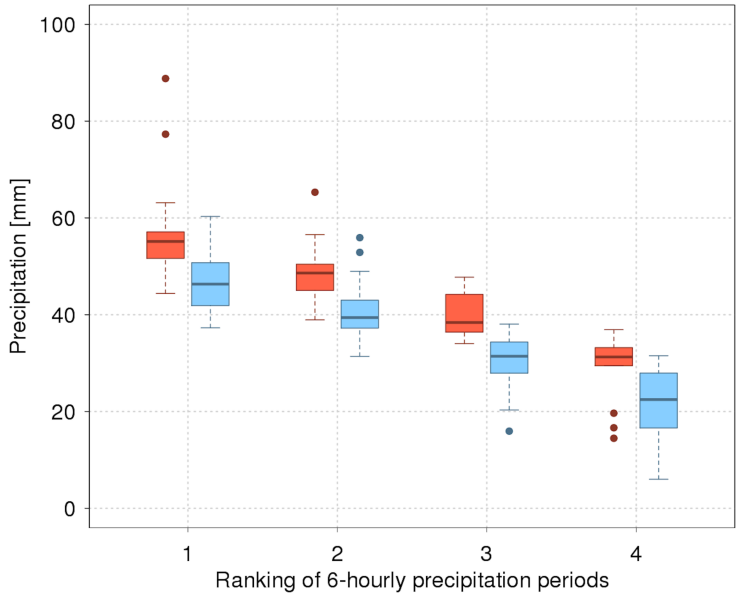

Figure A.5: Precipitation intensity distribution for the 6-hourly periods during (red) MEPEs and (blue) LEPEs over the Danube catchment, ranked by their precipitation intensity (descending).

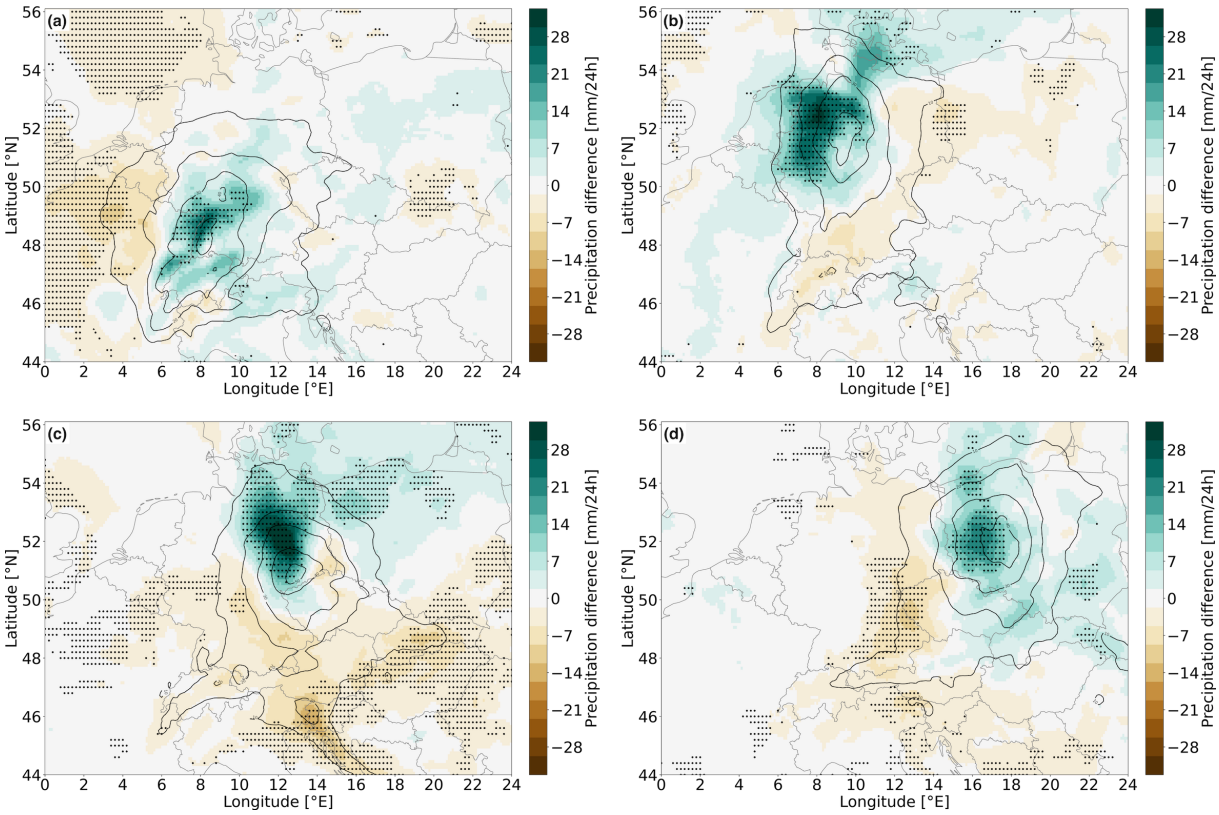

Figure A.6: Same as in Fig. 2.3b, but for events over the **(a)** Rhine, **(b)** Weser/Ems, **(c)** Elbe and **(d)** Oder catchment.

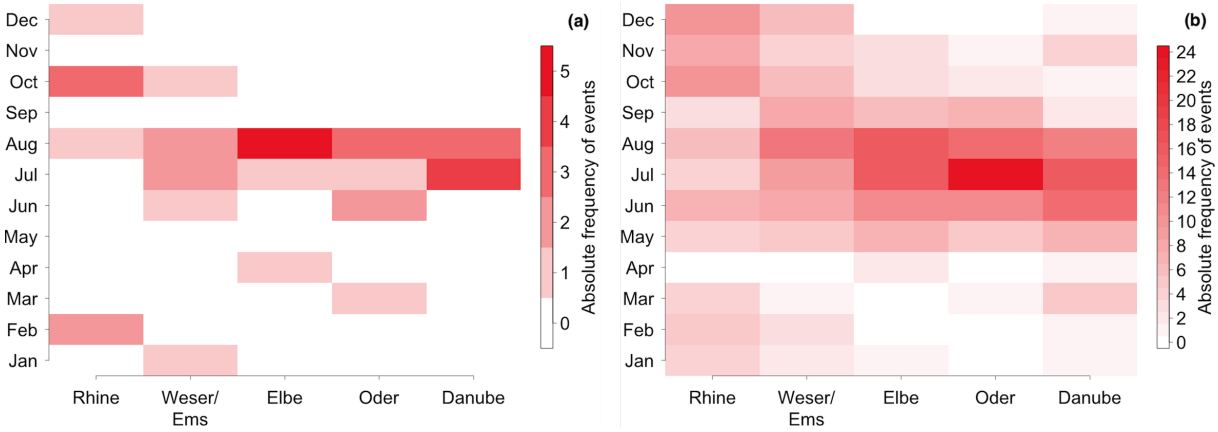

Figure A.7: Monthly distribution of the **(a)** 7 and **(b)** 65 most intense precipitation events for each river catchment based in HYRAS data. The events can simply be considered as **(a)** 10- and **(b)** 1-year precipitation events.

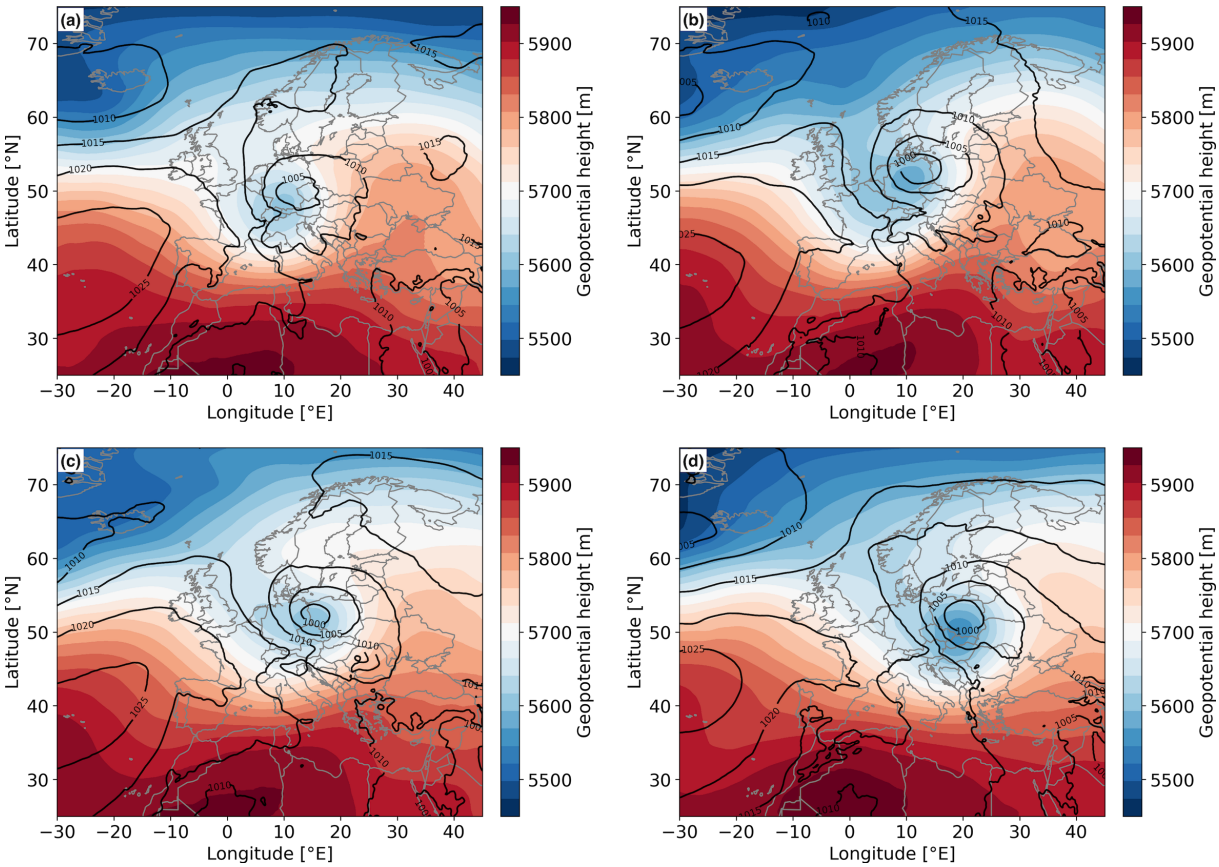

Figure A.8: Same as in Fig. 2.5a, but for events over the **(a)** Rhine, **(b)** Weser/Ems, **(c)** Elbe and **(d)** Oder catchment.

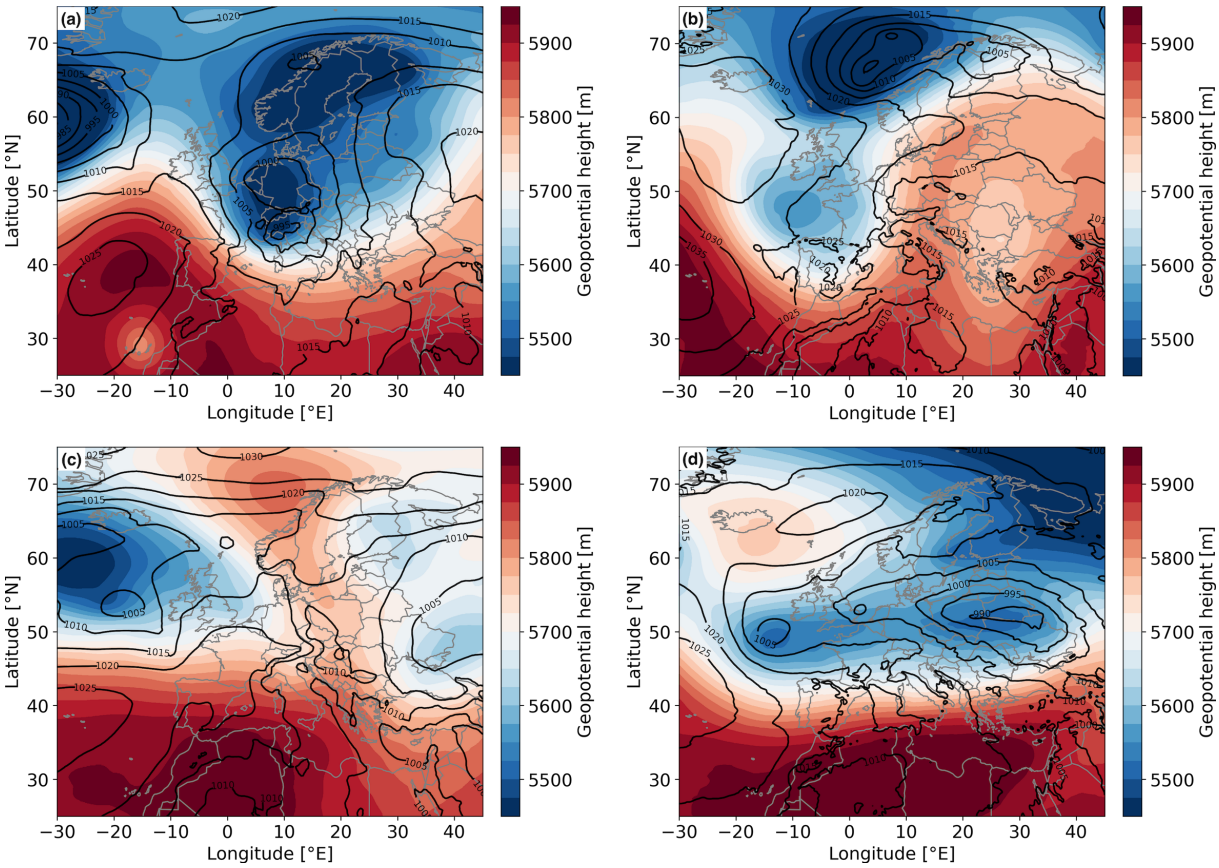

Figure A.9: Geopotential height at 500 hPa (colour shading) and sea level pressure (black contours) of single MEPEs, 12 hours after the events started, over the **(a)** Danube (here 12 hours before the event), **(b)** Weser/Ems, **(c)** Elbe and **(d)** Oder catchment. All events deviate from their specific catchment composite, as described in Sect. 2.4.2.

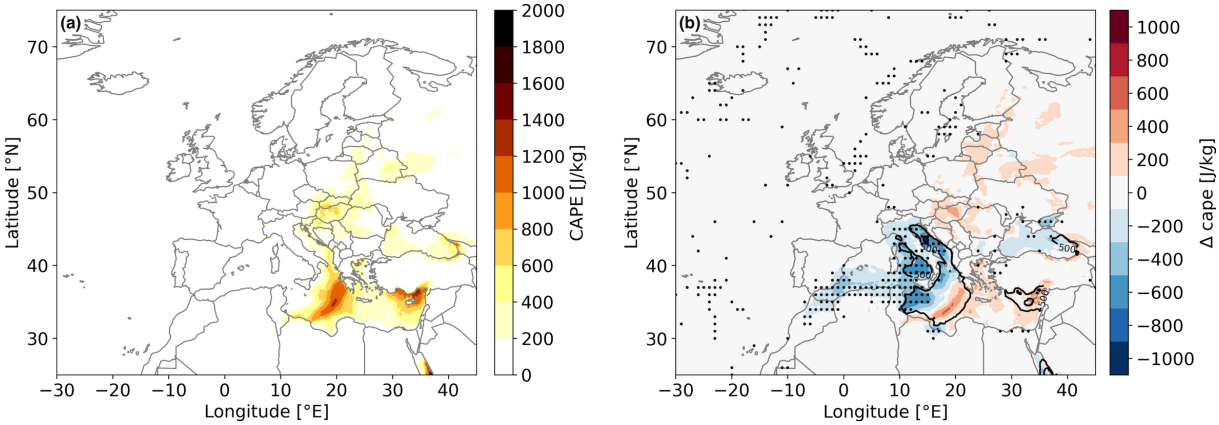

Figure A.10: **(a)** Composites of CAPE for all MEPEs and **(b)** difference between the MEPE and LEPE composites for events in the Danube catchment, 12 hours after the start of the events. In **(b)**, black dots mark significant differences and black contours indicate the LEPE composite.

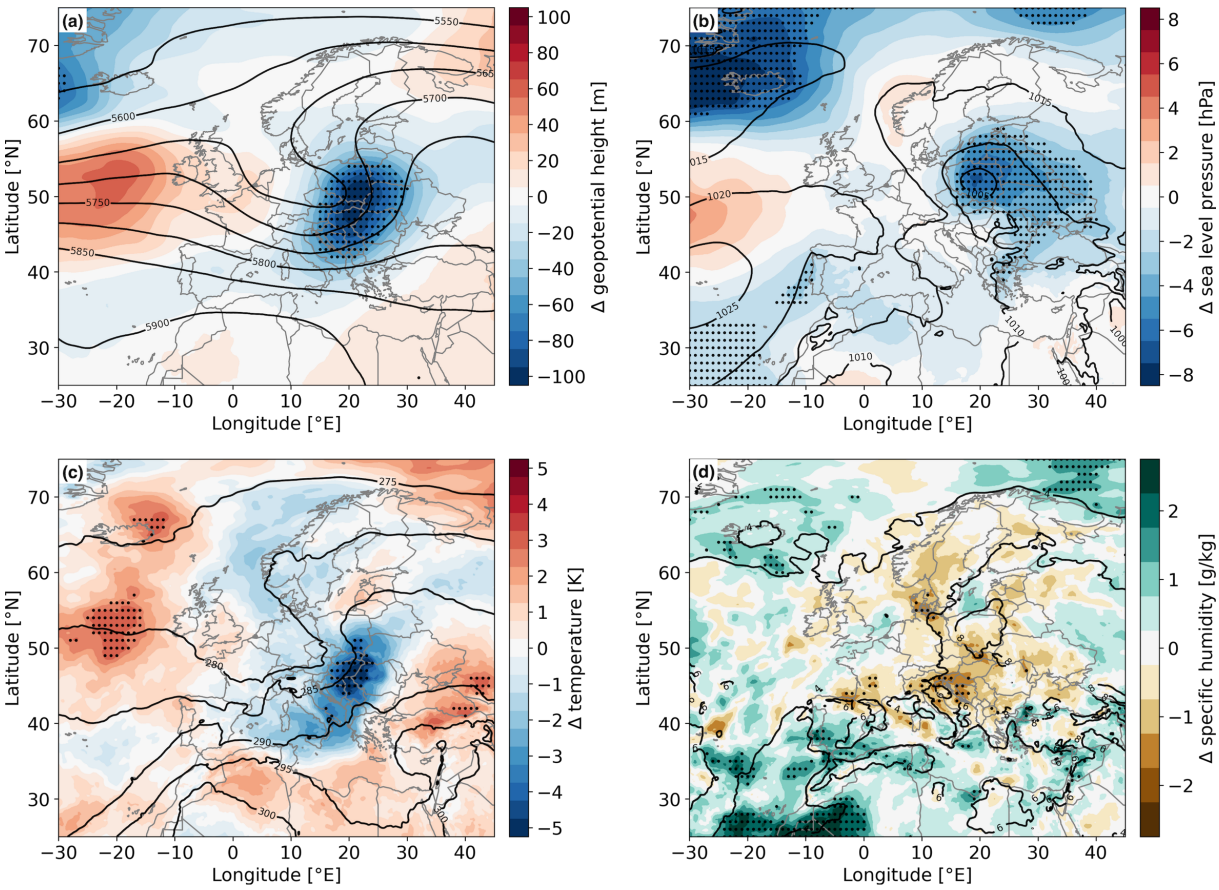

Figure A.11: Same as in Fig. 2.7, but for events over the Oder catchment.

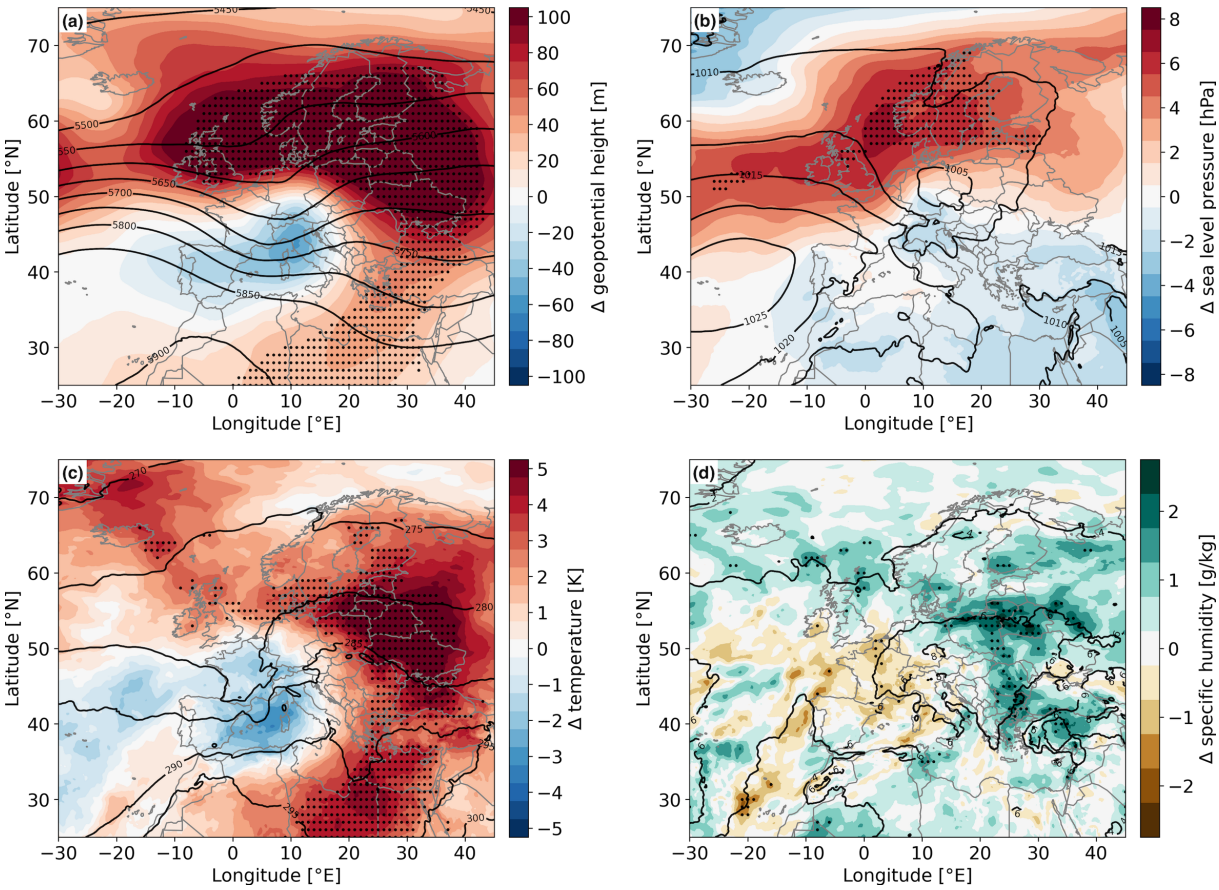

Figure A.12: Same as in Fig. 2.7, but for events over the Rhine catchment.

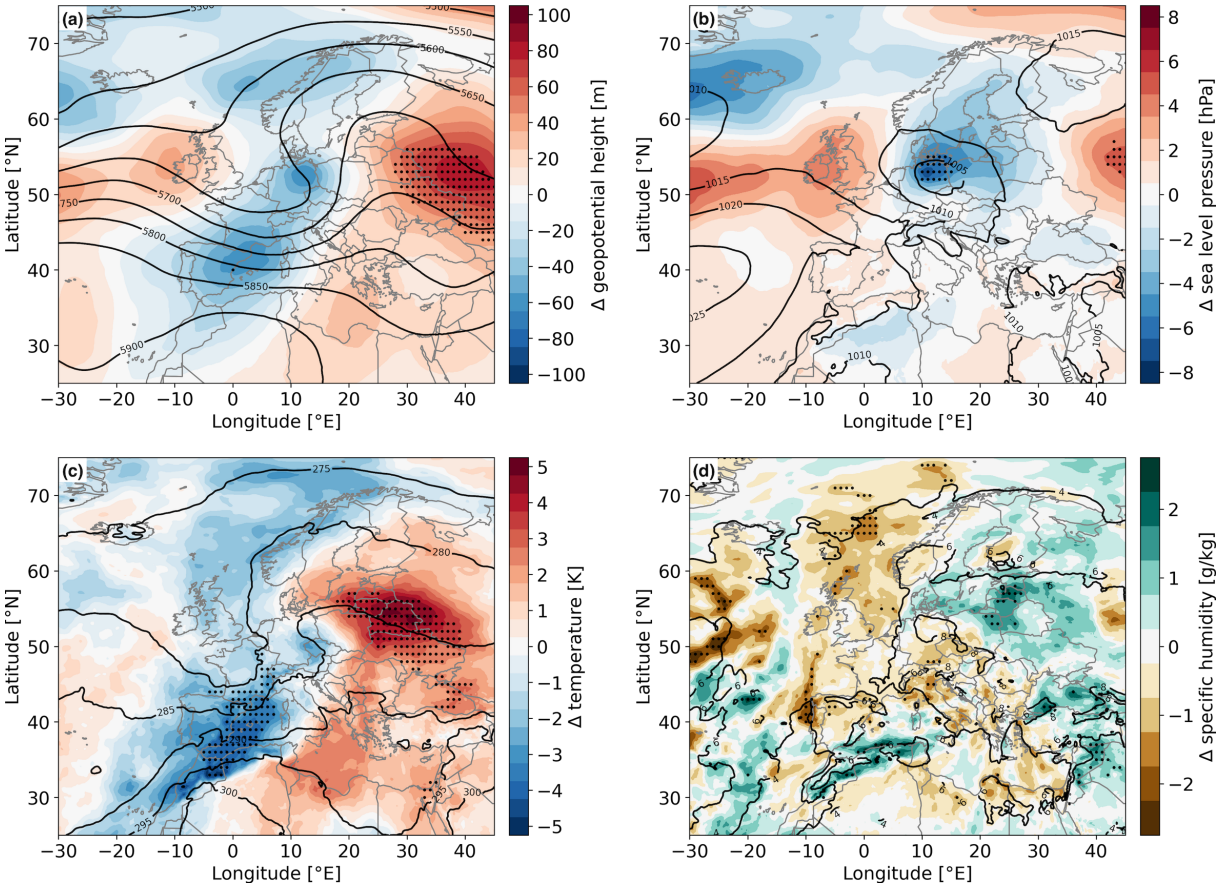

Figure A.13: Same as in Fig. 2.7, but for events over the Weser/Ems catchment.

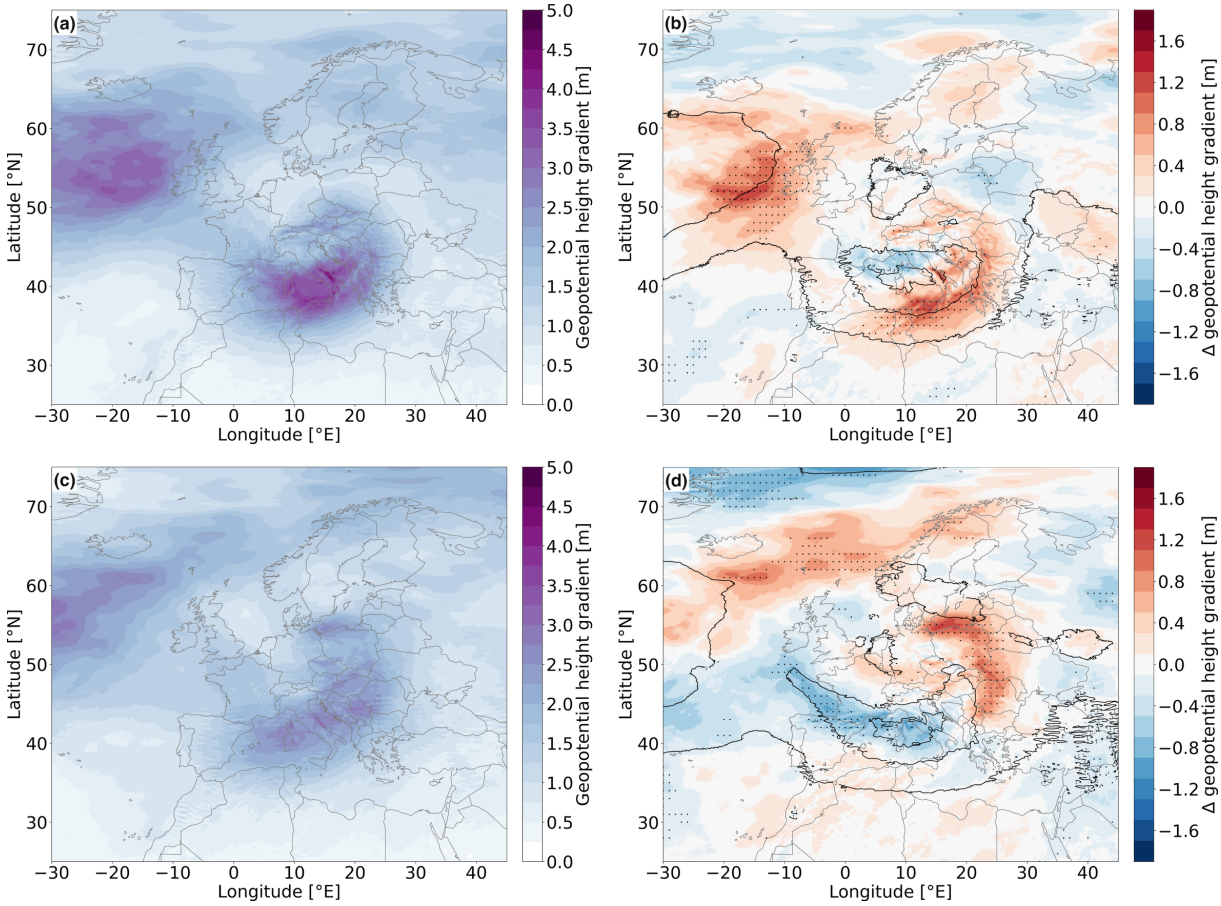

Figure A.14: **(Left)** MEPE composites of the absolute value of the geopotential height gradient at 500 hPa and **(right)** differences between MEPE and LEPE composites for events in the **(upper)** Danube and **(lower)** Elbe catchment, 12 hours after the start of the events. For the difference plots, black dots indicate statistical significance and black contours represent the LEPE composite.

Appendix B

Appendix of Chapter 3

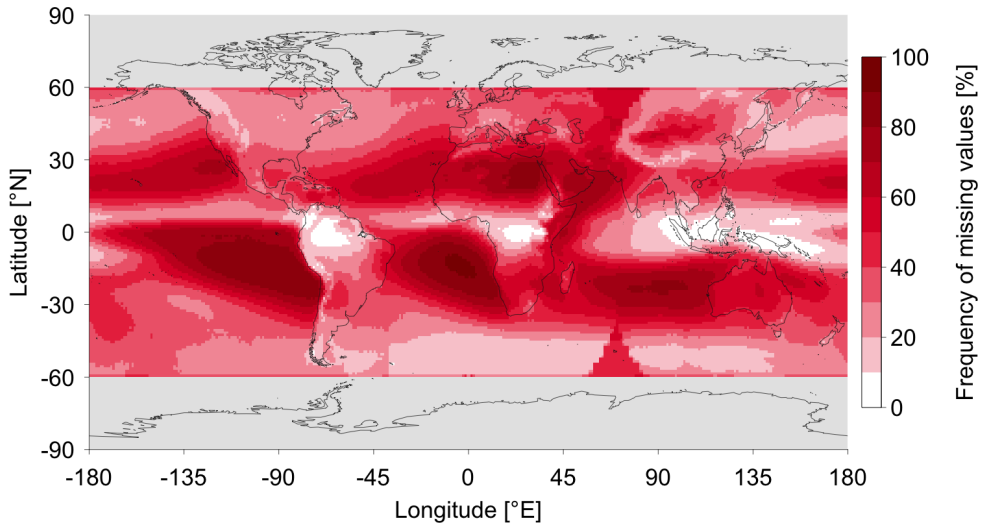

Figure B.1: Frequency of missing values (either dry days or days when satellite data are not available) in the original PERSIANN observations for a data period of 1983 to 2021.

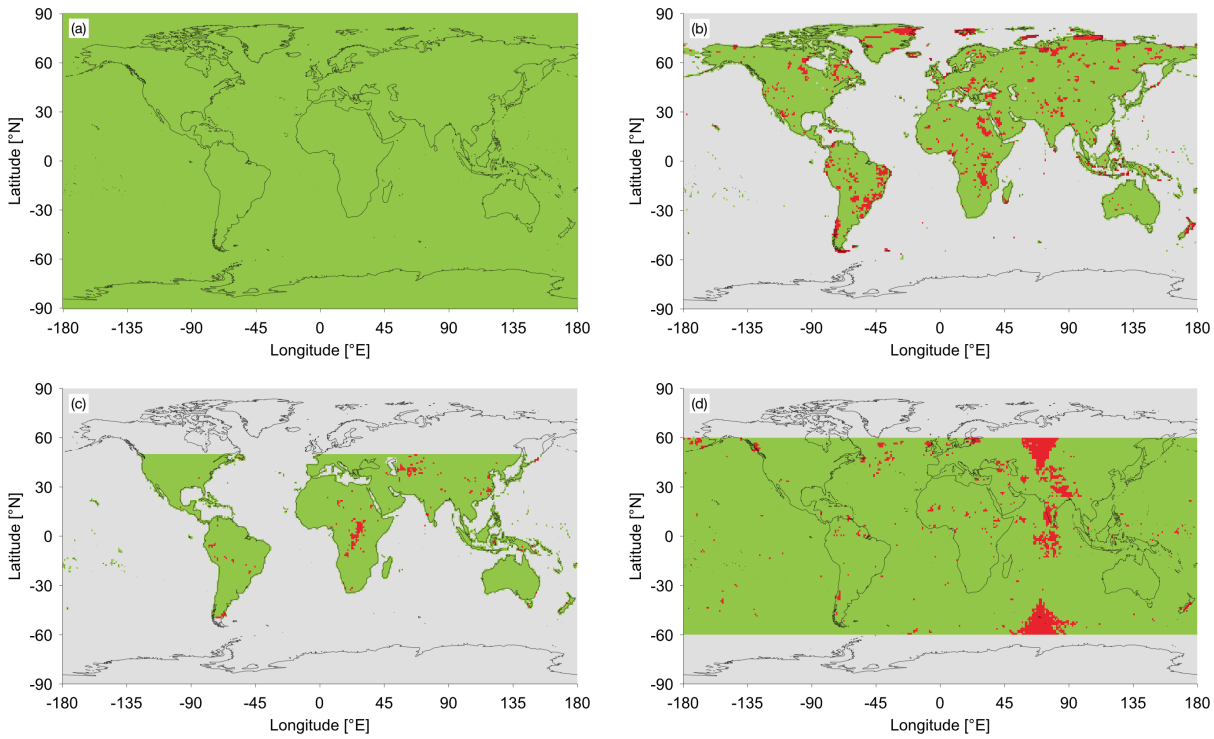

Figure B.2: Spatial distribution of statistical significant temporal trends (red grid points), obtained from the FDR test of Benjamini and Hochberg (1995), as described in Ventura et al. (2004), applied on multiple p values associated with the Mann-Kendall trend tests applied for the 99.9th percentile of daily precipitation for **(a)** the EPS data and the **(b)** REGEN, **(c)** CHIRPS and **(d)** PERSIANN observations.

Appendix C

Appendix of Chapter 4

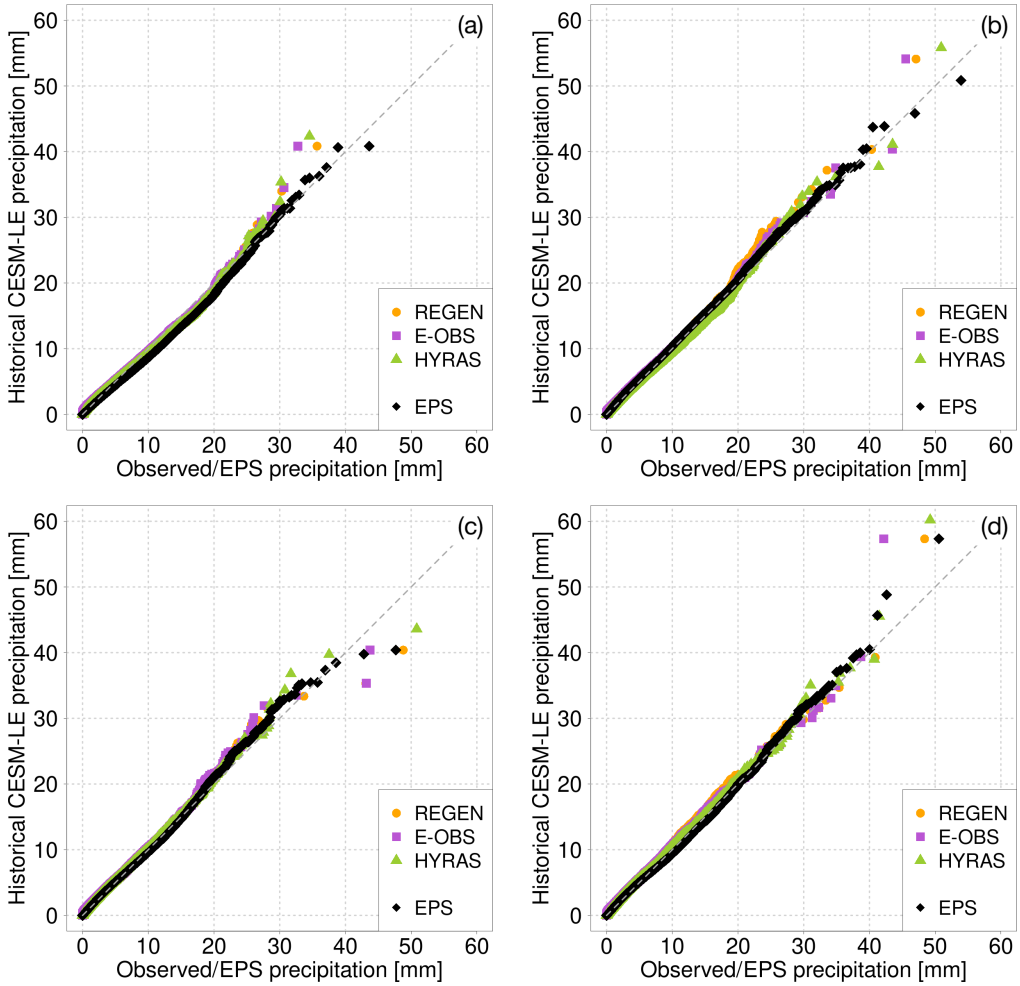

Figure C.1: The same as in Fig. 4.2b but for the **(a)** Rhine, **(b)** Weser/Ems, **(c)** Elbe and **(d)** Oder catchment.

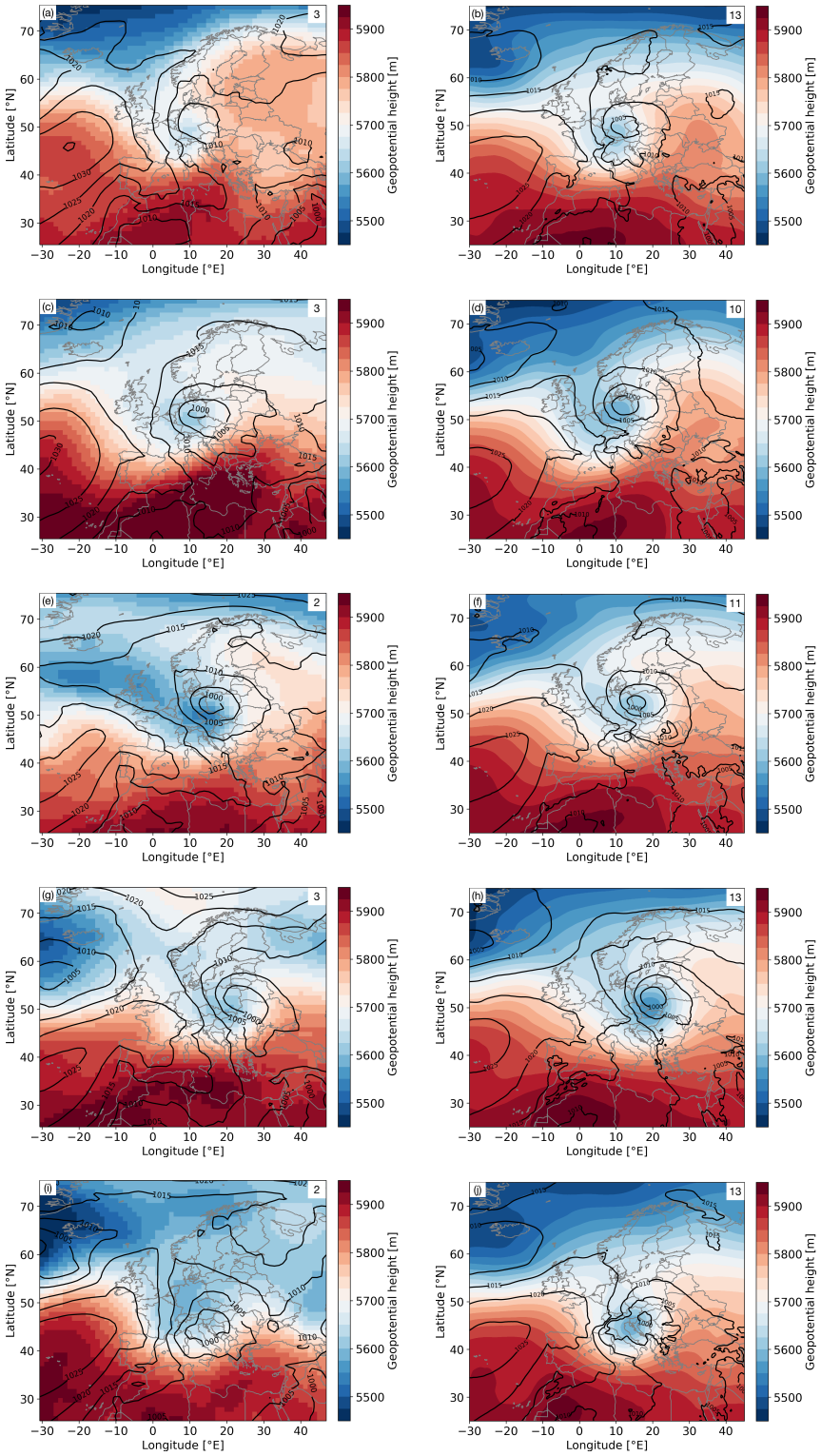

Figure C.2: The same as in Fig. 4.4 over the **(a,b)** Rhine, **(c,d)** Weser/Ems, **(e,f)** Elbe, **(g,h)** Oder and **(i,j)** Danube catchment but for **(left)** 100-year events from historical CESM-LE simulations.

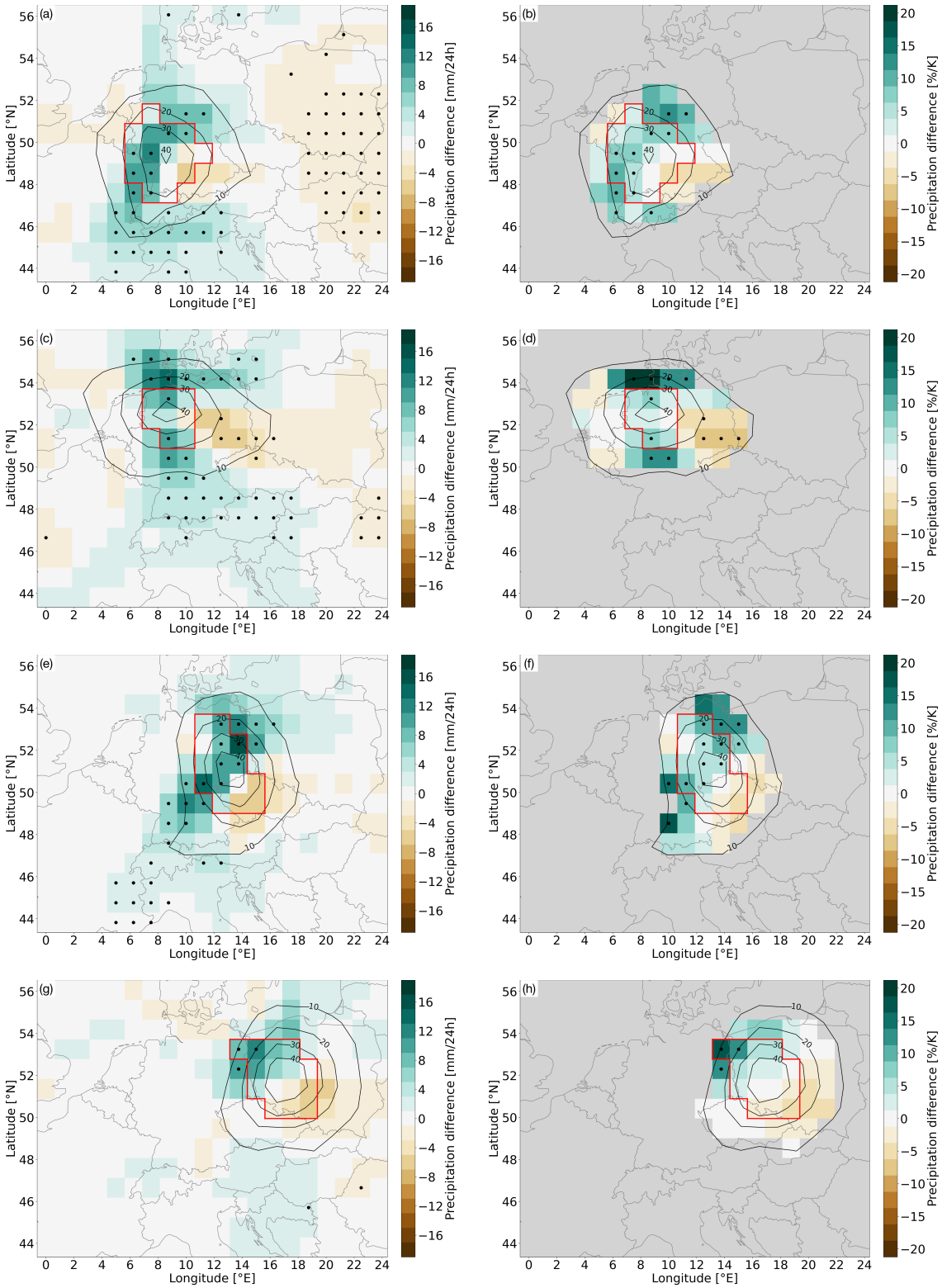

Figure C.3: The same as in Fig. 4.5 but for the **(a,b)** Rhine, **(c,d)** Weser/Ems, **(e,f)** Elbe and **(g,h)** Oder catchment.

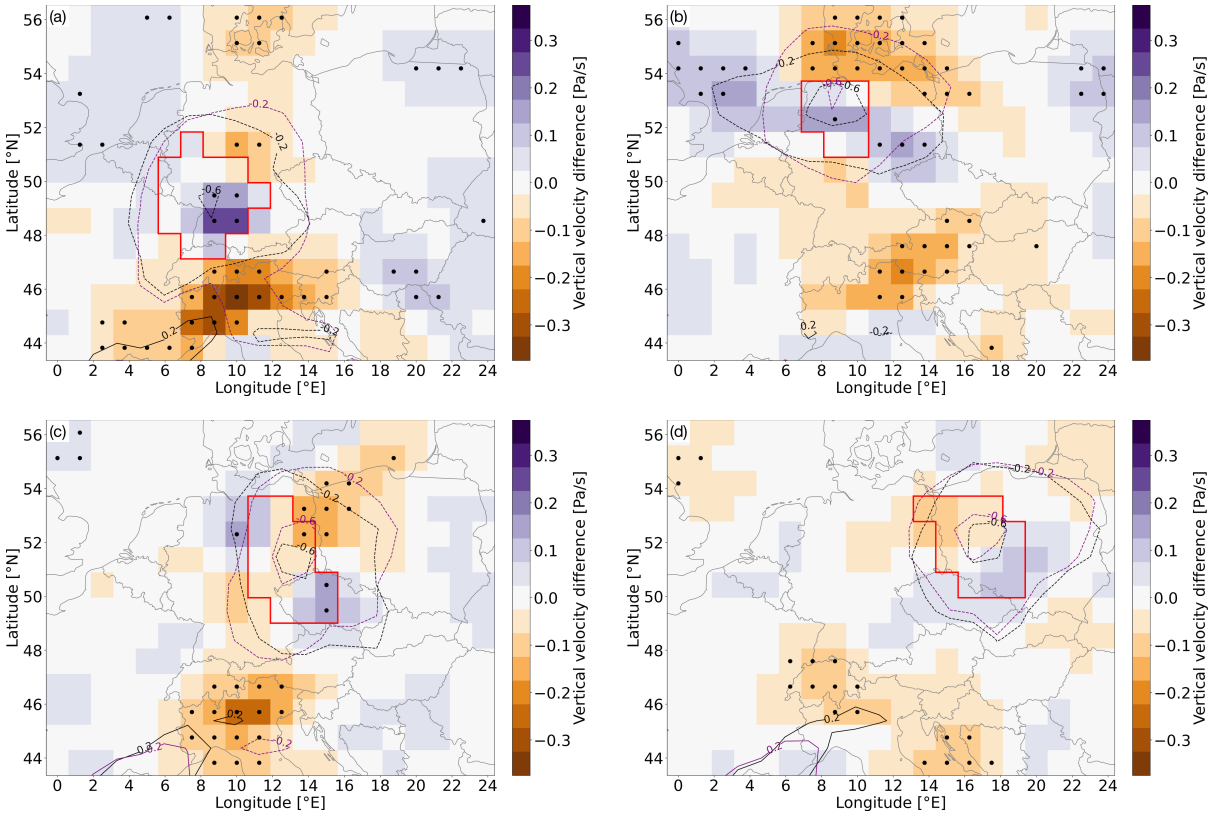

Figure C.4: The same as in Fig. 4.6 but for the **(a)** Rhine, **(b)** Weser/Ems, **(c)** Elbe and **(d)** Oder catchment.

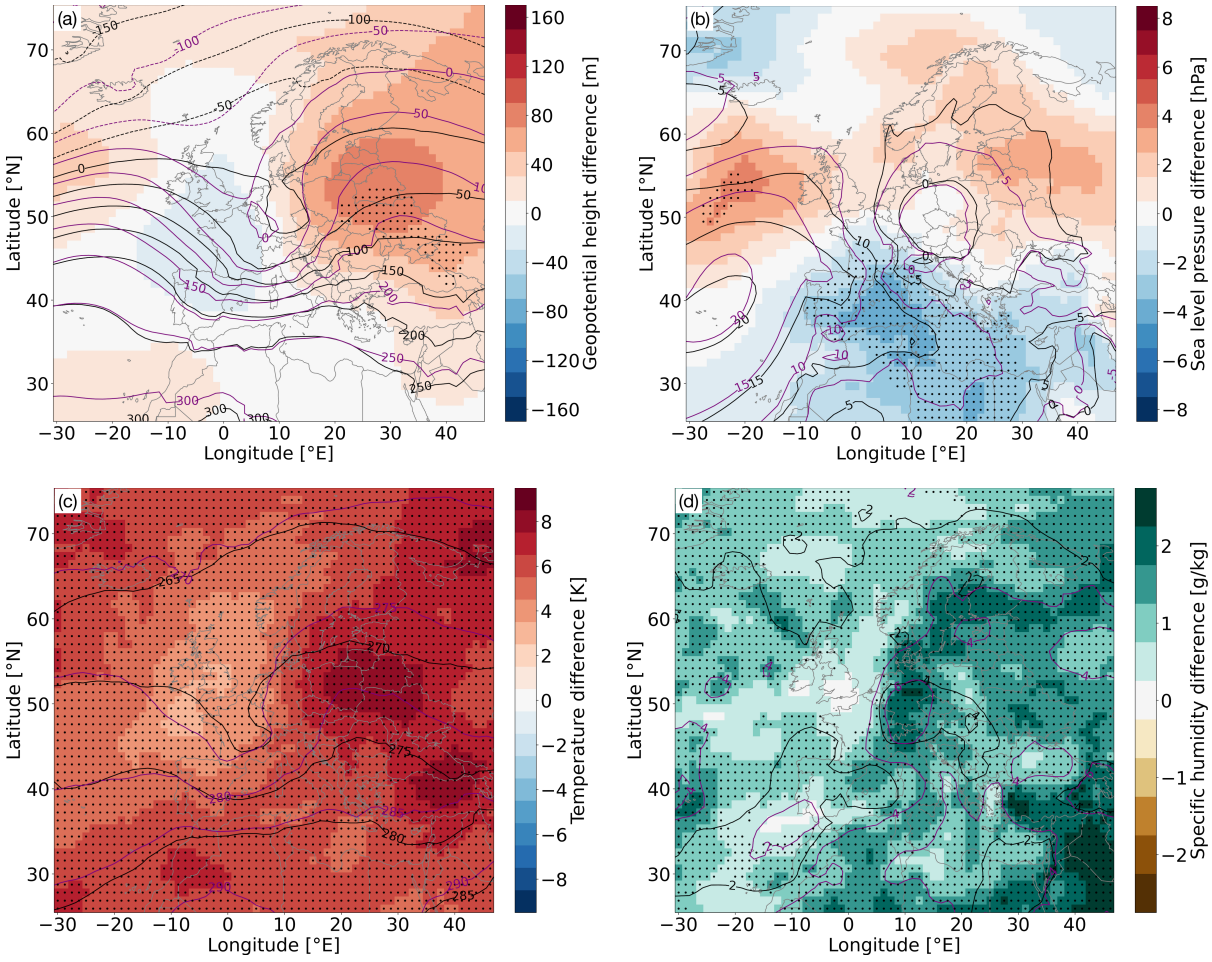

Figure C.5: The same as in Figs. 4.7 and 4.8 but for the Rhine catchment.

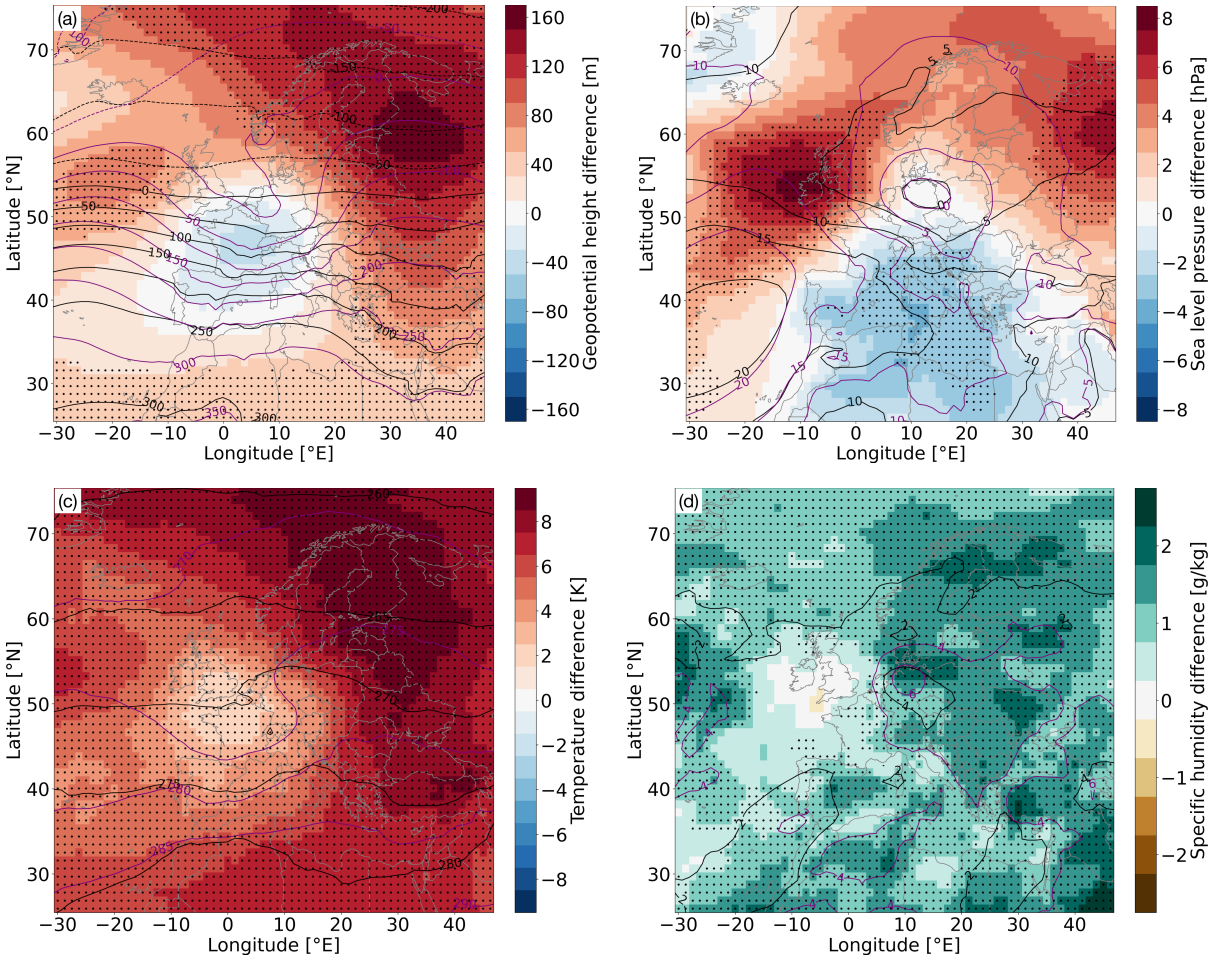

Figure C.6: The same as in Figs. 4.7 and 4.8 but for the Weser/Ems catchment.

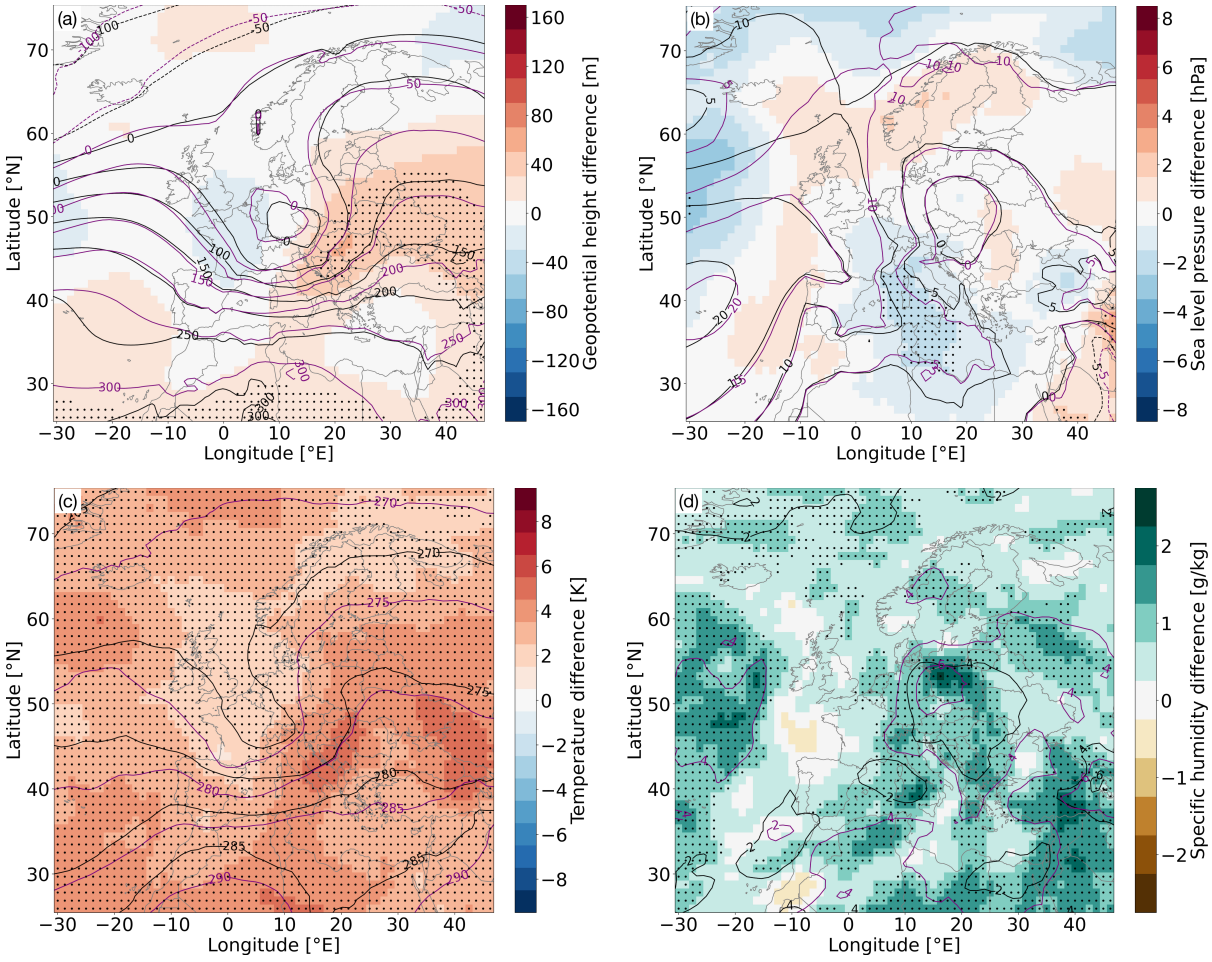

Figure C.7: The same as in Figs. 4.7 and 4.8 but for the Elbe catchment.

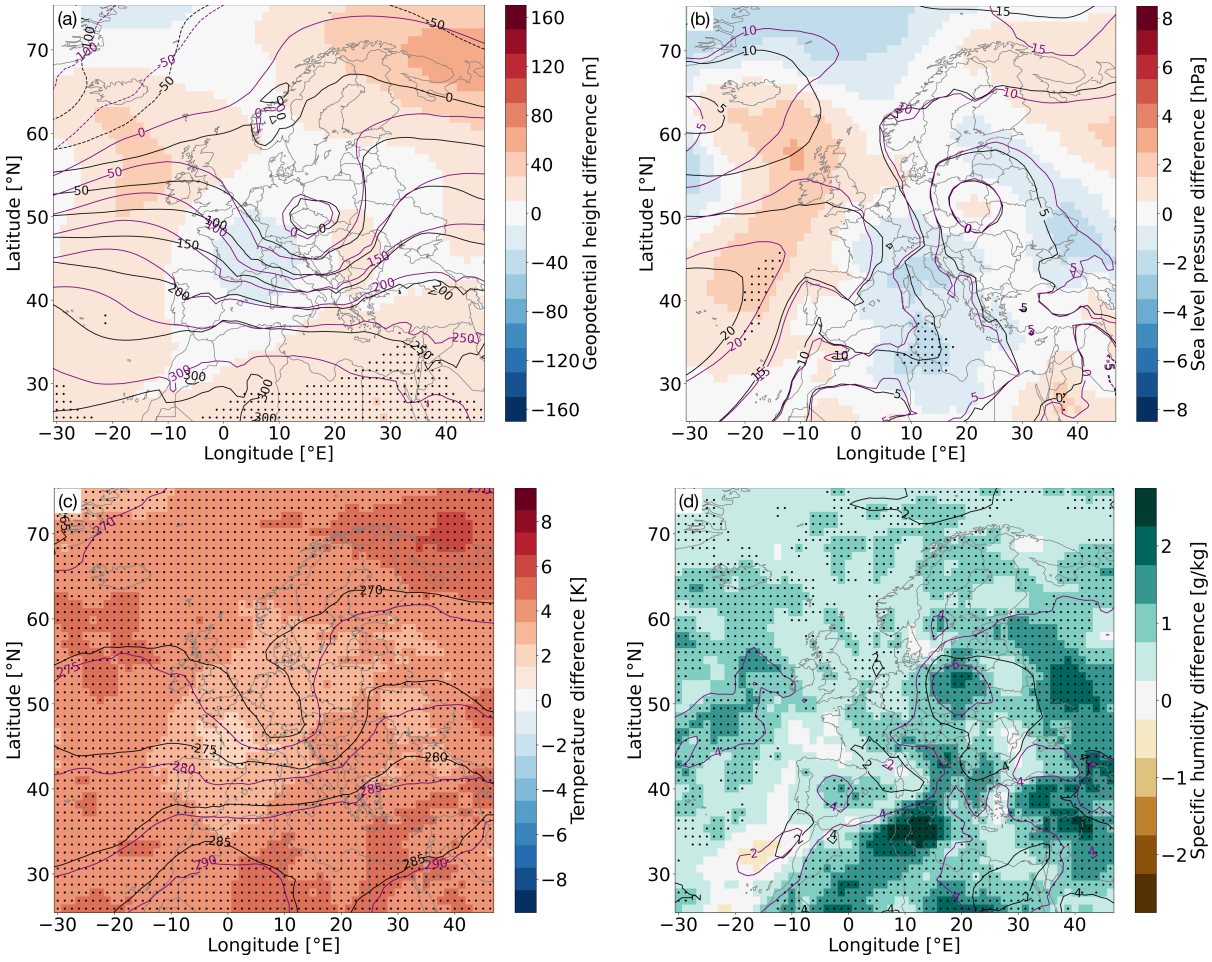

Figure C.8: The same as in Figs. 4.7 and 4.8 but for the Oder catchment.

Acknowledgement

I would like to thank Prof. Stephan Pfahl for the opportunity of working in his working group for the ClimXtreme project at the Freie Universität Berlin, his advice and support over the years, interesting discussions and the possibility of personally meeting people from international institutes and visiting international conferences. I also would like to thank Prof. Erich Fischer for being an external reviewer of this thesis.

This thesis has been funded by the German Ministry of Education and Research (Bundesministerium für Bildung und Forschung, BMBF) in its strategy Research for Sustainability (FONA) in the framework of the ClimXtreme programme, sub-project A2 (MExRain, grant number 01LP1901C). I acknowledge the German Meteorological Service DWD and the ECMWF for providing the operational IFS model data. This thesis used resources of the Deutsches Klimarechenzentrum (DKRZ), which is granted by its Scientific Steering Committee (WLA) under project ID bb1152. I also would like to acknowledge Urs Beyerle (ETH Zurich) for performing the re-runs of the CESM-LE climate simulations. In addition, the global estimates of 100-year return values and their confidence intervals from EPS and observational data (REGEN, CHIRPS and PERSIANN), presented in Ch. 3, can be downloaded from `http://dx.doi.org/10.17169/refubium-39650`. The operational IFS ensemble forecast data from ECMWF can be obtained from ECMWF (2023a) for the control run and from ECMWF (2023b) for the perturbed runs. The user's affiliation needs to belong to an ECMWF member state. The observational data sets are freely accessible from Contractor et al. (2020b) for REGEN, from Rauthe et al. (2013b) for HYRAS, from Cornes et al. (2018b) for E-OBS, from Funk et al. (2014b) for CHIRPS and from Ashouri et al. (2015a) for PERSIANN.

I would also like to thank the entire working group with Michael, Thomas, Patrick, Svetlana, George, Kalpana, Edgar, Ingo, Gregor, Henry and Angela for having nice talks, long lunch breaks (including Dönerstage) and funny events. I am grateful for being a part of the large ClimXtreme community, including nice conversations, discussions and conferences with such great colleagues. In particular, I thank Heini Wernli for his helpful comments and interesting discussions on the event process analysis, Felix Fauer and Henning Rust for their help on statistical approaches, Hendrik Feldmann for his suggestion of diverse data sets, and all colleagues of the Module D for their technical assistance.

Special thanks go to my family and my friends for always supporting me during each phase of the thesis and clearing my head for a change. Finally, I particularly want to thank Lisa for supporting me, mentally and scientifically. Thank you for being such an important person to me.

Declaration of originality

I hereby confirm that I have written this dissertation independently and have not used any other sources than those which are indicated as references. All statements taken from other sources have been identified. I am aware that the digital form of this thesis can be examined for the use of unauthorised aid and in order to determine whether the report as a whole or parts incorporated in it may be deemed as plagiarism. For the comparison of this thesis with existing sources I agree that it shall be entered in a data base where it shall also remain after examination, to enable comparison with future theses submitted. However, further rights of reproduction and usage are not granted here. This thesis was not previously presented to any other university for examination and has not been published, except for the two journal publications as indicated at the end of Ch. 1.

Berlin, 18th of September 2023

Florian Ruff